UNCLASSIFIED

AD NUMBER

AD817580

LIMITATION CHANGES

TO:

Approved for public release; distribution is unlimited.

FROM:

**Distribution authorized to U.S. Gov't. agencies and their contractors;
Administrative/Operational Use; 01 MAY 1967.
Other requests shall be referred to Office of Naval Research, Arlington, VA 22203.**

AUTHORITY

ONR ltr 27 Jul 1971

THIS PAGE IS UNCLASSIFIED

AD817580

SEMIANNUAL TECHNICAL SUMMARY REPORT
CONTRACT NO. NO 0014-67-C-0307
ARPA ORDER NO. 306

HUGHES
HUGHES AIRCRAFT COMPANY

CO_2 OPTICAL RADAR SYSTEM

1 NOVEMBER 1966 through 1 MAY 1967

HUGHES RESEARCH LABORATORIES • MALIBU

DISCLAIMER NOTICE

THIS DOCUMENT IS THE BEST QUALITY AVAILABLE.

COPY FURNISHED CONTAINED A SIGNIFICANT NUMBER OF PAGES WHICH DO NOT REPRODUCE LEGIBLY.

ERRATA FOR SEMIANNUAL TECHNICAL SUMMARY REPORT

Contract No. N00014-67-C-0237

Hughes Research Laboratories
Malibu, California

Table VI, page 57, should read as follows:

TABLE VI

Comparison of Amplifier Characteristics

Characteristic	Pulsed, 1000 pps, 100 μsec	cw
g_o	4 dB/m	3 dB/m
S_o	> 200 W/cm^2	60 - 90 W/cm^2
Current	200 mA peak	25 mA dc
Specific potential	8 kV/m	5 kV/m
Specific average power input	160 W/m	120 W/m
Gas flow	26 cfh CO_2 32 cfh N_2 126 cfh He } at 11.5 Torr	13 cfh CO_2 32 cfh N_2 178 cfh He } at 17 Torr

Table IX, page 71 — First line should read "same as Table X, except" instead of "same as Table XI, except"

HUGHES RESEARCH LABORATORIES
Malibu, California

a division of hughes aircraft company

CO_2 OPTICAL RADAR SYSTEM

Semiannual Technical Summary Report
Contract No. NO 0014-67-C-0237
ARPA Order No. 306

1 November 1966 through 1 May 1966

W. B. Bridges, Project Engineer
Electron Device Physics Department

[redacted]

Reproduction in whole or in part is permitted for any purpose of the United States Government.

The research conducted under this contract is part of project DEFENDER under the joint sponsorship of the Advanced Research Projects Agency, the Office of Naval Research, and the Department of Defense.

STATEMENT #2 UNCLASSIFIED

This document is subject to special export controls and each transmittal to foreign governments or foreign nationals may be made only with prior approval of

TABLE OF CONTENTS

LIST OF ILLUSTRATIONS

ABSTRACT

Progress is reported on a program to develop and build a 1 kW average power 10.6 μ amplifier for radar applications. Small signal gain and saturation measurements were made on 1-in. diameter amplifier tubes using a CO_2-N_2-He mixture with cw driving signals. Optimum values for cw discharge tubes were 3 dB/m and 60 to 90 W/cm^2; for pulsed discharges (at 500 pps), they were 4 dB/m and more than 200 W/cm^2.

Based on the above values, transmitter designs were made using pulsed operation or a combination of pulsed and cw operation at different stages. The most promising of these designs would use: (1) a 10 W cw oscillator, (2) a folded 16 m, 1 in. diameter tube, (3) a mechanical modulator with recollimating optics, and (4) a final amplifier of 8 m, 2 in. diameter tubes operated with a pulsed discharge. The device would be 32 ft long, including folding and recollimating optics.

The mechanisms of the CO_2-N_2-He laser are summarized and relevant rates and coefficients tabulated. The theory of gain saturation is reviewed and equations derived. Numerical values for small signal gain and saturation flux are calculated and compared with experimental values. Collisional cross relaxation among rotational levels appears to be important, and a method of treating it is presented. We solve the gain saturation equation for simplified cases. Diffraction beam spreading effects on amplifier performance are discussed, and a solution for the effect of gain saturation on the radial beam profile is given.

I. INTRODUCTION AND SUMMARY

This report gives the progress to date on the program to develop and build a 1 kW average power 10.6 μ amplifier suitable for radar applications. As outlined in our Technical Proposal 66M-7374/B1560 and the Final Technical Report* on the Laser Engineering Design Study (U) F29601-67-C-0034, the amplifier must be capable of pulsed operation to be suitable for radar use. The target values chosen as a result of the Design Study as most desirable for the final transmitter unit are: 25 kW peak power output, 20 μsec optical pulse length, and 2000 pps repetition rate, giving 1 kW average output at 0.04 duty cycle. The output will be near-diffraction limited and capable of being produced by a single-frequency driving source.

Small-signal gain and saturation measurements have been made on 1 in. diameter amplifier tubes. The resulting optimum values for a cw discharge were 3 dB/m and 60 to 90 W/cm^2; for a pulsed discharge at 500 pps the optimum value was 4 dB/m peak, $\gtrsim$ 200 W/cm^2 with a pulsed discharge at 500 pps. These values are for modest flow rates of CO_2-N_2-He mixture, and were obtained with cw driving signals.

Using these values (with some extrapolation for 2 in. diameter tubes), designs for the transmitter have been made on the basis of pulsed operation of the discharge or a combination of pulsed and cw operation of different stages. The most promising design consists of: (1) a 10 W cw oscillator, (2) a folded 8 m, 1 in. diameter tube (16 m active length) operated as a cw intermediate amplifier, (3) a mechanical modulator with recollimating optics producing 20 μsec pulses at 2000 pps with an exit diameter of 3.0 cm, (4) a final amplifier operated with a pulsed discharge and consisting of several 8 m sections of 2 in. diameter tubing. The over-all length of the device is 32 ft, including folding and recollimating optics. The exact number of 8 m sections required to reach the 25 kW level is dependent on the exact values of small signal gain and saturation flux obtained in the 2 in. pulsed discharge.

Section II-A of this report reviews and summarizes what is known of the CO_2-N_2-He laser mechanisms. A tabulation is made of the relevant rates and coefficients. In Section II-B the theory of gain saturation is reviewed and the equations to be used in the design procedure are derived on the basis of the model discussed in Section II-A. Numerical values for small-signal gain and saturation flux are calculated from the atomic constants and compared with experimentally determined values. From the comparison we conclude that collisional cross relaxation among the rotational levels is an important process; a method of treating collisional cross relaxation is included in Appendix B. Section II-C treats the solution of the gain saturation equation in simplified cases. The effects of diffraction beam spreading on amplifier

*Report classified SECRET.

performance are discussed, and a first-approximation solution for the effect of gain saturation on the radial beam profile is given. It appears that for small signal gains of 50 dB, the beam width is increased by more than a factor of two over the diffraction spread. Medium distortion measurements not due to saturation are given in Appendix A.

Section III gives the results of our measurements of small signal gain and saturation flux under cw and pulsed discharge conditions. The variation with gas mixture and pressure, discharge current and repetition rate, and gas flow rate are given. Cw small-signal gain values of 3 to 4 dB/m were obtained; peak pulsed gain values as high as 13 dB/m were observed, but only with very long ($\approx$ 1 msec) excitation pulses at low repetition rates (50 pps). In the useful range of repetition rates, the pulsed gain dropped to 4 to 5 dB. Saturation flux densities of 60 to 90 W/cm^2 were observed for cw discharges and $>$ 200 W/cm^2 for pulsed discharges. This latter value must be taken as somewhat tentative, because insufficient input power was available to obtain a good saturation curve.

Section IV-A presents the over-all design based on the experimental values obtained for g_o and S_o. The progress on fabrication of this design is given in Section IV-B. The 16 m intermediate amplifier is essentially complete and ready to be operated. Section V is a brief statement of the tasks to be completed in the next three-month period. Those include gain saturation measurements on the 16 m IA and on a 8 m test section of the final amplifier.

II. THEORY

A. Mechanisms of CO_2-N_2-He Laser

The excitation mechanisms and rate processes in the CO_2 laser are now reasonably well understood. The following will present a summary of the important processes and rates as they are known in the literature.

The CO_2 laser system is a four-level system as shown in Fig. 1; the lower laser level is at an energy $E_1 \approx 6$ kT at room temperature. The CO_2 laser medium generally consists of a mixture of CO_2, N_2 and a gas additive, such as helium or H_2O, excited in a glow discharge.

1. Excitation of Upper Laser Level

The upper laser level is the first vibrational level of the asymmetric stretching mode $CO_2(00^o1)$. Excitation is transferred to the upper laser level by a near-resonant vibrational energy transfer from excited N_2 molecules or from excited CO molecules produced in the discharge, by direct electron collisions with the ground state $CO_2(00^o0)$ and by cascade from the higher-lying ν_3 levels. The rate constant for the vibrational transfer process from N_2 has recently been measured,[1] ($k_e' = 1.7 \times 10^4$ sec^{-1} - Torr^{-1}). The excitation cross section for vibrationally exciting N_2 by electron collision has been measured by Schulz,[2] to be $\sigma = 3 \times 10^{-16}$ cm^2 for 2.2 eV electrons. The cross section for exciting $CO_2(00^o1)$ by electron collision has not appeared in the literature.

The vibrational transfer from N_2^* to CO_2^* occurs from the entire vibrational family of N_2 ($v = n$) to the corresponding family of $CO_2(00^on_3)$. Hocker, et al.,[3] have used a Q-switched laser as a probe to measure the excited population $CO_2(00^on_3)$ in a CO_2-N_2-He laser discharge. They found that levels as high as $n_3 = 4$ were heavily populated. They also determined that the relaxation time of the coupled $CO_2(00^on_3)$ levels was of the order of 10 μsec or less. Because of the strong coupling and rapid thermalization between the vibrational levels, the population of the $CO_2(00^o2, 00^o3, 00^o4)$ levels can contribute substantially to the cw saturated gain and power output of the CO_2 10.6 μ laser. Other Q-switched laser studies[4] indicate that the relaxation time of the rotational levels of $CO_2(00^o1)$ are of the order of 20 to 100 nsec.

2. De-excitation of Upper Laser Level

The upper laser level, $CO_2(00^o1)$ is depopulated by molecular collisions and by stimulated emission. Spontaneous emission is generally an unimportant depopulation mechanism in molecular laser

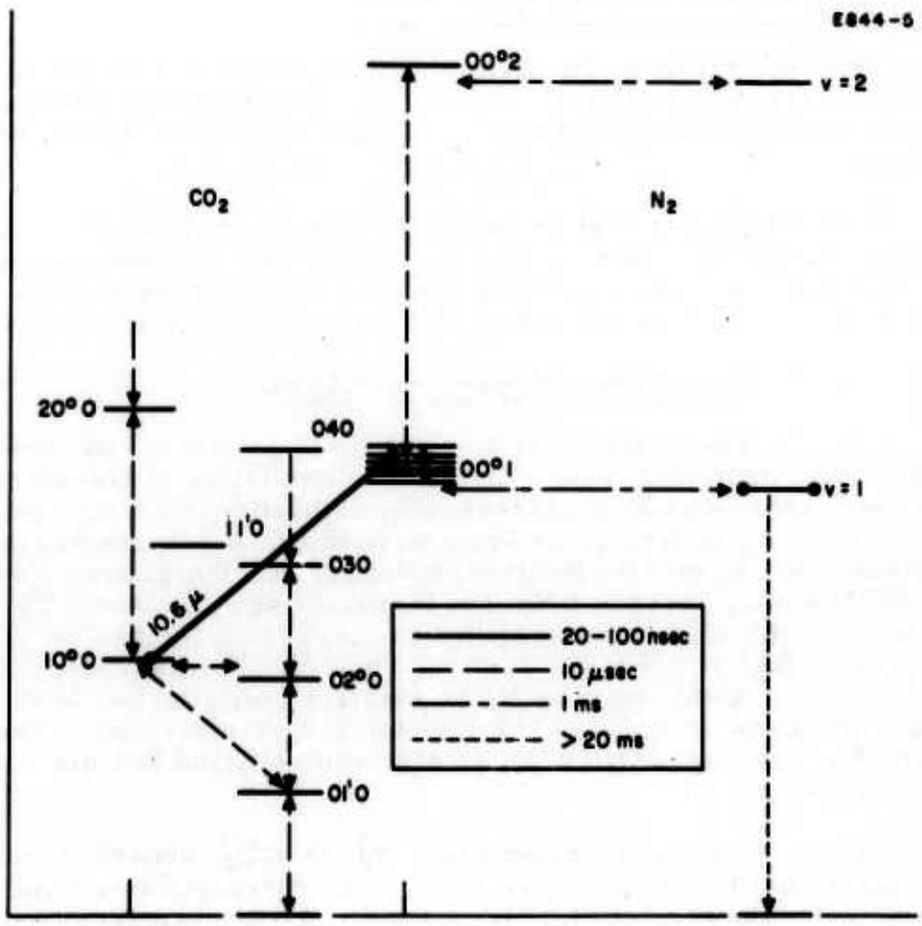

Fig. 1. Energy level diagram of the CO_2 molecule and N_2 metastable levels.

systems.[5] The spontaneous transition rate for the upper laser level is shown in Table I to be 200 sec^{-1}. However, in the presence of radiation trapping the transition rate A_{20} is decreased by a factor approximately 10^4 at 1 Torr CO_2. Thus, in the CO_2 laser system, collisional decay rates are at least 2 orders of magnitude greater than spontaneous emission decay rates.

TABLE I

Spontaneous Radiative Transition Probabilities in CO_2 (from Statz, et. al.[5])

Transitions	Dominant Branch	A_{ij}, sec^{-1}
$00^0 1 \rightarrow 10^0 0$	P	0.34
$00^0 1 \rightarrow 02^0 0$	P	0.20
$10^0 0 \rightarrow 01^1 0$	Q	0.53
$02^0 0 \rightarrow 01^1 0$	Q	0.48
$01^1 0 \rightarrow 00^0 0$	Q	1.07
$00^0 1 \rightarrow 00^0 0$	P	2×10^2

The $CO_2(00^0 1)$ can transfer its vibrational energy to an adjacent energy level during a collision.

$$CO_2(00^0 1) + M \rightarrow CO_2(n_1, n_2^{\ell}, n_3) + M + KE \quad . \qquad (1)$$

The molecule M, which can be a CO_2 or a foreign molecule, serves to catalyze the reaction. Collisions of this sort are most probable when the transfer energy levels are closely matched.[6, 7] Therefore, the most probable reactions in CO_2 are:

$$CO_2(00^0 1) + M \rightarrow CO_2(04^0 0) + M - 204\ cm^{-1} \qquad (2)$$

$$CO_2(00^0 1) + M \rightarrow CO_2(11^1 0) + M + 273\ cm^{-1} \quad . \qquad (3)$$

The collisional rate constants for de-excitation of $CO_2(00^o1)$ by various molecular additives are summarized in Table II. The rate constant is defined as follows

$$\frac{d}{dt}\ (N_2) = -\ (k_2\ p_M)\ N_2 \qquad (4)$$

where N_2 is the upper laser level number density and p_M is the partial pressure of molecule M.

3. De-Excitation of Lower Laser Level

The lower laser level $CO_2(10^o0)$ must rely upon collisions to provide a sufficiently rapid depopulation rate for the observed laser output. Because of the close proximity in energy, the lower laser level can communicate with the bending mode through a Fermi resonance interaction

$$CO_2(10^o0) + M \rightarrow CO_2(02^o0) + M + 103\ cm^{-1} \qquad (5)$$

$$CO_2(10^o0) + CO_2(00^o0) \rightarrow 2\ CO_2(01^{1}0) + 53\ cm^{-1}\ . \qquad (6)$$

The importance of electron collisions on the excitation or de-excitation of the lower laser level is not known at this time.

The primary role of the gas additives in the CO_2 laser discharge is to assist in depopulating the lower laser level. Table III indicates the effectiveness of various molecules for depopulating the $CO_2(10^o0)$ level. The rate constant is defined as follows

$$\frac{d}{dt}\ \left[N_1\right] = -\ (k_1\ p_M)\ N_1 \qquad (7)$$

where N_1 is the number density of the lower laser level, k_1 is the rate constant per Torr of gas additive, and p_M is the partial pressure of the gas additive.

From Table III it is evident that most of the molecules listed would be effective additives. However, reference to Table I indicates that most of the additives also depopulate the upper laser level as well,

TABLE II

Collisional-Depopulation Rate Constants k_2

$CO_2(00^01) + M \rightarrow CO_2(n_1, n_2, n_3) + M + KE$

Additive	k_2, $sec^{-1} - Torr^{-1}$	Source
CO_2	350	Moore, et al.[1]
	385	Hocker, et al.[3]
He	85	Moore, et al.[1]
H_2	3,840	Moore, et al.[1]
D_2	271	Moore, et al.[1]
H_2O	24,000	Moore, et al.[1]
N_2	106[(a)]	Moore, et al.[1]
	165[(b)]	M. J. Weber and T. F. Deutsch[8]

Resonant-Excitation Rate Constant, k_e'

k_e', $sec^{-1} - Torr^{-1}$	Source
1.7×10^4	Moore, et al.[1]

[(a)] Moore, et al.,[1] observed two exponential decays in their relaxation experiments with CO_2-N_2. They selectively excited the $CO_2(00^01)$ level of a CO_2-N_2 gas sample with a Q-switched CO_2 laser pulse. Following the excitation, $CO_2(00^01)$ molecules rapidly transferred their excitation to ground state N_2. This process resulted in a rapid decay of the $CO_2(00^01)$ level population until the N_2 attained vibrational equilibrium with the CO_2. Subsequently, the $CO_2(00^01)$ and $N_2(v = 1)$ relaxed together at a slower rate, transferring energy to the translational modes. Moore, et al.,[1] have correctly interpreted the two distinct relaxation times to yield values for the resonant excitation rate constant and the collisional-depopulation rate constant due to collision of CO_2 with N_2.

[(b)] Weber and Deutsch[8] have made relaxation rate measurements in the afterglow of a pulsed CO_2-N_2 discharge. They evidently did not observe the initial rapid transfer of energy from $N_2(v = 1)$ to $CO_2(00^00)$ and have erroneously associated the slower decay of $CO_2(00^01)$ with the resonance transfer process. Their experimental data can be reinterpreted, taking into account the equilibrium relaxation between the CO_2 and N_2 vibrational levels, to yield a value for the collisional-depopulation rate of $CO_2(00^01)$ due to collisions with N_2. This rate is presented above.

TABLE III

Collisional-Depopulation Rate Constants, k_1

$CO_2(01'0) + M \rightarrow CO_2(00^0 0) + M + kE$

Additive	k_1, sec^{-1} - $Torr^{-1}$	T ^oK	Source	Discussion
CO_2	188 - 220	300	Cottrell and McCoubrey[9]	a
	2180		Cheo[10]	b
N_2	660	291	Wallman[11]	
CO	66×10^3	273	Metter[12]	c
He	6600	291-293	Cottrell and McCoubrey[9]	
	3400	303	Cottrell and Day[13]	
Xe	< 44	303	Cottrell and Day[13]	
H_2O	44×10^4 - 26×10^3	300-673	Cottrell and McCoubrey[9]	d
D_2O	16×10^4	294	Van Itterbeek and Mariens[14]	
H_2	73×10^3	293	Küchler[15]	

[a] According to Cottrell and McCoubrey[9] this range of values is the most reliable average based on a multitude of ultrasonic measurements by various experimenters.

[b] The rate measured by Cheo[10] is an order of magnitude higher than the ultrasonic measurements. Cheo's data were obtained in the afterglow of a pulsed CO_2 discharge. A 3% concentration of CO (due to dissociation of CO_2) would yield the high value obtained.

[c] Metter's[12] results are open to question because he does not give any details of his experimental work. However, no other data are available.

[d] These results are obtained by various authors and are summarized by Cottrell and McCoubrey. The negative temperature coefficient was obtained by Eucken and Nümann.[16]

which is undesirable. Helium has been determined empirically to be most effective in lasers in depopulating the lower laser level while ignoring the upper laser level. While water vapor has also been shown to behave selectively, there is some question of whether the H_2O is dissociated in the discharge.

4. Role of Helium in the CO_2 Laser Discharge

In addition to its effect on the depopulation rates of the two laser levels (i.e., not interacting with the upper laser level while depopulating the lower laser level), the helium additive performs two other functions. Because of its small mass and large collision frequency, the helium maintains the rotational levels of the CO_2 molecule in thermal equilibrium at the translational temperature of the helium,[17] thereby increasing the gain. Smith and Clark[18] have shown that a large amount of helium can be used without disturbing the electron temperature in the CO_2 laser discharge and hence does not disturb the excitation rate of $N_2(v = 1)$. Helium has this property because of its high lying energy levels which essentially divorce it from the energetics of the discharge.

B. Theory of Gain Saturation

In this section, we treat some questions which arise in choosing equations to describe accurately the amplifier gain saturation. The treatment follows closely that given by Gordon, White, and Rigden[19] with appropriate changes* for the pecularities of the CO_2 system (e.g., the radiative decay terms are replaced by collisional decay terms).

The rate equations for the upper (2) and lower (1) laser levels may be written

$$\dot{N}_2(\nu', z) = C_2'(\nu') - N_2(\nu', z)\left[T_2^{-1} + B_{21}'(\nu', \nu)\, S(\nu, z)/4\pi\right] + N_1(\nu', z)\, B_{12}'(\nu', \nu)\, S(\nu, z)/4\pi \qquad (8)$$

*The notation has also been changed to agree with that used in this report. For those readers familiar with the Gordon, White, and Rigden paper, laser levels "3" and "2" have been replaced by "2" and "1" while S and I now become C and S; the natural linewidth $\Delta\nu_N$ is replaced by the homogeneous linewidth $\Delta\nu_H$ (pressure broadened).

$$\dot{N}_1(\nu', z) = C_1'(\nu') - N_1(\nu', z)\left[T_1^{-1} + B_{12}'(\nu', \nu)\, S(\nu, z)/4\pi\right]$$

$$+ N_2(\nu', z)\, B_{21}'(\nu', \nu)\, S(\nu, z)/4\pi \qquad (9)$$

N_2 and N_1 are the number densities of atoms in upper and lower laser levels in a unit frequency range about a frequency ν' at a plane z along the direction of propagation. (The amplifier input is taken to be $z = 0$). C_2' and C_1' are the creation rates of the upper and lower levels by collisions per unit volume and per unit frequency interval. These collisions are assumed to produce a line with doppler profile of width $\Delta\nu_D$, so that C_2' and C_1' have the form

$$C_i' = \frac{2\sqrt{\ell n 2}}{\sqrt{\pi}\,\Delta\nu_D}\, C_i \exp\left\{-4\ell n 2 \left(\frac{\nu' - \nu_o}{\Delta\nu_D}\right)^2\right\} \qquad (10)$$

where C_i is the total creation rate of the i^{th} level per unit volume and ν_o is the frequency at line center. In eqs. (8) and (9) the times T_2 and T_1 are the collisionally determined lifetimes of upper and lower laser level; $S(\nu, z)$ is the monochromatic signal intensity in W/cm^2 at frequency ν and position z; $B_{ij}(\nu', \nu)$ is the stimulated emission coefficient (in dimensions of probability/molecule/sec/(W/cm^2)/unit frequency interval) giving the rate of simulation from the i^{th} to the j^{th} level of a molecule with doppler shifted frequency ν' by a signal S at frequency ν. The stimulated emission coefficients are assumed to have Lorentzian line shapes with width $\Delta\nu_H$ determined by collisions.

$$B_{ij}'(\nu', \nu) = B_{ij}\, \frac{\left(2/\pi\Delta_H\right)}{1 + \left[2(\nu - \nu')/\Delta\nu_H\right]^2} \qquad (11)$$

where B_{ij} is the more usual B coefficient, the total probability/molecule/sec/(W/cm^2). $\Delta\nu_H$ is essentially the width of the hole that is burned in the doppler broadened line of width $\Delta\nu_D$.

Spontaneous emission processes, with probability rates A_2, A_1, A_{21} have all been ignored in eqs. (8) and (9) since these are much smaller than T_2^{-1}, T_1^{-1}, as discussed in the previous section. (Of course we will not ignore A_{21} when it is used to evaluate B_{21}: $A_{21} = B_{21}\, 2hc/\lambda_o^3$.)

The equation governing the signal amplification is simply

$$\frac{dS(\nu,\ z)}{dz} = h\nu \int_0^\infty \left\{ \left[B'_{21}(\nu',\ \nu)\ N_2(\nu',\ z)\ S(\nu,\ z)/4\pi \right] \right.$$

$$\left. - \left[B'_{12}(\nu',\ \nu)\ N_1(\nu',\ z)\ S(\nu,\ z)/4\pi \right] d\nu' \right\}. \qquad (12)$$

The intergrand in eq. (12) is obtained from the simultaneous solution of eqs. (8) and (9) for the steady state $\dot{N}_2 = \dot{N}_1 = 0$. Equation (12) can then be written in the form

$$\frac{dS}{dz} = \frac{Sk_o}{\pi} \int_{-\infty}^{\infty} \frac{\exp\left[-(\epsilon x)^2\right] dx}{1 + x^2 + S/S_o} \qquad (13)$$

where

$$x = 2(\nu' - \nu_o)/\Delta\nu_H \qquad (14)$$

$$k_o = \frac{h\nu\ B_{21}\sqrt{\ell n 2}}{2\pi^{3/2}\ \Delta\nu_D} \left[C_2T_2 - C_1T_1 \right]$$

$$= \frac{\lambda^2\ A_{21}\sqrt{\ell n 2}}{4\pi^{3/2}\ \Delta\nu_D} \left[C_2T_2 - C_1T_1 \right] \qquad (15)$$

$$S_o = \frac{2\pi^2\ \Delta\nu_H}{B_{21}} \left[T_2 + T_1 \right]^{-1}$$

$$= \frac{4\pi^2\ \Delta\nu_H\ h\nu}{\lambda^2\ A_{21}} \left[T_2 + T_1 \right]^{-1} \qquad (16)$$

$$\epsilon = \frac{\Delta\nu_H \sqrt{\ell n 2}}{\Delta\nu_D} \tag{17}$$

The integration over x (that is, over ν') can be carried out, as in Ref. 19, to yield

$$\frac{dS}{dz} = Sg(S, \epsilon) \tag{18}$$

where

$$g(S, \epsilon) = \frac{k_o}{\left(1 + \frac{S}{S_o}\right)^{1/2}} \left[1 - \mathrm{Erf}\left(\epsilon \left\{1 + \frac{S}{S_o}\right\}^{1/2}\right)\right] \exp\left[\epsilon^2\left(1 + \frac{S}{S_o}\right)\right] . \tag{19}$$

The two familiar cases of pure homogeneous and pure inhomogeneous (Doppler) broadening can easily be derived from eq. (19), as shown in Ref. 19. For a pure doppler broadened line $\Delta\nu_D \gg \Delta\nu_H$, so that $\epsilon \to 0$. In this limit, eq. (19) becomes

$$g(S) = \frac{k_o}{\left(1 + \frac{S}{S_o}\right)^{1/2}} . \tag{20}$$

At the opposite extreme, the case of a pure homogeneously broadened line $\Delta\nu_H \gg \Delta\nu_D$ requires $\epsilon \to \infty$, so that we have

$$g(S) = \frac{k_o \Delta\nu_D/\Delta\nu_H \sqrt{\pi \ell n 2}}{1 + \frac{S}{S_o}} . \tag{21}$$

Even though $\Delta\nu_D \to 0$, the product $k_o \Delta\nu_D$ remains finite. Using expression (15) for k_o,

$$g(S) = \frac{\frac{\lambda^2 A_{21}}{4\pi^2 \Delta\nu_H}\left[C_2T_2 - C_1T_1\right]}{1 + \frac{S}{S_o}} \,. \qquad (22)$$

For a typical CO_2 laser, $\Delta\nu_D \approx \Delta\nu_H$ so that neither limiting case applies exactly; however, the homogeneous interaction limit represents a closer approximation if a simple form is desired for the gain expression. We will base our further calculations on that approximation and assume that the gain has the form

$$g(z) = \frac{g_o}{1 + \frac{S(z)}{S_o}} \,, \qquad (23)$$

where g_o is the numerator given in eq. (22).

The quantities g_o and S_o thus specify the behavior of the gain and control the design of the device. Both quantities must be measured accurately under optimum conditions before a realistic design can be realized. The expressions given in eqs. (16) and (22) in terms of fundamental constants are accurate, of course, but the quantities $\Delta\nu_H$, $C_{1,2}$, $T_{1,2}$ depend rather critically on discharge conditions. Nevertheless, it is interesting to try to estimate g_o and S_o from eqs. (16) and (22) for later comparison with experiment. If we take

$$\lambda = 10.6\ \mu$$

$$A_{21} = 0.25\ \text{sec}^{-1}\ \text{(Ref. 5)}$$

$$\Delta\nu_H = 50\ \text{mHz}$$

$$T_2 = 0.3\ \text{msec}$$

$$T_1 < 30\ \mu\text{sec} \ll T_2$$

$$C_1 \ll C_2 \,.$$

Then,

$$S_o = 0.44 \text{ W/cm}^2 \tag{24}$$

and

$$g_o = [4.25 \times 10^{-20} C_2]\,\text{cm}^{-1} . \tag{25}$$

We do not know the excitation rate C_2, but we may estimate it from the specific power output typical of CO_2 lasers. Statz, et al.,[5] have taken 0.25 W/cm^3 as an experimental power generation rate. Our experimental values obtained with CO_2 oscillators are consistent with this number. To achieve this rate, C_2 must be at least

$$C_2 > \frac{0.25 \text{ W/cm}^3}{h\nu} \approx 1.3 \times 10^{19} \text{ cm}^{-3} \text{ sec}^{-1} \tag{26}$$

which would imply a small signal gain of

$$g_o = 0.55 \text{ cm}^{-1} . \tag{27}$$

Experimentally, we find $g_o(\text{dB}) \approx 3 - 5$ dB/m, or

$$g_o \approx 0.01 \text{ cm}^{-1} \tag{28}$$

which would imply a pump rate 50 times lower than that given by eq. (26). The difficulty apparently lies in the fact that the several rotational levels are closely coupled together. Equation (26) gives the gain of a single rotational level in terms of the pumping rate to that particular level in the absence of oscillation; that is the way in which C_2 is defined. However, eq. (26) estimates the total equivalent pumping rate to all rotational levels, whether all are oscillating independently or all are feeding a single oscillating level by collisional cross relaxation. To account properly for the cross relaxational pumping of the upper laser level, we should return to the rate equations (writing M simultaneous equations

for the M rotational transitions) and include the coupling terms. This procedure was followed in analyzing the effect of coupled levels for the case of pure homogeneous broadening and infinitely rapid lower level relaxation in Appendix B of our Proposal No. 66M-7374/B1560. That work is also included here as Appendix B. Under the approximation that the rotational levels are uniformly populated, the net result is to increase the pump rate of the oscillating level by M and increase the saturation flux for that level by M.

This result can also be obtained by argument from the present analysis if we associate M with $\Delta\nu_H$, the "hole" width, $\Delta\nu_H$ physically represents the width, in frequency, over which a signal taps population. If M levels relax into one lasing level, the effect is the same as increasing $\Delta\nu_H$ to $M\Delta\nu_H$, at least for the homogeneously broadened line. From eq. (22) we see that for the same pump rate C_2 into the lasing level, an increase of $\Delta\nu_H$ to $M\Delta\nu_H$ makes the appropriate correction to the gain, and from eq. (16) the appropriate increase to S_o. Comparison of eqs. (27) and (28) would indicate a value of $M \approx 50$ (which may seem a bit large until we recall that there are certainly this many rotational levels with significant populations, even if they are not inverted enough to oscillate). A factor of 50 for M would imply an S_o of ≈ 20 W/cm^2. Actually, larger values than this have been observed by Kogelnik and Bridges (ref. 20) and by ourselves (see Section III).

As a sidelight, we can compare the results of the analysis given in Appendix B with that of this section to clarify the terminology. Equation B-6 (using z instead of x) states that

$$\frac{d\mu}{dz} = \frac{\mu\sigma Wn_o}{\frac{1}{\tau} + \sigma\mu} \tag{29}$$

where μ is the photon flux, Wn_o the pump rate, σ the stimulated emission cross section and τ the upper level relaxation time. Identifying $Wn_o \equiv C_2$, and $S = h\nu\mu$, $\tau \equiv T_2$ we obtain

$$\frac{dS}{dz} = \frac{S\sigma(C_2T_2)}{1 + \frac{S}{\left(\frac{h\nu}{\sigma\tau}\right)}} \tag{30}$$

evidently

$$\sigma = \frac{\lambda^2 A_{21}}{4\pi^2 \Delta\nu_H} \tag{31}$$

and

$$S_o = \frac{h\nu}{\sigma\tau} \tag{32}$$

which is obviously true by comparison with eqs. (22) and (16).

C. Solution of the Gain Saturation Equation

In the previous section we discussed the theory of gain saturation and some of the restrictions and uncertainties concerning assumptions of the proper interaction and use of the proper form of equation. Acknowledging those restrictions and uncertainties, we choose the case of pure homogeneous interaction as a first model for gain saturation computations and laser design; the governing equation is

$$\frac{dS(z)}{dz} = \frac{g_o S(z)}{1 + \frac{S(z)}{S_o}} \quad . \tag{33}$$

If S(z) is the intensity of an infinitely broad plane wave passing through a laser of length L, eq. (33) can be integrated directly to yield the over-all gain G.

$$G = \exp\left[g_o L - \frac{S_{in}}{S_o}(G - 1)\right] \tag{34}$$

where S_{in} is the input intensity (W/cm^2). Unfortunately, the solution given by eq. (34) is not explicit in G. While it is easy to solve this transcendental equation for G numerically by trial and error, it is even easier to integrate eq. (33) numerically on a small computer with S_{in} as the initial condition and obtain S_{out} and the gain as outputs.

The use of a small computer is even more strongly recommended if S(z) is not the intensity of a plane wave, but has instead a radial intensity distribution – for example, that of a Gaussian beam spreading by diffraction. That is,

$$S(r, z) = S_1 \exp\left[-2(r/w(z))^2 \right] \tag{35}$$

$$w^2(z) = w_o^2 \left[1 + \left\{ \frac{\lambda (z - z_o)}{\pi w_o^2} \right\}^2 \right] , \tag{36}$$

where w_o is the beam radius at the $(1/e^2)$ intensity point and z_o is the position of the waist. Equations (35) and (36) are, of course, the equations governing the propagation of a gaussian beam through a linear medium (e.g., free space); saturation in the amplifier must change the functional form of S(r, z). The problem may be further complicated if g_o or S_o are themselves functions of the radial coordinate r. In any case, a closed-form solution of eq. (33), including radial dependencies, is not generally possible.

We have elected to solve simplified models first rather than tackle the complete self-consistent system. The solutions are easier to obtain and they serve as guides for the amplifier design effort. Different mathematical models are constructed to answer specific questions relative to the design:

- How does the diffraction beam spread affect the design?
- How do g_o and S_o affect the over-all performance of an amplifier?
- How is the beam distorted in a saturable amplifier?

Some first order answers are given in the remainder of this section.

1. Effect of Beam Expansion

To estimate the effect of the beam expansion on the gain saturation, we simplify our model by ignoring the change in radial distribution with z. We assume that instead of a gaussian distribution, the radial distribution is uniform over an area A(z) [but which expands like the gaussian beam, eq. (36)]

$$A(z) = \frac{\pi w^2(z)}{2} = \frac{\pi w_o^2}{2}\left[1 + \left\{\frac{\lambda(z - z_o)}{\pi w_o^2}\right\}^2\right] . \qquad (37)$$

The factor of 1/2 on the right hand side arises from the requirement that the total power in this uniformly-distributed beam be equal to the power in the gaussian beam (at least at the input to the amplifier z_o, where the Gaussian is yet undistorted). That is,

$$\int_o^\infty S_{in} \exp\left[-2(r/w(o))^2\right] 2\pi r dr \equiv S_{in} A(0) . \qquad (38)$$

The distributions are compared in Fig. 2.

With this approximation, eq. (33) is easily integrated numerically. The method of solution and typical programs are described in Appendix C. Several variations on the basic program have been used to generate specific outputs. The input parameters specified or generated are

(1) beam waist diameter, w_o

(2) position of the beam waist with respect to input end of the amplifier, z_o

(3) small-signal gain coefficient, g_o

(4) saturation flux, S_o

(5) length of tube, L

(6) input power, P_{in} .

Two of the last four parameters are redundant; only the product $g_o L$ and the ratio $P_{in}/S_o A(0)$ must be specified. For design purposes, however, it is convenient to list these parameters explicitly. The output of a typical program consists of the power output at L and the gain at L (and possibly the power and gain at several intermediate points between $z = 0$ and $z = L$).

Figure 3 shows the results of beam expansion for a particular tube. The parameters chosen are appropriate to the 16 m intermediate amplifier described in Section IV. They are:

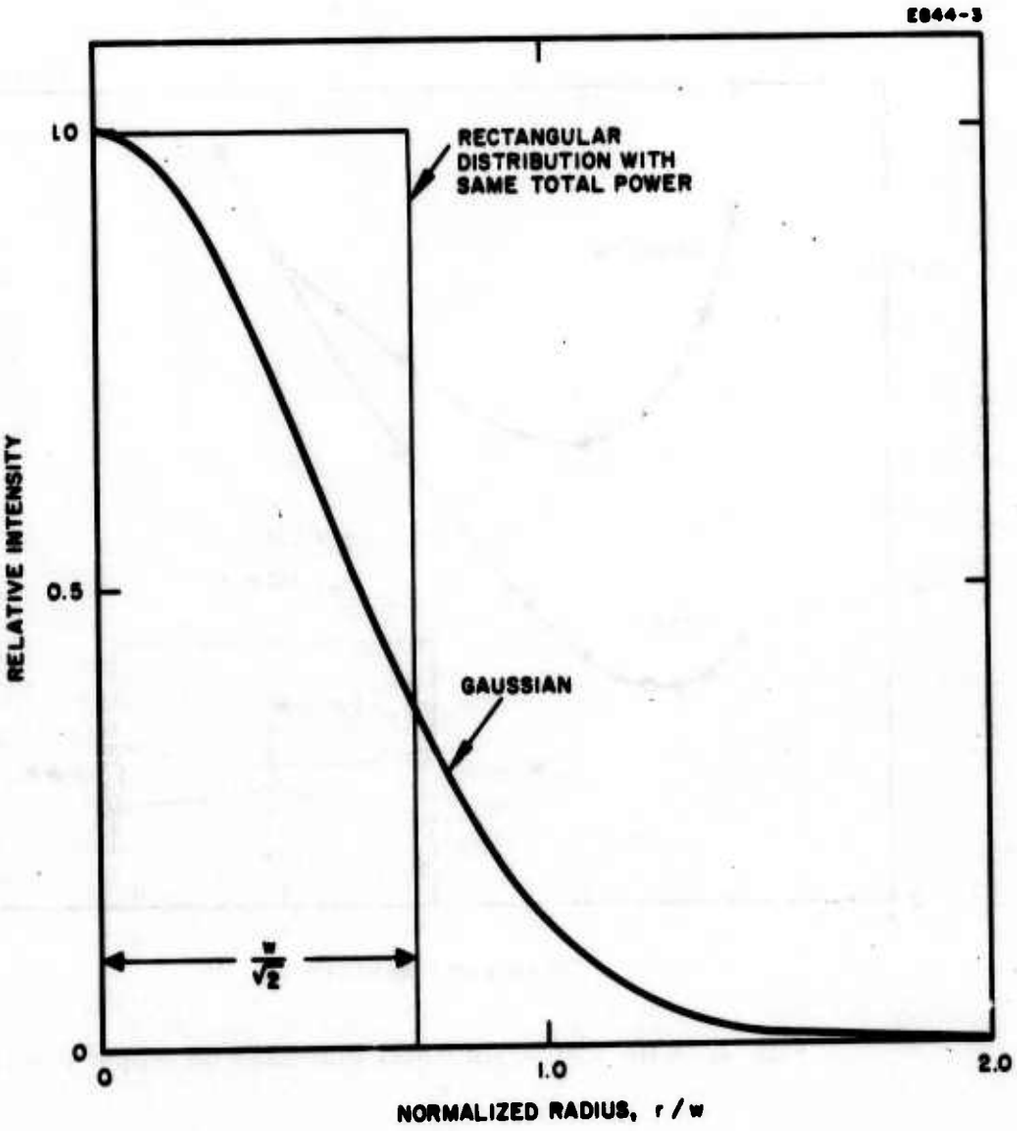

Fig. 2. Comparison of gaussian and rectangular distributions containing the same total power.

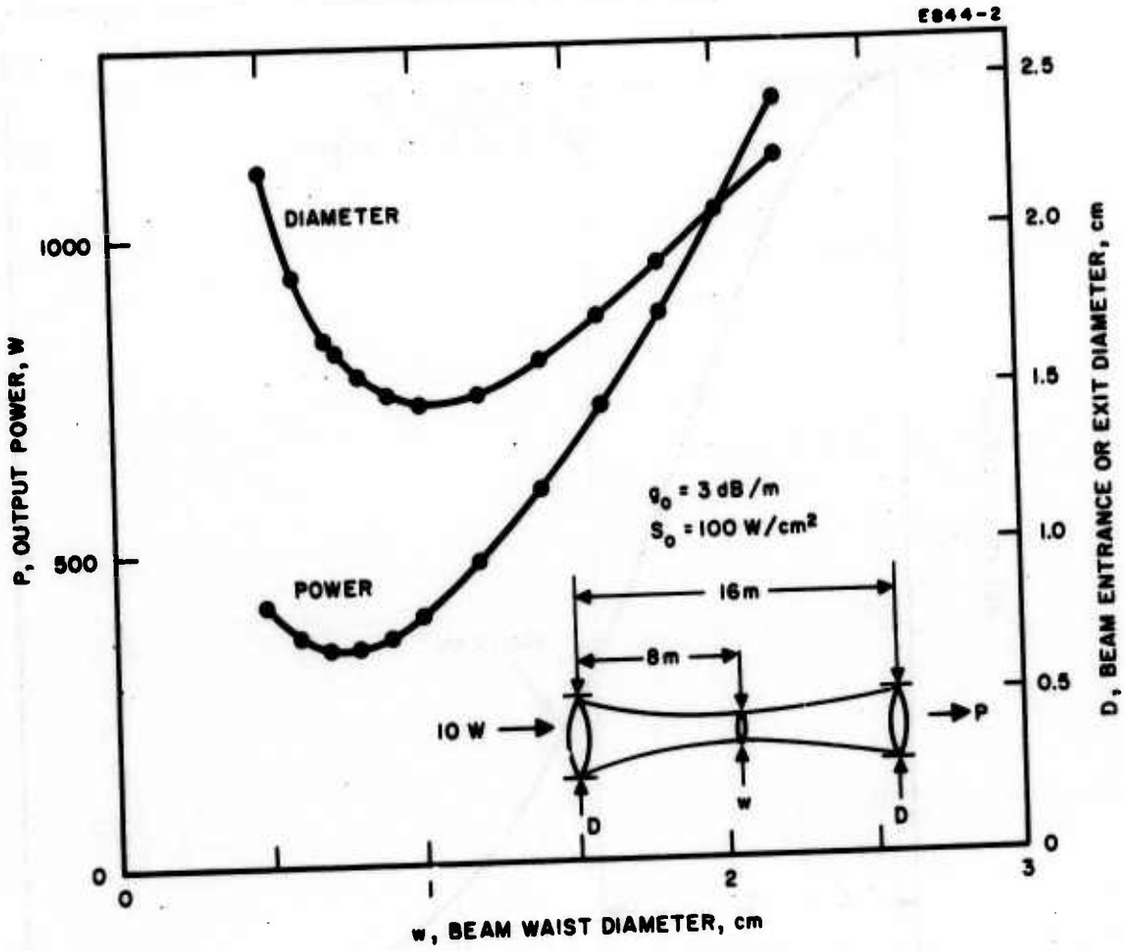

Fig. 3. Effect of beam waist diameter on output power.

$$z_o = 8 \text{ m}$$

$$g_o = 3 \text{ dB/m}$$

$$S_o = 100 \text{ W/cm}^2$$

$$L = 16 \text{ m}$$

$$P_{in} = 10 \text{ W}.$$

The output power and exit beam diameter are plotted as a function of the beam waist diameter. It is obvious from the curves (and intuitively obvious) that we would wish to operate the largest possible beam waist (for the example given $(2w_o)_{max} \approx 2$ cm, since the values of g_o, S_o are appropriate to a 1 in. diameter tube). Figure 2 shows the drastic reduction in performance (from 1000 W output to 330 W output) that could occur with improper focusing of the collimating optics to produce a beam waist of ≈ 0.7 cm instead of ≈ 2 cm.

2. Effect of g_o and S_o on Amplifier Design

The small signal gain g_o and the saturation flux S_o are, of course, the main controlling parameters of the amplifier design. As an example, Fig. 4 shows the change in the gain saturation curves for a particular amplifier (the 16 m intermediate amplifier described in Section IV) as the small-signal gain is varied. The curves are plotted as (G - 1) dB versus input power in dB above a 1 W reference (dBW). (G-1) rather than G is used in order to exhibit the (- 1) slope of the curves in the saturated region. Figure 5 shows the gain and power output for the same tube, with 10 W input (+ 10 dBW) as a function of g_o. For a g_o of 3 to 4 dB/m (the experimentally determined range of values for a 1 in. diameter (see Section III)), $G \approx 18$ to 20 dB and $P_{out} = 700$ to 1000 W (provided, of course, $S_o = 100$ W/cm^2).

Figure 6 shows the effect of S_o on the gain saturation for the same tube, with $g_o = 3$ dB/m. In this case, the curves are identical in shape, but simply translated in ordinate (i.e., the solution depends only on the ratio S_{in}/S_o). Because of the high over-all gain (48 dB), the small signal portion of the curves occurs off the graph for the range of input powers shown (0.01 W to 1 kW). Figure 7 shows the gain and power output for the same tube with an input power of 10 W. Power outputs of 400 to 600 W are expected with S_o in the experimentally determined range of 60 to 90 W/cm^2 (see Section III) (provided, of course, $g_o = 3$ dB/m).

Many sets of curves could be computed and used for amplifier design. Instead, we prefer to work out the design step by step using the computer on-line. Examples of designs using this procedure are given in Section IV and in Appendix C (reduction of Kogelnik and Bridges' results[20]).

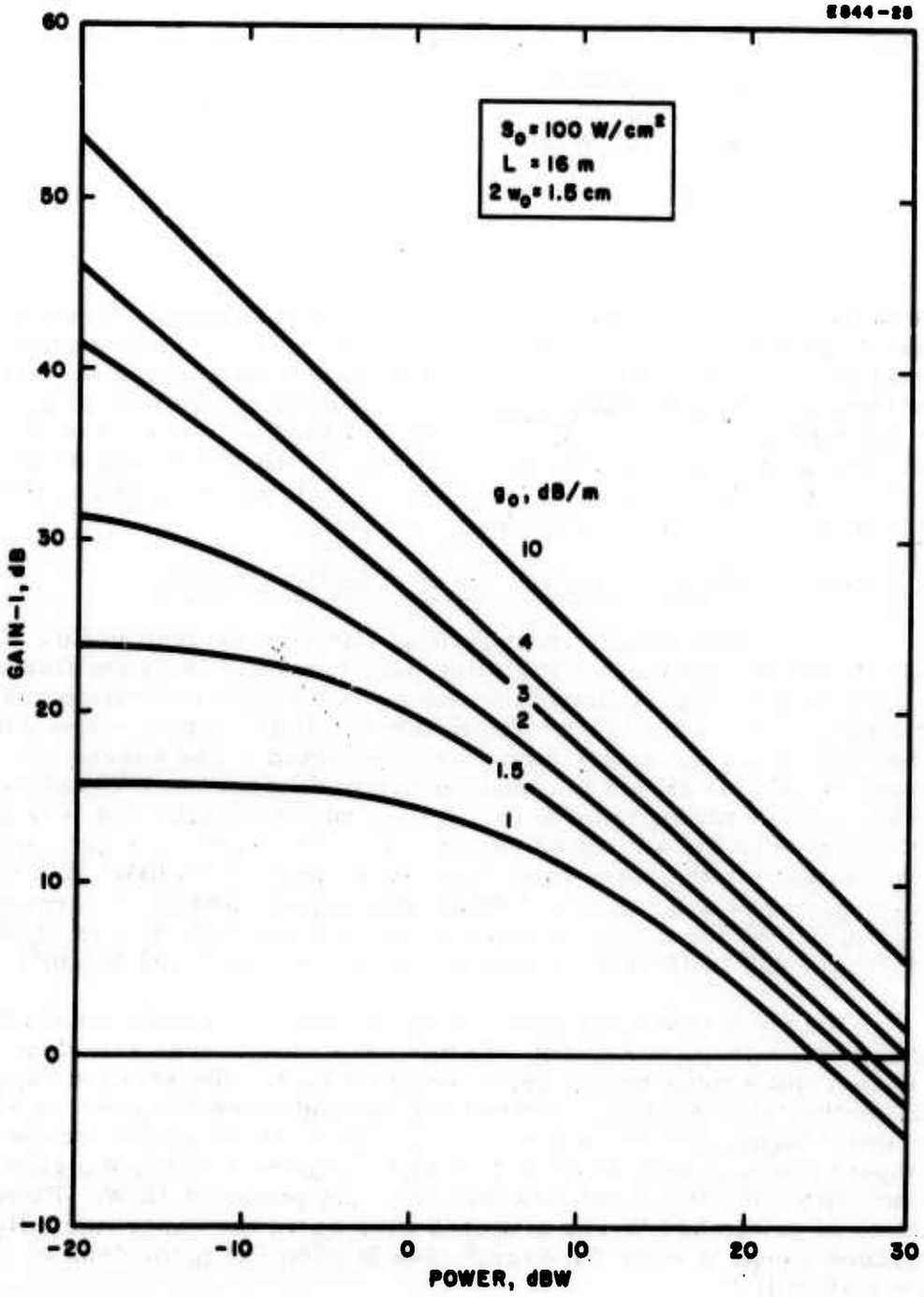

Fig. 4. Gain saturation curves with g_o as the parameter.

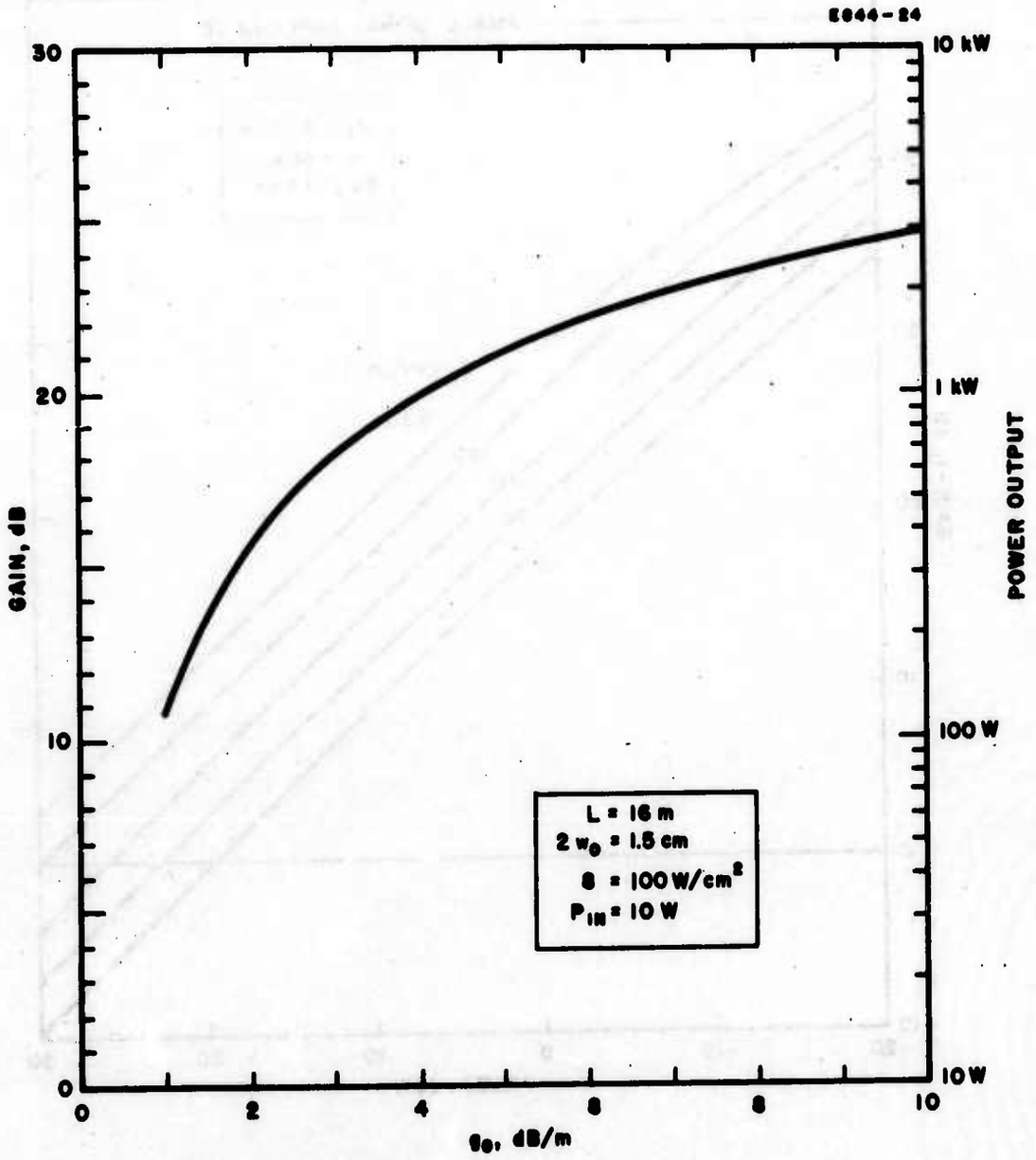

Fig. 5. Power output from 16 m amplifier as a function of small-signal gain.

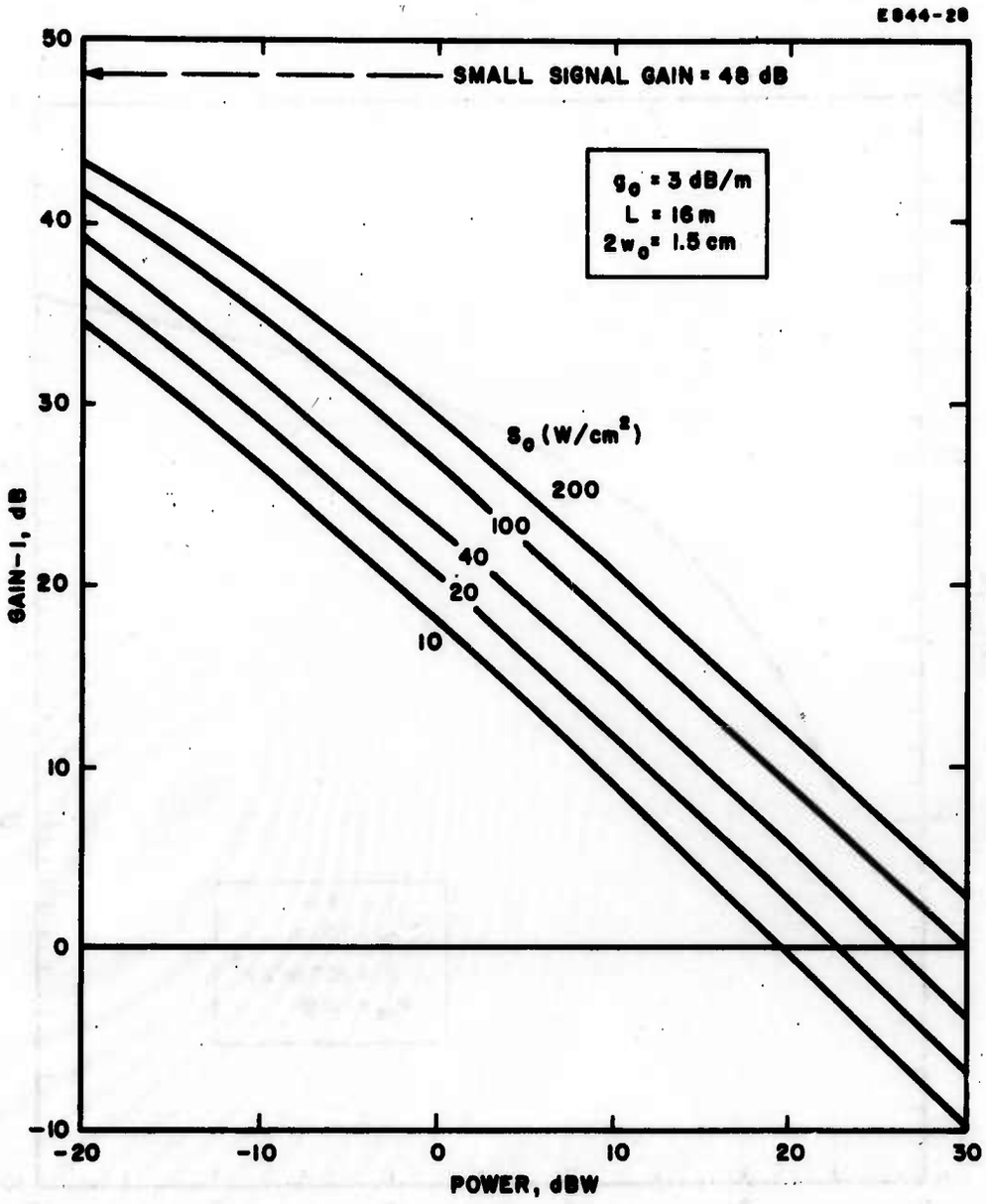

Fig. 6. Gain saturation curves with S_o as the parameter.

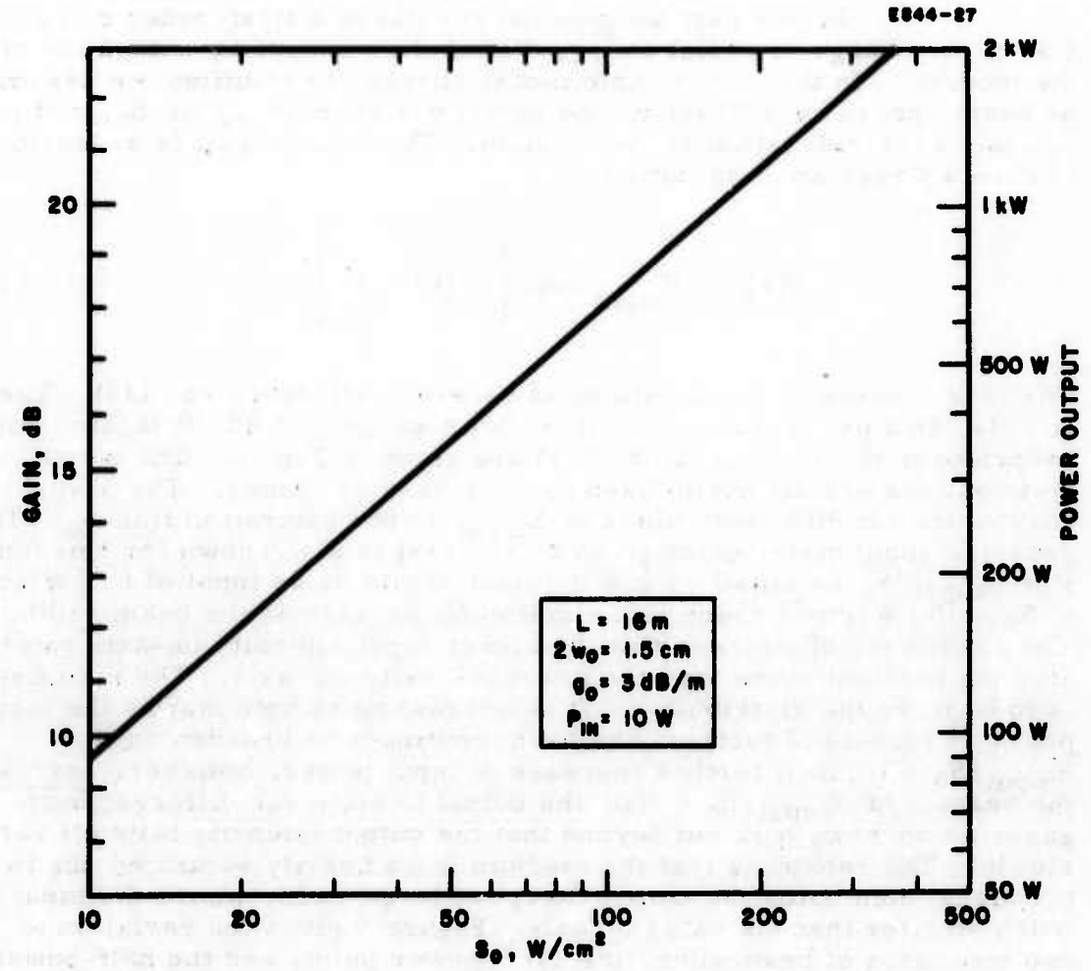

Fig. 7. Power output from 16 m amplifier as a function of the saturation flux density.

3. The Effect of Saturation on Radial Distribution

In this part we give the results of a first-order calculation of the change in radial energy distribution caused by saturation of the medium. In the very simple model chosen for solution, we assume no beam spread by diffraction, no radial variation of g_o or S_o, and no spatial cross-relaxation of the medium. The input signal is assumed to have a Gaussian distribution

$$S(r) = S_{input} \exp\left[-2(r/w_o)^2\right] \tag{39}$$

The output intensity is calculated at several radii using eq. (33). The results for a particular tube with an over-all gain of 48 dB (again, appropriate to the 16 m preamplifier) are given in Fig. 8. The output distributions are all normalized to their on-axis values. The several curves are for different values of S_{input} to the saturation flux S_o. The gaussian input distribution given by eq. (39) is also shown for reference. For S_{input}/S_o as small as 0.001 (which would be an input of 0.1 W/cm^2 if $S_o \approx 100$ W/cm^2) there is a significant increase in the beam width. The reason is, of course, that the higher input intensity on-axis saturates the medium more than the lower intensity off-axis. The net effect is to broaden the distribution. It is interesting to note that as the input power is increased further, the beam continues to broaden until $S_{input}/S_o \approx 1$. Still further increase in input power, however, narrows the beam. At $S_{input}/S_o = 100$, the output is not much different from gaussian to $r/w_o \approx 1$, but beyond that the output intensity falls off very slowly. The reason is that the medium is so heavily saturated the input signal dominates the output except at large radii, where the input is much smaller than its value on axis. Figure 9 gives the variation of two measures of beamwidth, the $1/e^2$ power point, and the half-power point as a function of signal power. The beam is largest at its half-power point when $S_{input} \approx S_o$, while the maximum radius to the $1/e^2$ points occurs at a somewhat higher input power (the computer program, ONR 9, described in Appendix C was only run out to $r/w_o = 2$). Figure 10 shows the same kind of result for a lower gain tube. The value 11.1 dB is appropriate to the 3.7 m tube on which the saturation measurements described in Section III-B were made. The effect is much smaller for this lower gain value, and was not actually observed in the 3.7 m tube. The saturation measurements were made with a maximum S_{input}/S_o of -7 dB, so that we were not at the peak of the spread; the values given by Fig. 10 for -7 dB would be about equal to our experimental error in determining beam profile.

It is clear that the beam spreading in the 48 dB tube caused by saturation cannot be neglected. According to Fig. 9, a 10 W input in a 1 cm diameter beam with $S_o \approx 100$ W/cm^2 will produce a 2x beam spread;

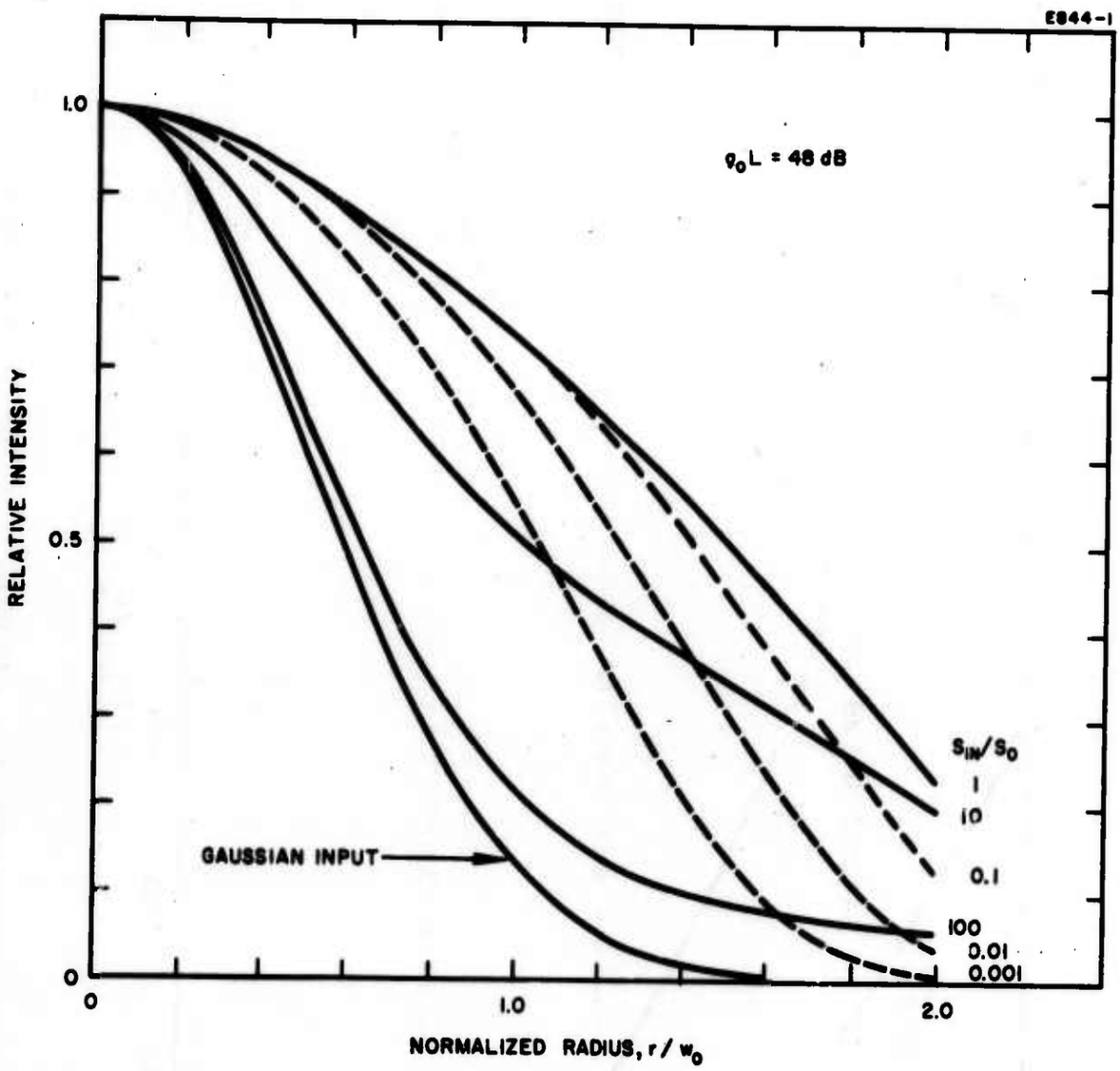

Fig. 8. Change in radial beam profile with saturation.

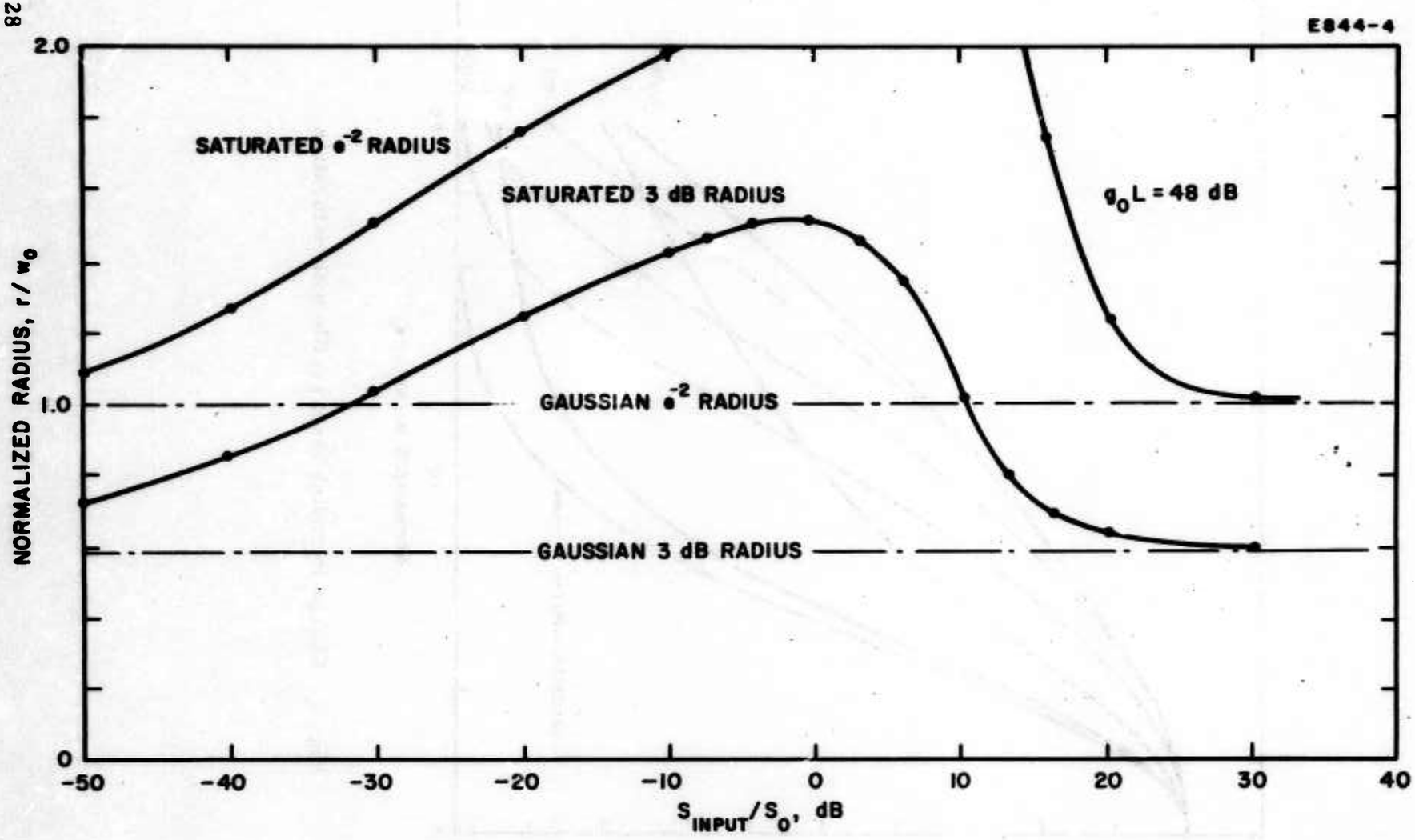

Fig. 9. Variation of beam width with input power for the 16 m amplifier.

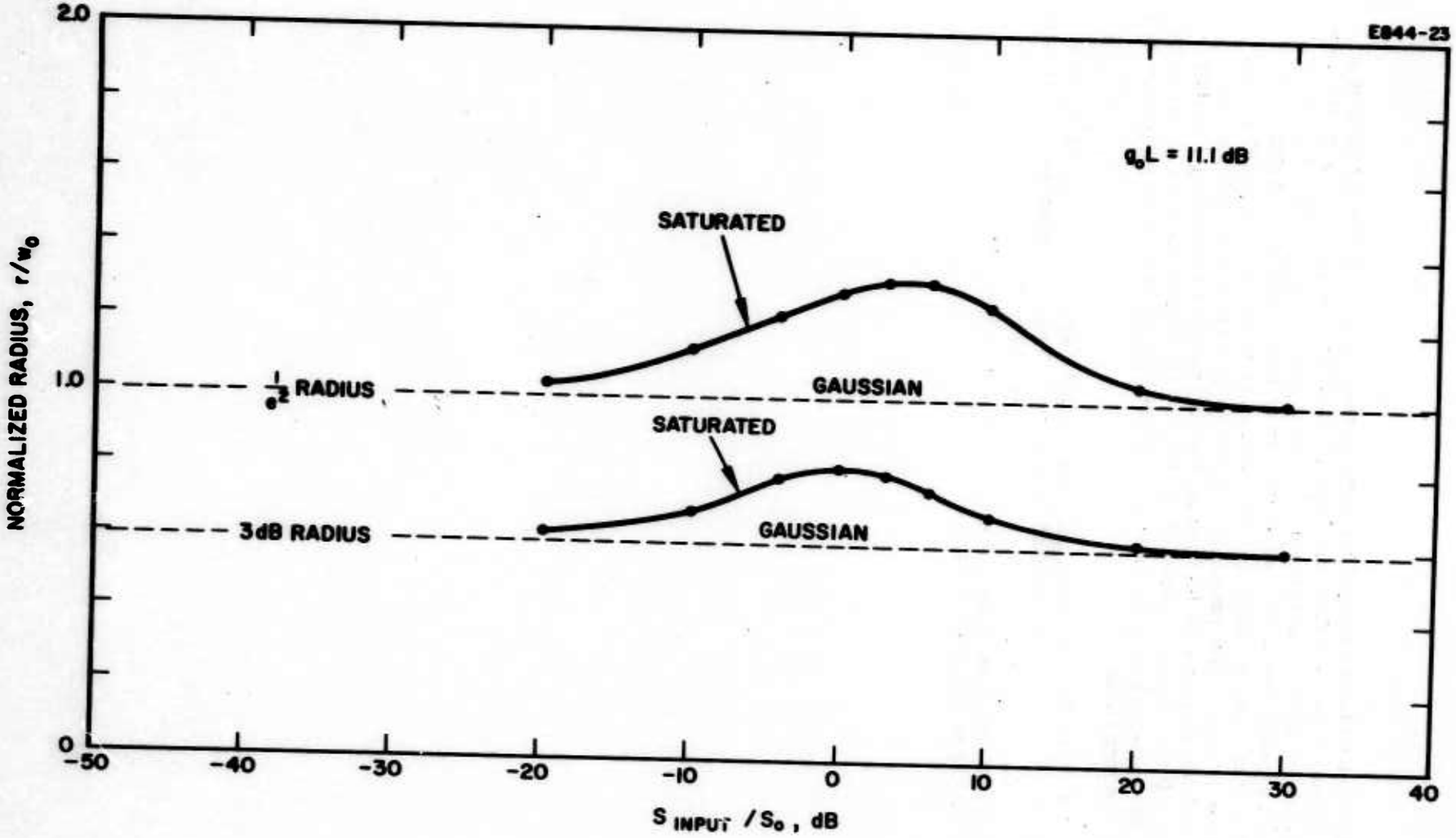

Fig. 10. Variation of beam width with input power for the 3.7 m amplifier.

this amount added to the diffraction spread may require the use of a bore diameter larger than anticipated in order to get the beam through the amplifier without interception. Compensating for the additional spread by prefocusing the wavefront may prove difficult since it is doubtful that simply "adding" the two beam spreads will yield a very accurate result. The problem should be solved again, taking into account both saturation distortion and diffraction spreading simultaneously. If the simple model chosen here for calculation is at all correct, the effect should be readily measurable in the 16 m amplifier now under construction.

We should also note that any radial variation in g_o or S_o will certainly change the degree of distortion. These variations are easily added to the computer program, and some estimate of the magnitude of these effects will be made, even though measurements of $g_o(r)$ and $S_o(r)$ have not yet been made.

III. PARAMETER MEASUREMENTS

A. Small Signal Gain Measurements

Small-signal gain measurements were initially made on a 20 mm diameter by 60 cm long discharge. The experimental apparatus is described in the schematic shown in Fig. 11. A low power, single-frequency 10.6 μ source laser was collimated with a 10:1 off-axis reflecting telescope. (The characteristics of the single frequency source are described in Appendix D.) The source beam was modulated with a rotating chopper and after traversing the amplifier section the signal was measured with a liquid-helium-cooled Ge:Cu detector. A 10.6 μ band pass filter was necessary to block the strong spontaneous signals between 4 to 5 μ occurring at higher pulsed currents. A portion of the incident beam was extracted through a beam splitter and was monitored continuously with a grating monochromator. Brewster's angle NaCl windows were used on the amplifier test section. The small-signal gain characteristics of the amplifier were measured as a function of gas mixture, pressure, and flow rate, peak discharge current, current duration, and current pulse repetition rate.

1. CW Discharge

The optimum cw small-signal gain in the 20 mm diameter tube occurred with flowing gas mixtures of $2CO_2 + 3N_2 + 5He$ at a total static pressure of 10 Torr. The unsaturated gain as a function of discharge current is shown in Fig. 12. Although it is not shown in Fig. 12, the gain decreases at $I > 100$ mA. For maximum efficiency in a saturated amplifier we wish to operate on the low current side of the optimum point. The value of $g_o \gtrsim 3$ db/m is in good agreement with the measurement of Kogelnik and Bridges.[20]

The variation of cw unsaturated gain with gas flow rate is illustrated in Fig. 13. The data show that g_o increases with increasing flow rate, but increase at a diminishing rate above about 0.1 cfm (STP).

2. Pulsed Discharge

Gain measurements on the 20 mm tube operated with a pulsed discharge were made by synchronizing the current pulse with the "on" time of the chopped signal source. (It was desirable to modulate the signal source so that an absolute zero-signal level could be established.) Typical detector signals are shown in Fig. 14. In these oscillograms, the upper trace is the detector signal, the middle trace is the amplifier discharge current, and the lower trace is the amplifier discharge voltage. The gain is then the ratio of the peak value during the current pulse to the pedestal value, as scaled from the oscilloscope photographs.

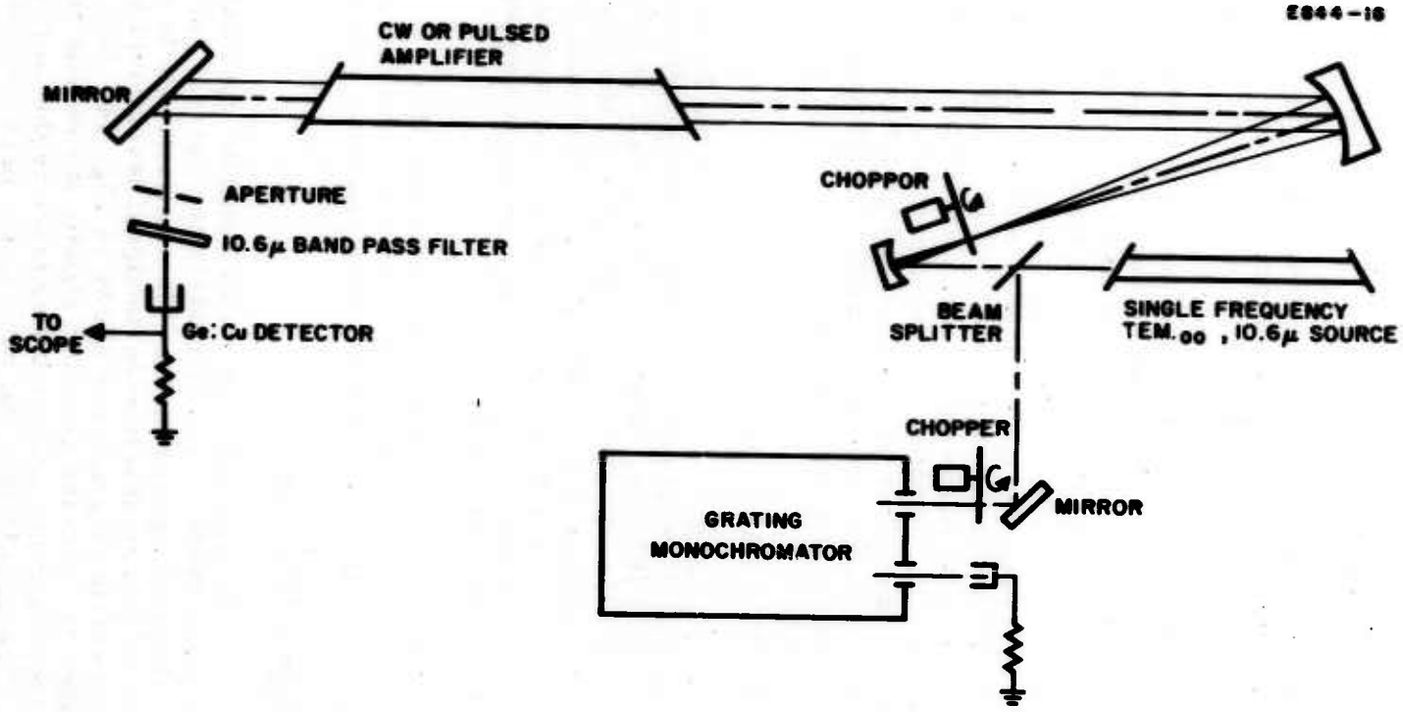

Fig. 11. Small signal gain measurement arrangement.

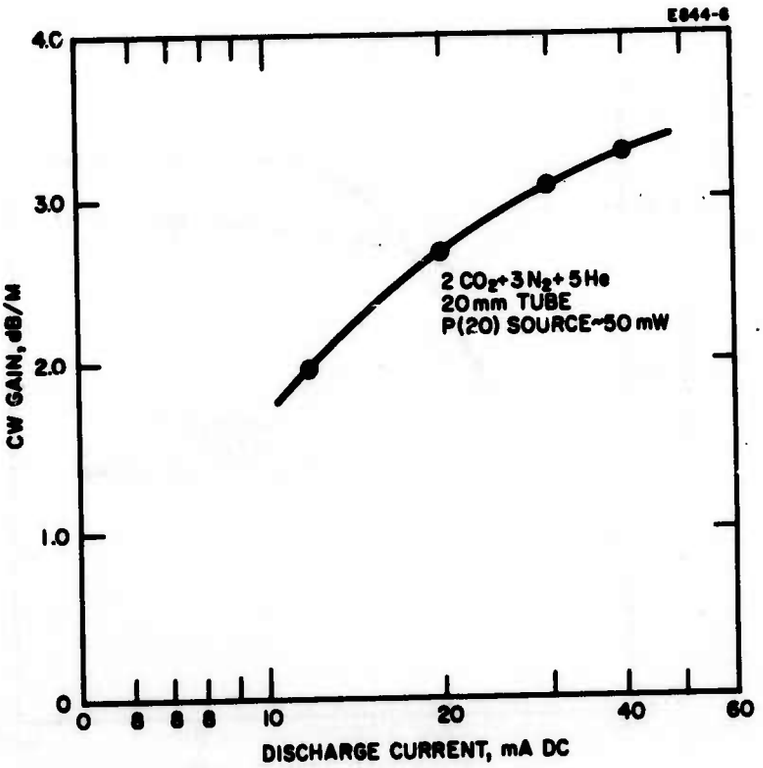

Fig. 12. Small signal gain versus discharge current for a cw discharge.

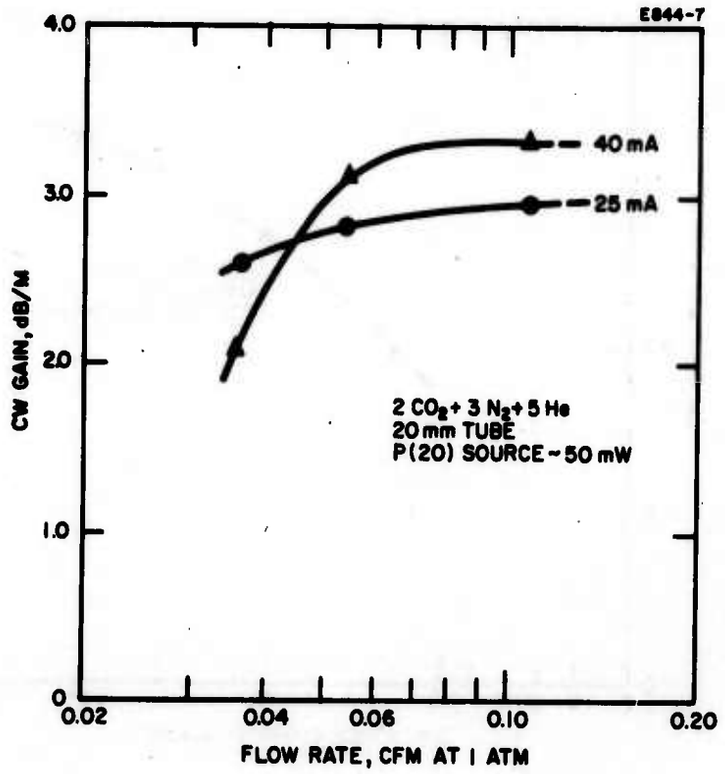

Fig. 13. Small signal gain versus gas flow rate.

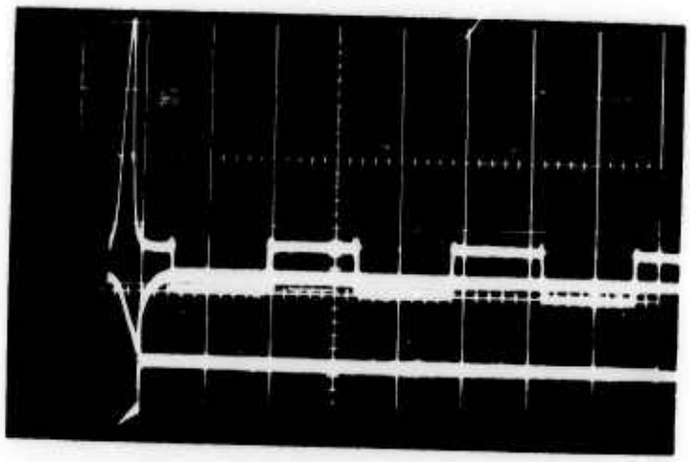

(a) 1000 μsec current pulse duration

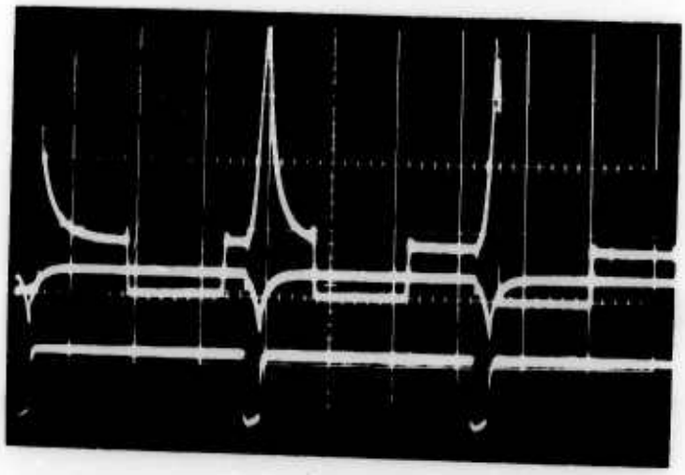

(b) 500 μsec current pulse duration

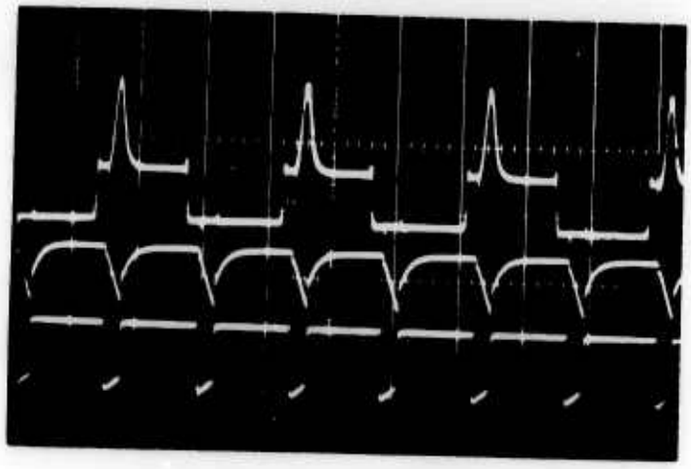

(c) 500 μsec current pulse duration

Fig. 14. Oscilloscope photographs for pulsed gain measurements. The upper trace in each photograph is the output, the middle trace is the discharge current, and the lower trace the discharge voltage. The time scale is 2 msec/div. The pulse repetition rate increases from (a) to (c). The amplifier contains a flowing gas mixture of $4CO_2 + 1N_2 + 4He$.

The variation of g_o with pressure, mixture, flow rate, etc., is somewhat more complicated in the pulsed discharge case. Different processes enter in with changing importance depending on the pulse duration time and repetition rate. For this reason, we give some explanation of these processes as determined from the pulsed gain data before giving the data on g_o itself.

When the amplifier is excited with a short current pulse ($\approx$ 10 μsec), the resulting time variation of the gain gives a measure of the excitation and de-excitation processes involved in the CO_2 gain mechanism. Figure 15 shows the time variation of the gain on the P(16) transition following a 10 μsec current pulse. Photograph (a) occurred with a pure CO_2 discharge at 4 Torr, (b) for a flowing mixture of $2CO_2 + 3N_2 + 1He$ and (c) for $2CO_2 + 3N_2 + 7He$. The time scale is 500 μsec/div. The lower trace of each pair is the discharge current pulse. The results of many photographs are summarized in Fig. 16. For pure CO_2, both the rise time and decay time of the gain pulse decrease with increasing CO_2 pressure. This is in agreement with the mechanism model in which the rise of the gain pulse is determined by the collisional de-excitation time of the lower laser level, and the decay of the gain pulse is determined by the collisional de-excitation time of the upper laser level. The addition of helium to a $2CO_2 + 3N_2$ mixture does not affect the gain pulse rise time and causes an increase in the gain pulse decay time. Both of these latter observations are in disagreement with Cheo's results (Section II-A). (However, Cheo found that the exponential time constant, not the time to reach peak gain, decreased with increasing helium pressure.) A possible explanation for the lengthened gain pulse with helium pressure is that the increased heat conductivity of the gas with helium added can reduce the net thermal population rate of the lower laser level following the current impulse. This would allow the gain to persist for a longer time.

The variation of small-signal gain with current pulse duration is illustrated in Fig. 17. For the data in this figure the gas mixture and flow rate were the same as those used in the cw measurements (Fig. 2); these values are not optimum for pulsed operation, however. The discharge was pulsed at 60 pps. It is evident that the magnitude of the peak gain is highly dependent upon current pulse duration. Figure 18 shows similar results with an approximately optimum gas mixture and pressure ratio for pulsed operation. The peak gain is substantially increased with amplifier current pulse durations greater than 100 μsec; values of $g_o \approx 13$ dB/m were obtained with 1000 μsec pulses.

Small-signal gain data were also taken for non-optimum gas mixtures to obtain information on excitation mechanisms. The results are summarized below.

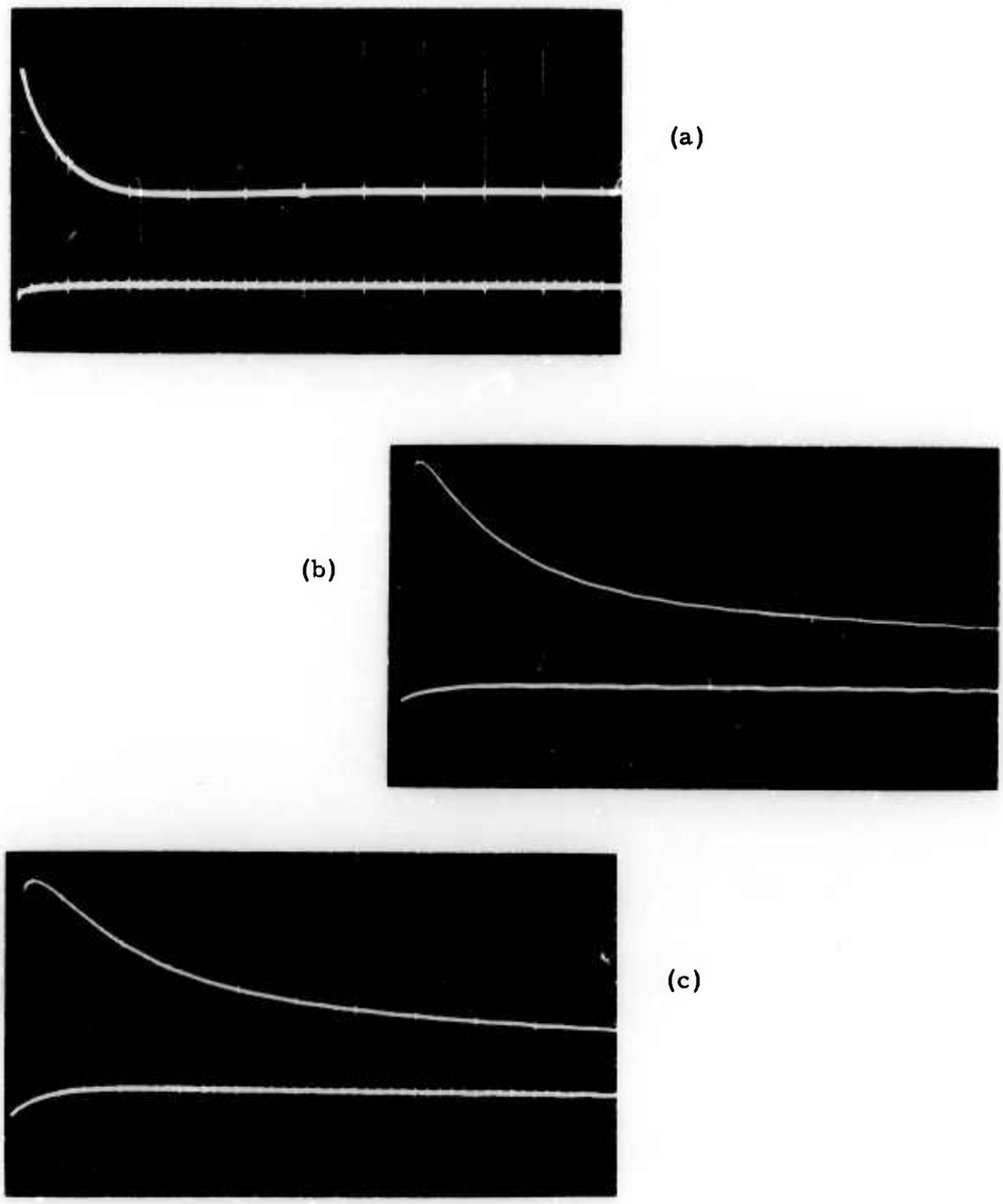

Fig. 15. Time variation of gain for (a) pure CO_2, (b) $2CO_2 + 3N_2 + 1He$, and (c) $2CO_2 + 3N_2 + 7He$.

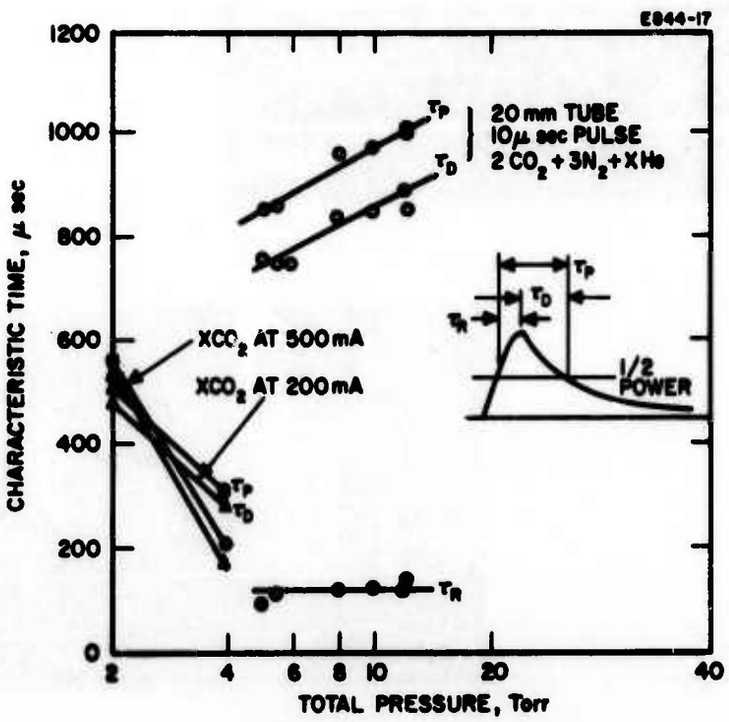

Fig. 16. CO_2 molecular decay time as a function of gas pressure.

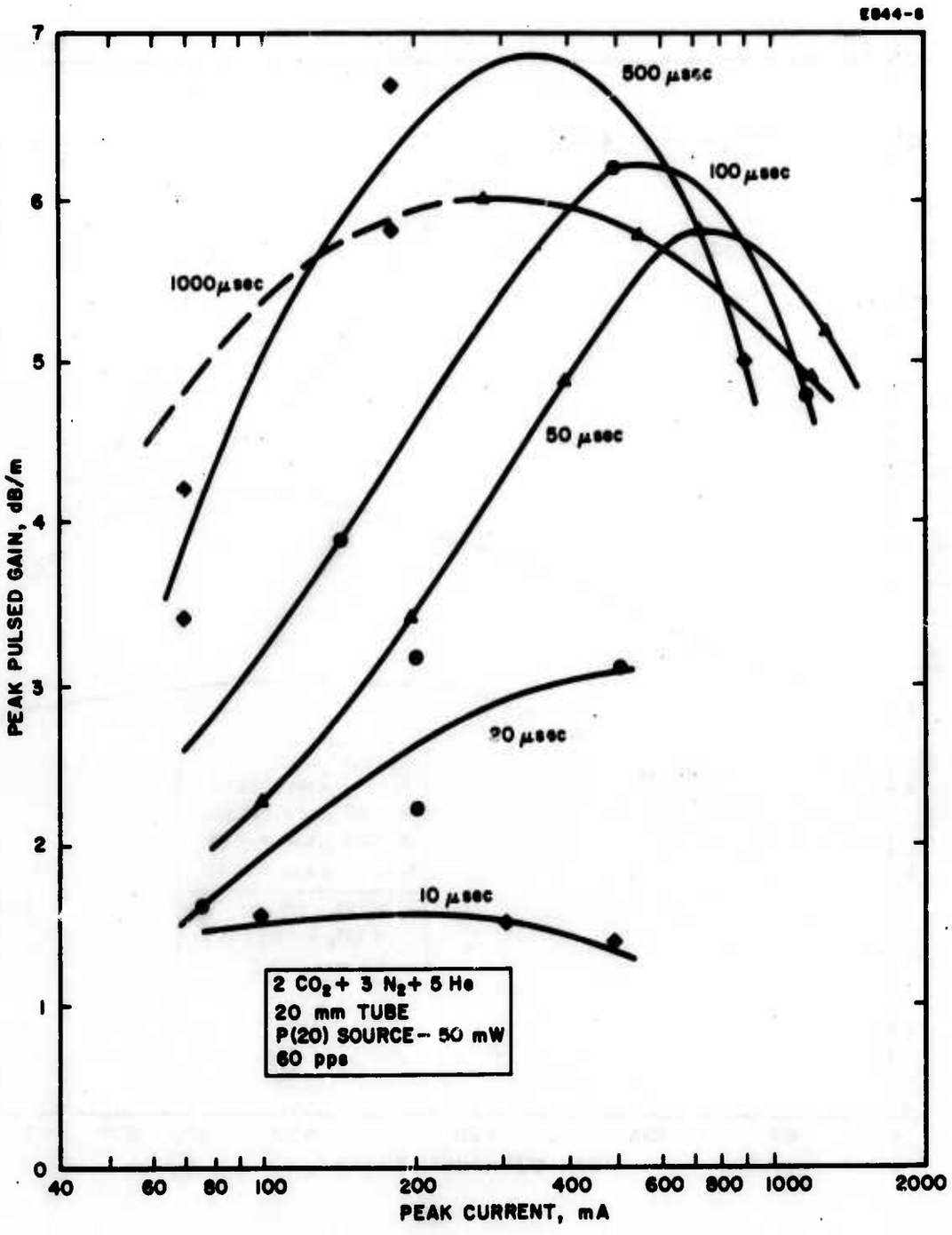

Fig. 17. Peak small signal gain as a function of discharge current.

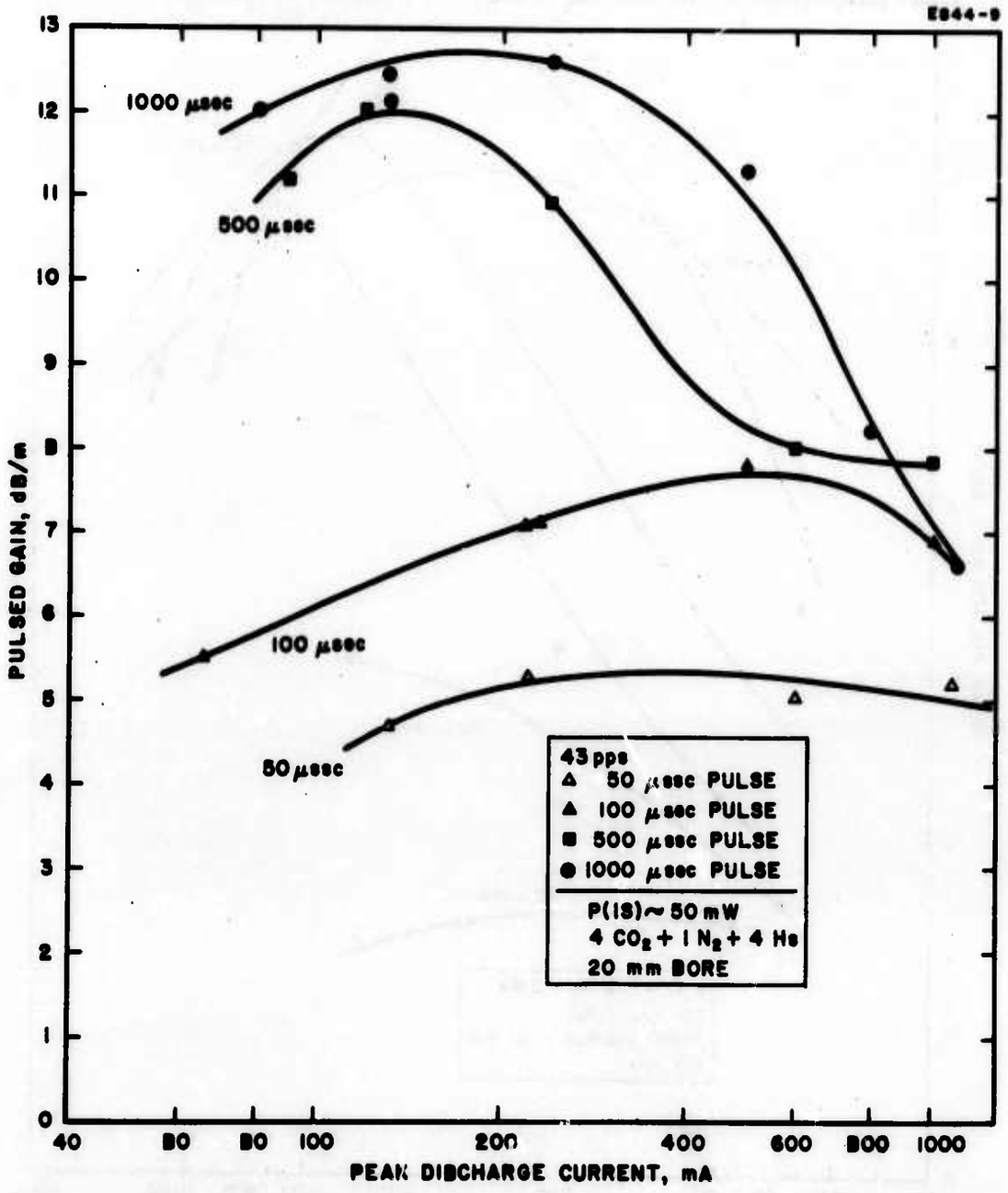

Fig. 18. Variation of small signal gain with current with optimum gas mixtures for low repetition rate pulsed operation.

In pure CO_2, the optimum CO_2 pressure for pulsed operation was approximately 5 Torr, as illustrated in Fig. 19. The optimum CO_2 + He ratio was found to be $4CO_2$ + 4He, as shown in Fig. 20. The addition of small amounts of N_2 greatly increased the peak small-signal gain, provided that the current pulse duration was longer than 100 μsec. This is illustrated in Fig. 21. The pulsed gain decreases with repetition rate, as illustrated in Fig. 22, for a mixture of $4CO_2$ + 4He with a pulse duration of 100 μsec.

Extensive data were not taken on the variation of pulsed gain with the J-value of the P-branch transitions. However, Fig. 23 illustrates the variation for $4CO_2$ + $1N_2$ mixture with 500 μsec pulse duration. The variation is as expected, based on Patel's gain theory.[21] The maximum gain switches to the P(20) transition at higher currents (that is, at higher gas temperature). The absolute values of g_o are not substantially different for the two J values shown.

We may summarize the results of these small-signal measurements as follows: peak gains of > 13 dB/m are exhibited by pulsed discharges at low repetition rates and long (~ 1 msec) pulse durations. At the high repetition rates of interest (1000 to 2000 pps) to this program, the best values obtained with pulsed discharges were only 1 dB/m or so greater than the cw discharge values (≈ 3 dB/m).

B. Saturated Gain

Because of the small differences in the measured values of small-signal gain between cw and high repetition rate pulsed discharges, we decided that it was necessary to measure the saturation flux S_o for pulsed and cw discharges. The original rationale for using pulsed discharge excitation was based on the relatively high peak power outputs obtained from pulsed CO_2 oscillators; they were 10 to 50 times the cw discharge values.[22,23] These oscillator experiments were performed at low repetition rates, and it appears now that part of the increase results from higher values of g_o obtainable at these low repetition rates as we have seen in the previous section. However, the maximum increase in g_o observed in the pulsed amplifier measurements was 3 to 4 times, so that an increase in S_o is also needed to yield a 15 to 50 times increase in the saturated volume generation rate $g_o S_o$, as was observed in the pulsed oscillator experiments.

1. Experimental Apparatus

In order to make the indicated saturation flux measurements, it was necessary to build both a higher power signal source and a higher gain test section. It is necessary to know the signal spatial distribution accurately so that the equivalent area can be used to calculate power densities from total power measurements.

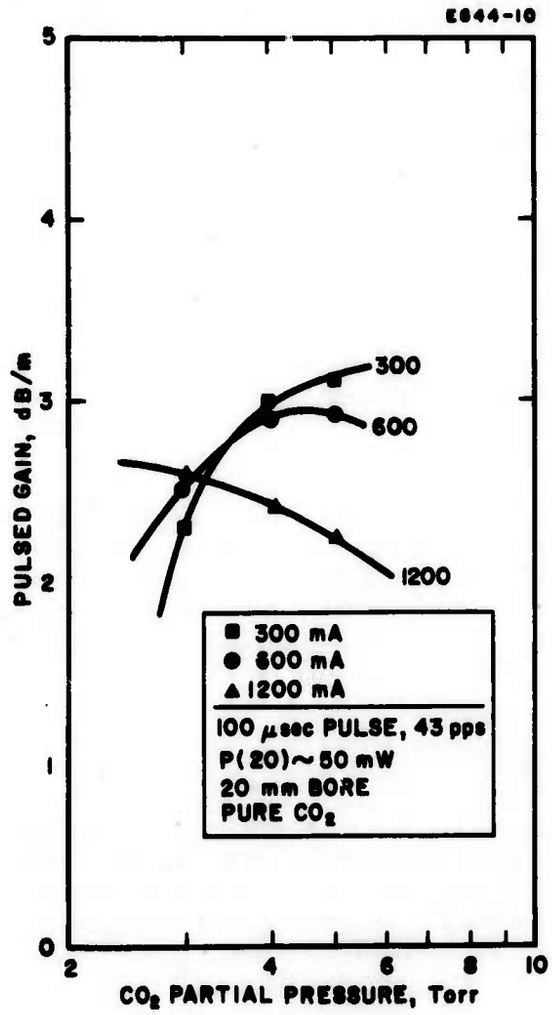

Fig. 19.
Variation of pulsed gain with CO_2 pressure in a pure CO_2 discharge.

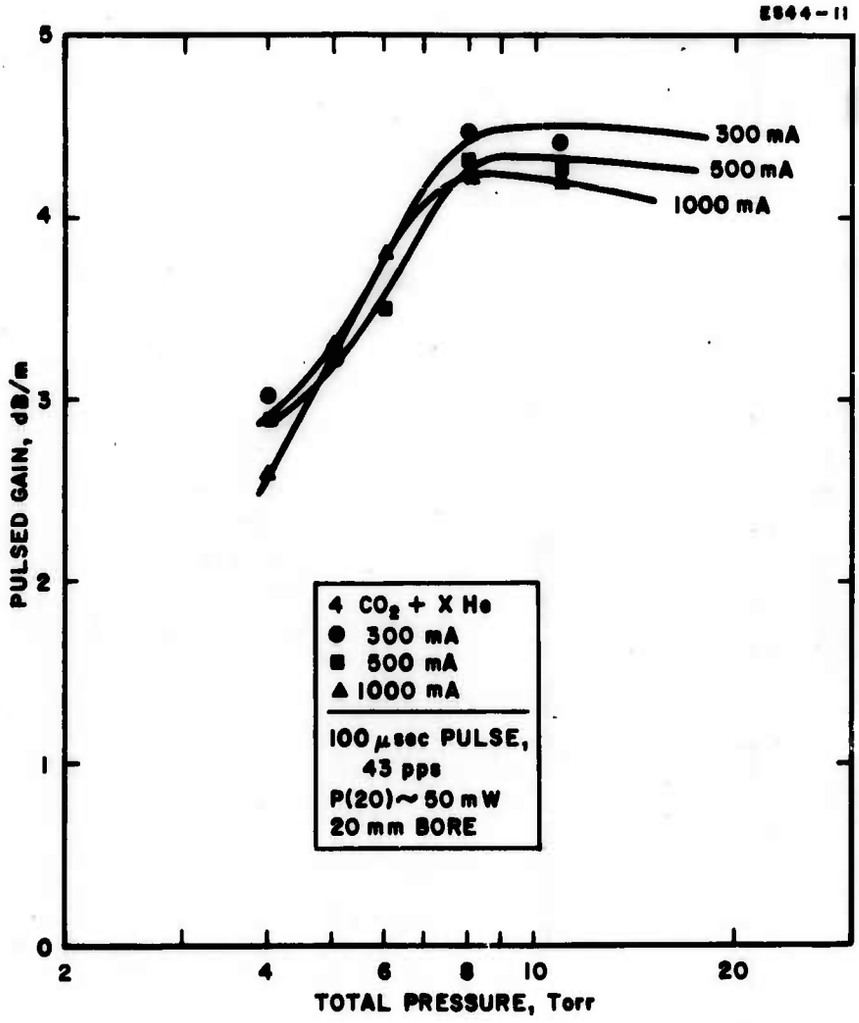

Fig. 20. Variation of pulsed gain with helium pressure in a CO_2-He discharge.

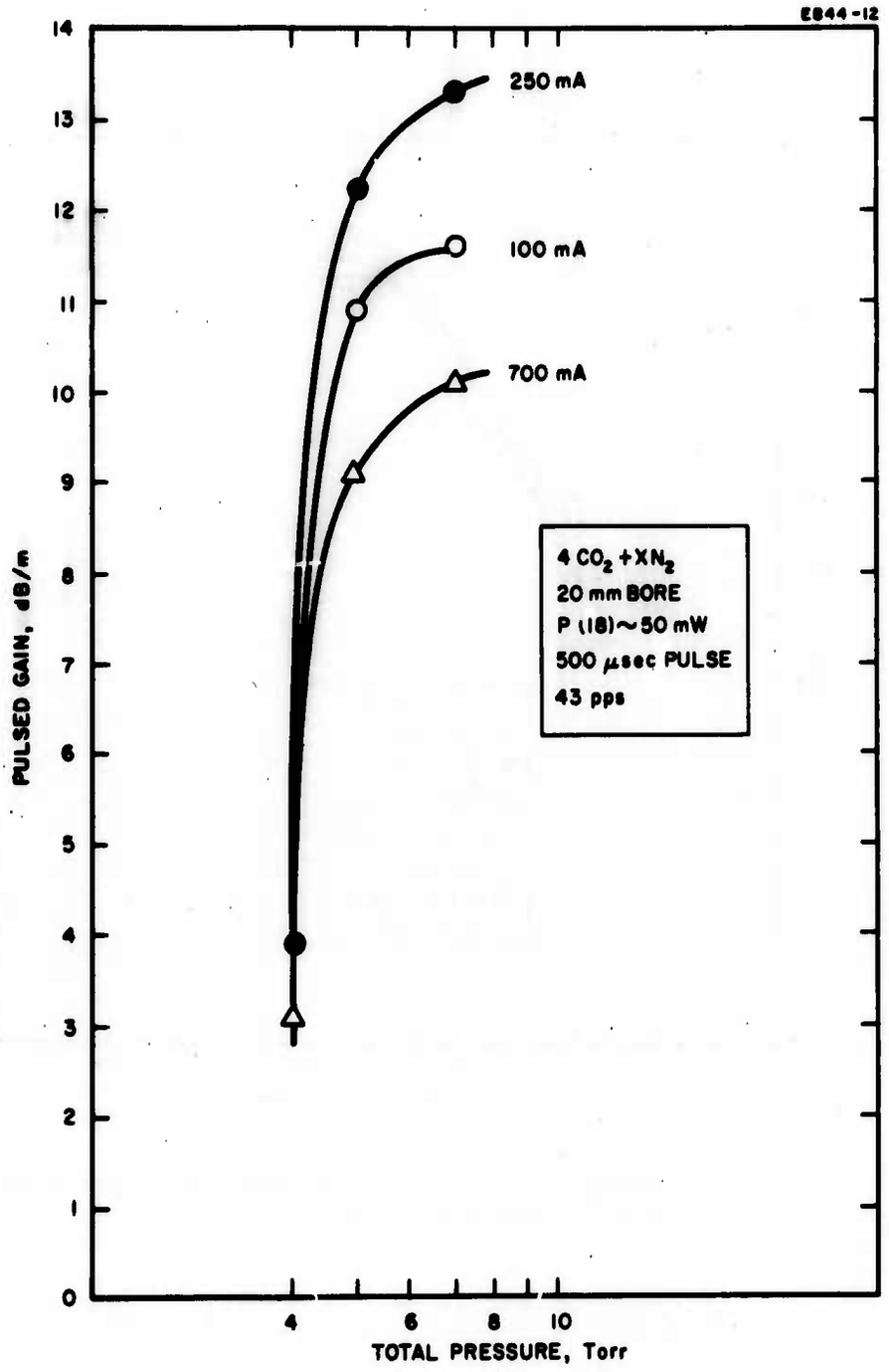

Fig. 21. Variation of pulsed gain with nitrogen pressure in a CO_2-N_2 discharge.

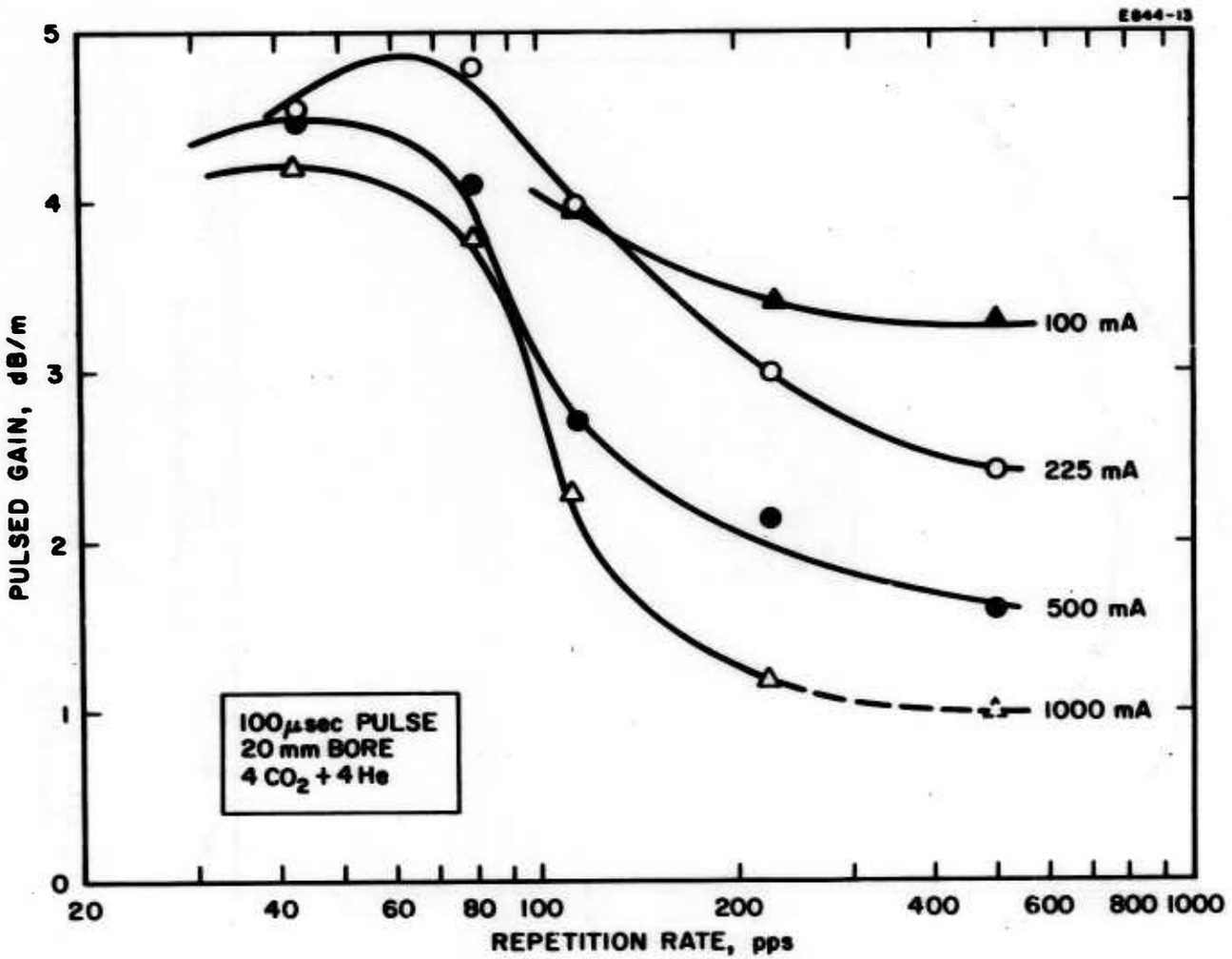

Fig. 22. Variation of pulsed gain with repetition rate in a CO_2-He discharge.

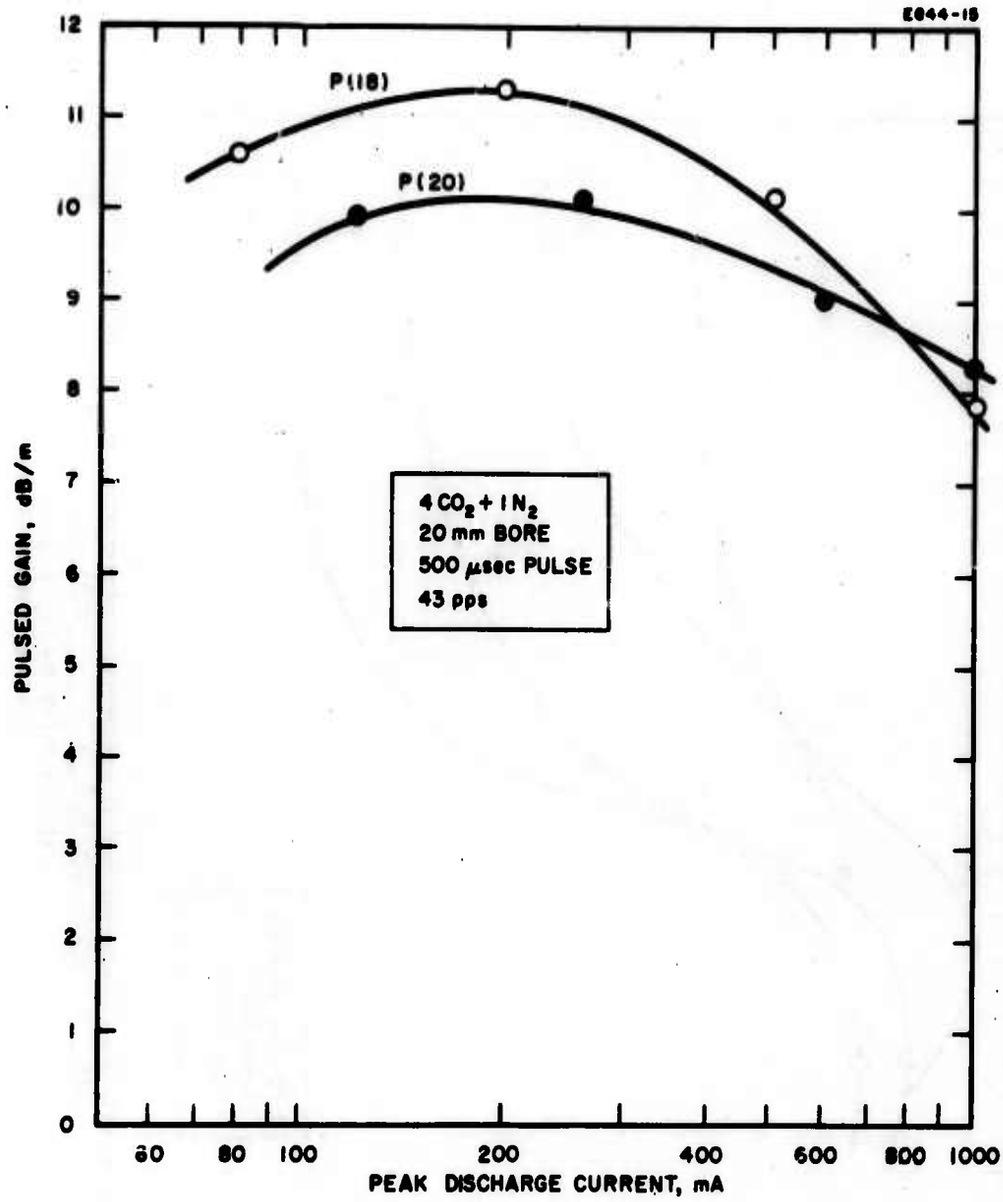

Fig. 23. Effect of discharge current on the gain of two rotational transitions.

A schematic of the apparatus used to make the saturated gain measurements in the 1 in. diameter amplifier section is shown in Fig. 24. A 5 W output source laser with a TEM_{00} output beam was collimated with a 2.5:1 off-axis reflecting telescope and was beamed through the 3.7 m amplifier section. The fabrication techniques used in the 3.7 m tube were similar to those used in the 16 m tube described in Section IV. The 3.7 m tube served as a test vehicle for these techniques. A liquid-nitrogen-cooled Ge:Au detector was used at the exit of the amplifier to measure the pulsed signal, and average power measurements were made with a CRL laser power meter.

With the amplifier section removed temporarily, the 10.6 μ beam propagation was studied with a rotating mirror-pinhole-detector arrangement. The collimating optics were adjusted to place the beam waist approximately at the center of the amplifier. A typical measured beam profile is shown in Fig. 25. The profile is compared with a gaussian beam having the same $1/e^2$ intensity width. The beam is seen to be nearly TEM_{00}. The far field diffraction angle of the beam was measured to the $1/e^2$ intensity points, and the divergence angle from the beam waist was found to be $\theta = 1.55\ \lambda/D$, which is 1.2 times diffraction limited divergence.

As a comparison with previous measurements in the short test section, the small-signal gain was remeasured in the 3.7 m section. Figure 26 shows the gain versus dischage current for pulsed operation under approximately optimum mixture and flow conditions. A gain of about 4 dB/m was obtained with 100 μsec current pulses at 500 pps, in good agreement with the 60 cm test section values. Cw discharge gain measurements on the 3.7 m section yielded $\approx$ 3 dB/m under optimum conditions, also in good agreement with the 60 cm section results.

2. Gain Saturation Measurements

Gain saturation was measured in the 1 in. diameter 3.7 m tube under cw discharge conditions with a flowing gas mixture of 13 cfh CO_2, 32 cfh N_2, 178 cfh He at a total pressure of 17 Torr and a discharge current of 21 mA. The small signal, cw gain in the 3.7 m section was 3.0 dB/m, or $\approx$ 11 dB over-all. The cw gain saturation data are shown in Fig. 27. The power density scale in this figure is based on the beam area at the half-power points ($r/W_o \approx 0.6$). A curve based on the beam waist diameter at the half-power points (computed from the output diameter using the previously measured relation $\theta = 1.55\ \lambda/D$) is shown. Figure 27 is intended only to show the saturation schematically. Actual values of S_o were calculated by fitting the experimental points to computed saturation curves based on the equivalent area of the TEM_{00} gaussian beam ($r/w_o = 0.707$) at the beam waist. Values of S_o of 60 to 90 W/cm^2 were required to fit the experimental points. The actual data and values of S_o are given in Table IV. The more accurate values are those for the highest power, since these are the least dependent on the exact value of g_o.

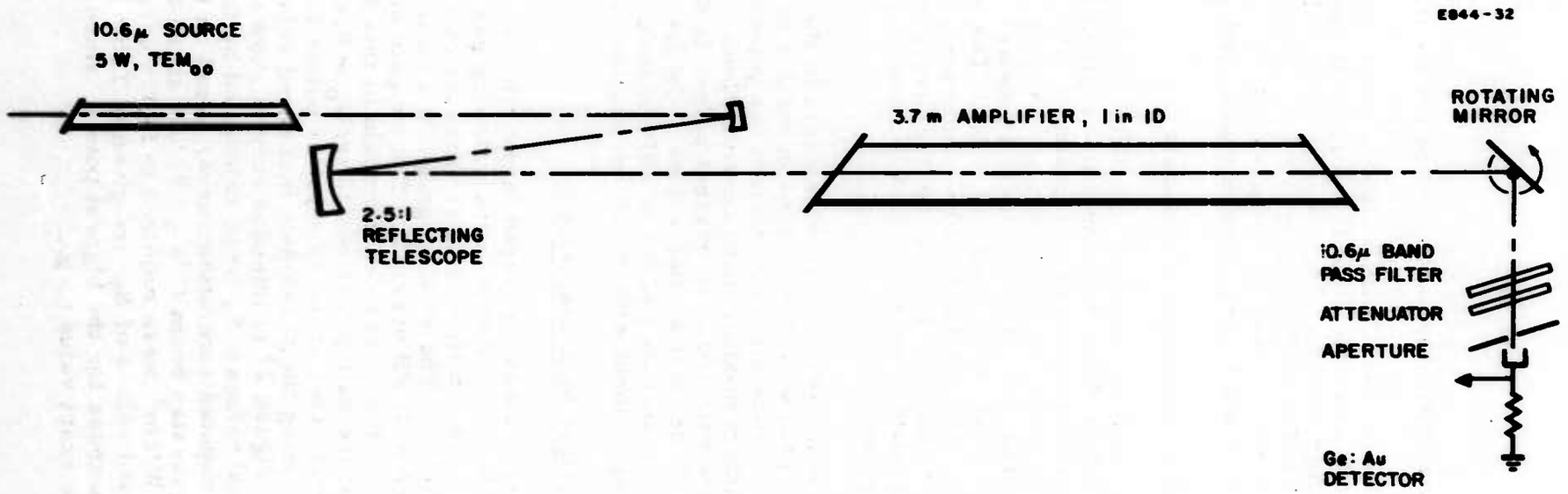

Fig. 24. Saturation flux density measurement arrangement.

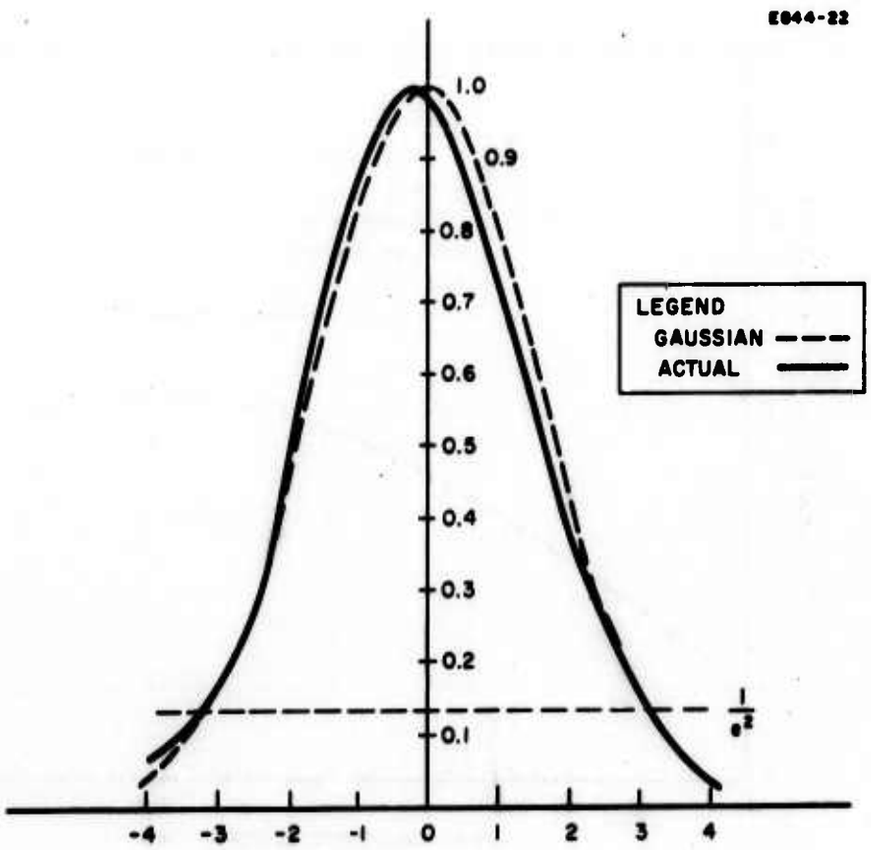

Fig. 25. Comparison of TEM_{00} 10.6 μ beam from output hole coupled laser with a gaussian curve matched at $1/e^2$ intensity point.

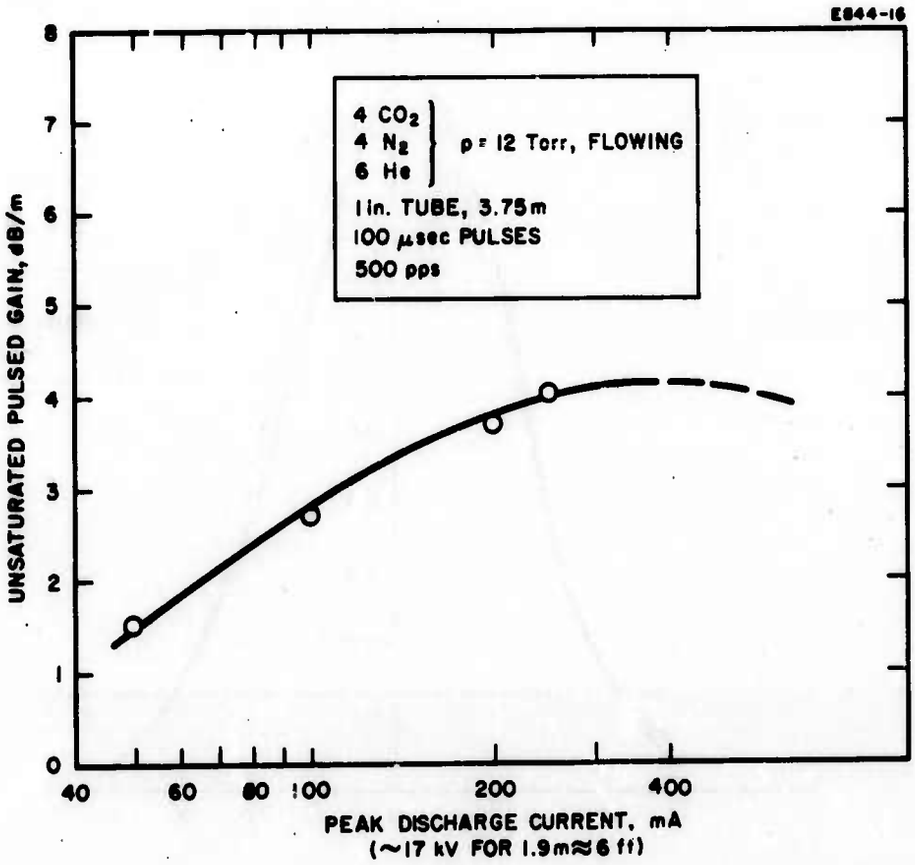

Fig. 26. Small signal gain in the 3.7 m tube with pulsed discharge excitation.

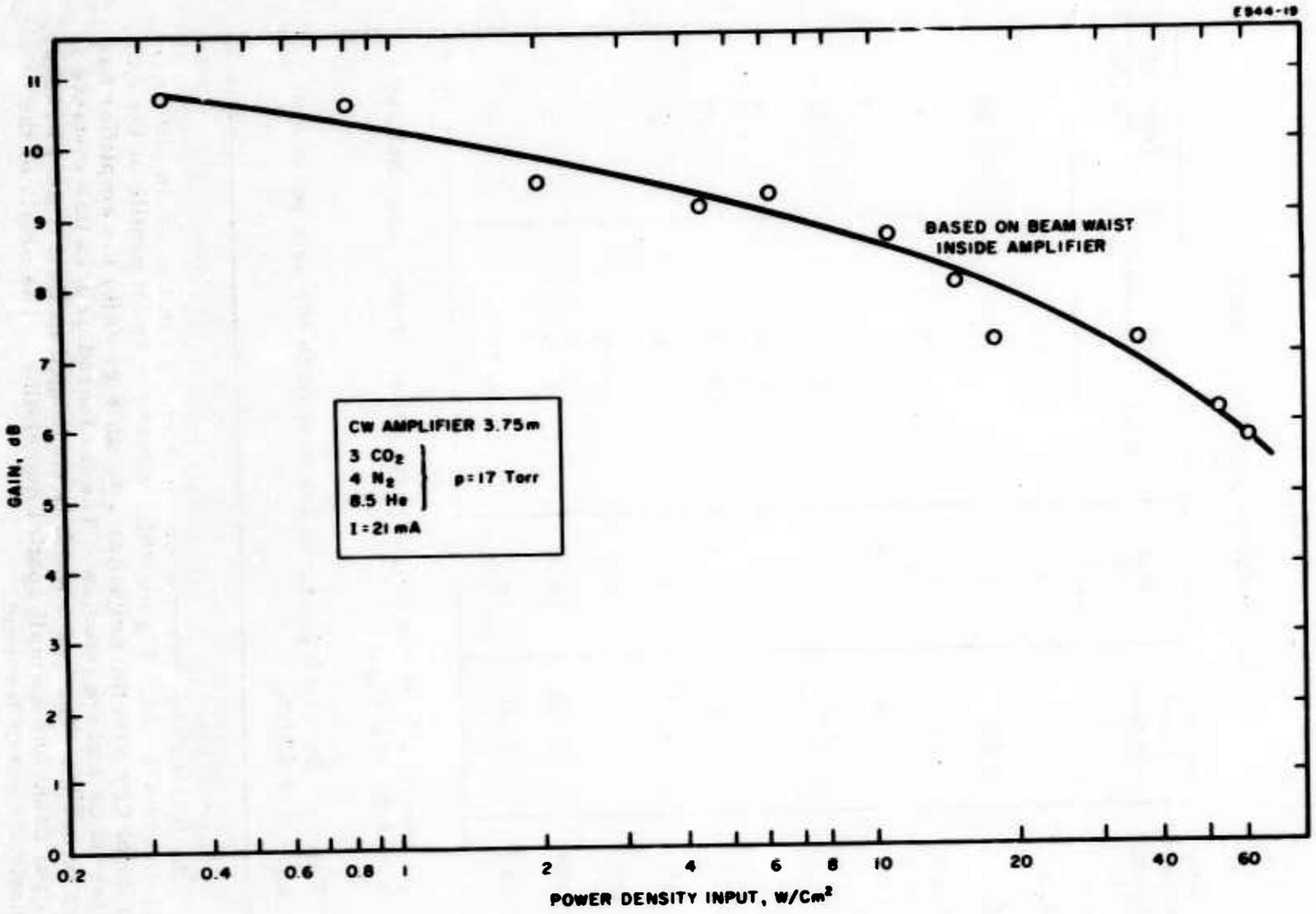

Fig. 27. Gain saturation curve for the 3.7 m tube with a cw discharge.

TABLE IV

CW Gain Saturation Measurements

Power Input, W	Power Output, W	Gain, dB	Beam Waist Diameter, cm[a]	Value of S_o, W/cm^2[b]
4.9	19	5.9	0.53	80
3.5	15	6.3	0.48	80
2.4	13	7.3	0.48	90
1.5	7.6	7.1	0.53	44
1.2	7.3	7.8	0.51	57
1.0	7.4	8.7	0.56	72
0.73	6.2	9.3	0.58	78
0.40	3.3	9.2	0.56	40
0.20	1.8	9.5	0.59	–
0.080	0.92	10.6	0.59	–
0.040	0.46	10.6	0.58	–

[a] As inferred from the output beam diameter measurement and $\theta = 1.55\,\lambda/(2W_o)$.

[b] Value of S_o which produced the best fit to the data point with $g_o = 3.0$ dB/m.

An interesting phenomenon which occurs in the cw amplifier is illustrated in Fig. 28. Figure 28(a) shows the beam profile at the exit of the amplifier with the amplifier off. In Fig. 28(b) the amplifier has been turned on and operated cw. The measured gain in this instance is 9.5 dB in 3.7 m. The beam width is unchanged to first order; however, the output beam has a small spatial modulation. The origin of the modulation is not understood.

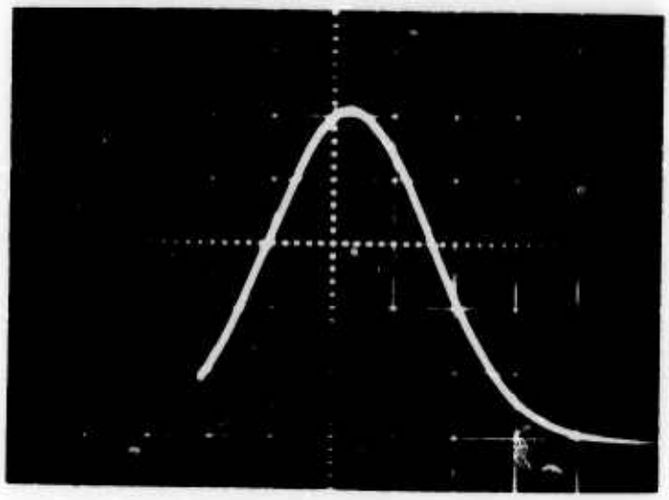

(a)

(b)

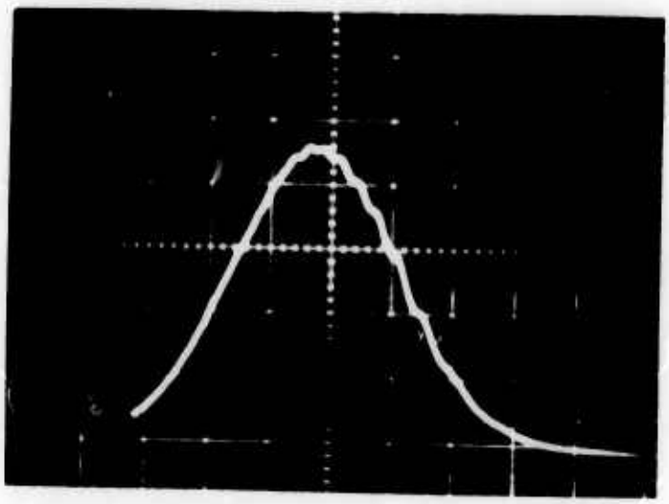

Fig. 28. Beam profile at the output of the 3.7 m tube (a) with discharge off, (b) with discharge on. Note the small spatial modulation on the profile in (b).

The gain saturation of the 3.7 m section was also measured with a pulsed discharge at 500 pps repetition rate and 100 μsec pulse length. A flowing gas mixture of 26 cfh CO_2, 32 cfh N_2, and 126 cfh He at a total pressure of 11.5 Torr was used. The small-signal gain under these conditions was 3.5 to 4 dB/m. By curve fitting the measured data as shown in Table V, an S_o of > 200 W/cm^2 was estimated. Unfortunately, with the signal source power available and the short length of test section, the degree of saturation was too small to obtain accurate values of S_o. The estimate of > 200 W/cm^2 is sufficiently promising that a more accurate measurement on the 16 m amplifier described in Section IV is warranted.

TABLE V

Pulsed Gain Measurements

Power Input, W	Power Output, W	Gain, dB	Beam Waist Diameter, cm (a)	Value of S_o, W/cm^2 (b)
4.5	51	10.6	0.63	445/253
3.6	58	12.0	0.63	> 1000/453
1.6	32	13.0	0.63	–
0.70	14	13.0	0.63	–
0.34	6.3	12.7	0.63	–
0.14	4.2	14.7	0.63	–
0.12	2.4	13.0	0.63	–

(a) As inferred from the output beam diameter and $\theta = 1.55\,\lambda/(2W_o)$.

(b) First value quoted is the best fit to the data point with $g_o = 3.5$ dB/m; the second value is the best fit with $g_o = 4.0$ dB/m.

C. Electrical Characteristics

The electrical characteristics of the CO_2 laser amplifier have been measured for various mixtures and pressures of interest for both cw and pulsed excitation. In general, for short current pulses, the peak voltage required is larger than the cw value. This is illustrated in Fig. 29. As the pulse duration increases, the pulsed voltage-current characteristics obviously approach the cw characteristics as seen in Fig. 29.

D. Comparison of CW and Pulsed Amplifier Characteristics

The results of the measurements which were made on the cw and pulsed amplifier are summarized in Table VI. The comparison is made between a pulsed amplifier operating at 1000 pps (extrapolated from 500 pps data) with 100 μsec pulse duration, i.e., a duty factor of 1/10, and a cw amplifier, both at optimum conditions. The pulsed amplifier has slightly higher small-signal gain and its saturation flux density is twice (or more) that of the cw amplifier. Both of these factors would contribute to a considerably smaller pulsed device than the equivalent cw device. The cw amplifier is slightly more efficient per unit length and has the advantage of added simplicity over the pulsed amplifier.

The decision to use a pulsed or a cw intermediate amplifier (IA) is not clearly indicated on the basis of the characteristics listed above, since the IA operates partially unsaturated. The final decision must weigh the relative complexity of the pulsed circuitry against the slightly higher gain; other practical considerations are discussed in the next section. It seems clear, however, that the final amplifier portion of the 1 kW transmitter should be operated in the pulsed discharge mode for maximum over-all electrical and volumetric efficiency.

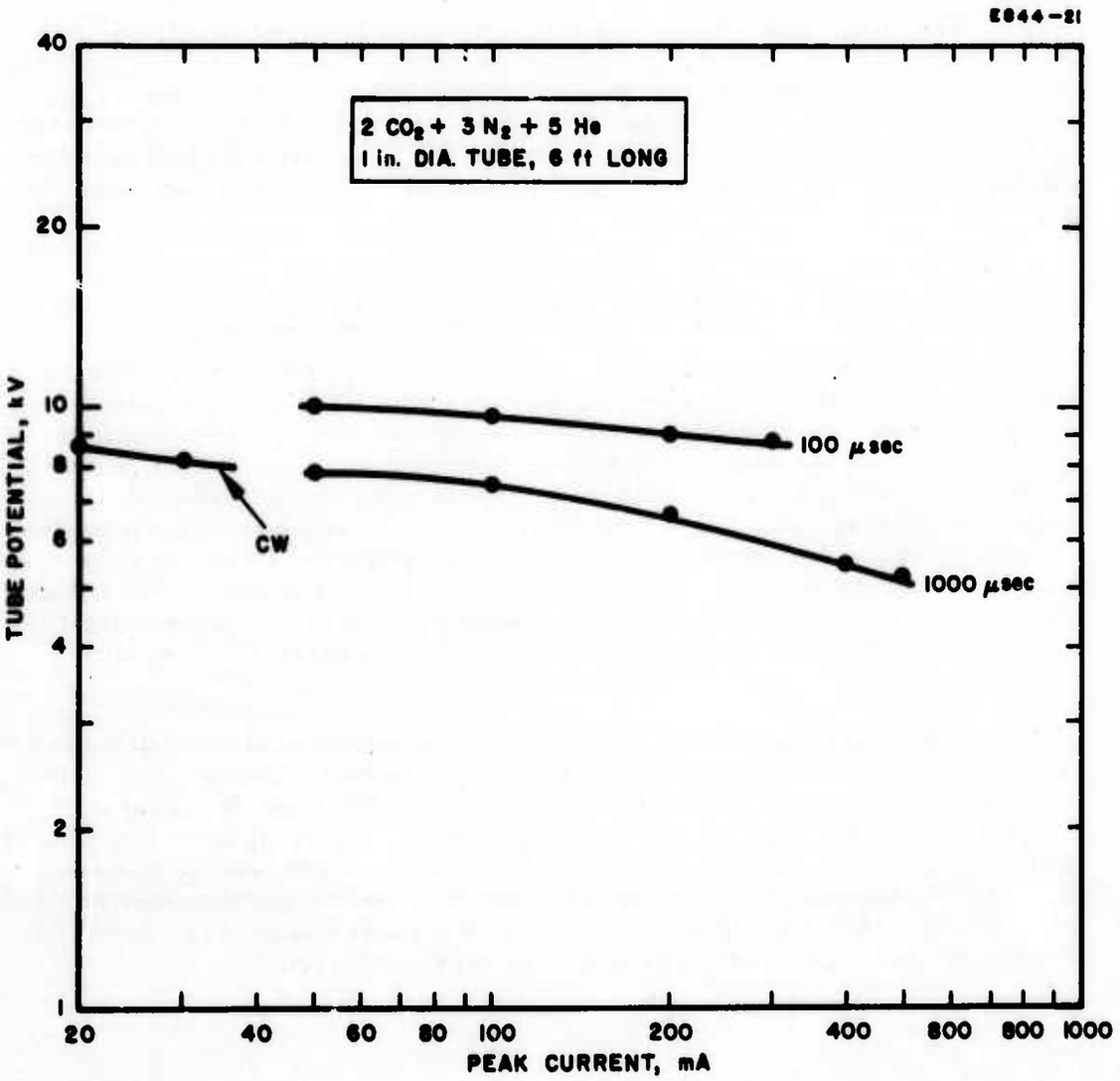

Fig. 29. Tube voltage as a function of discharge current for pulsed and cw discharge current for pulsed and cw excitation.

TABLE VI

Comparison of Amplifier Characteristics

Characteristic	Pulsed, 1000 pps, 100 μsec	cw
g_o	4 dB/m	3 dB/m
S_o	> 200 W/cm^2	60 - 90 W/cm^2
Current	200 mA peak	25 mA dc
Specific potential	3 kV/m	1.8 kV/m
Specific average power input	62 W/m	46 W/m
Gas flow	26 cfh CO_2 32 cfh N_2 126 cfh He } at 11.5 Torr	13 cfh CO_2 32 cfh N_2 178 cfh He } at 17 Torr

IV. TRANSMITTER DESIGN

In this section we present our design for the delivered hardware, the present status of that hardware, and the program plan for the next quarter.

A. Design

Figure 30 outlines schematically the configuration presently envisaged for the transmitter. The amplifier has been divided into two main units, an intermediate amplifier (IA) and a final amplifier (FA). The intermediate amplifier has been designed to reach saturation flux approximately at its output in the shortest discharge length. For this reason, a smaller diameter (1 in.) discharge is used. Two sections of discharge, each 8 m long, are used to amplify the 10 W oscillator output to the 0.5 to 1.5 kW level. Recollimating optics are used to match the oscillator output beam diameter and slope to the IA diameter and slope, so as to produce a 1.5 cm beam waist diameter (at the $1/e^2$ intensity points) in the center of the IA. The oscillator signal drives the IA continuously, in order to minimize the chance of self-oscillation. (The 16 m length will yield 48 dB small signal gain if driven cw or > 64 dB if pulsed.) The decision on whether to run the IA discharge pulsed or cw has been deferred until the two methods can be compared; the measurements of g_o and S_o on the 3.7 m discharge were not sufficiently accurate in the pulsed mode to provide a firm basis for decision, as mentioned in Section III. The apparent improvement in g_o and S_o must be weighed against the additional complexity of the power supply, so that it is reasonable to make the comparison carefully on the actual amplifier.

The IA output is recollimated to a larger (3 cm) diameter by a second set of optics. These also provide a focal plane for the mechanical modulator which produces 20 μsec pulses at a 2000 pps rate. (It would be an advantage here to have the IA operate in a pulsed discharge mode so that the chopper blade would not be subjected to the peak power on an average basis, provided, of course, that the increased gain in the pulsed mode does not overcome the 0.2 duty cycle of the pulsed IA and result in the same average power.) The collimated beam enters the final amplifier with its 3 cm waist at the input to the first stage. The beam thus continues to spread as it passes through the 2 in. inside diameter, final amplifier section. Figure 31 shows a schematic representation of the optical path, giving the critical dimensions. Final amplifier sections are 8 m long, with pairs of folding mirrors at the ends. Except for the diameter and the number of folds, the FA is identical in construction to the IA.

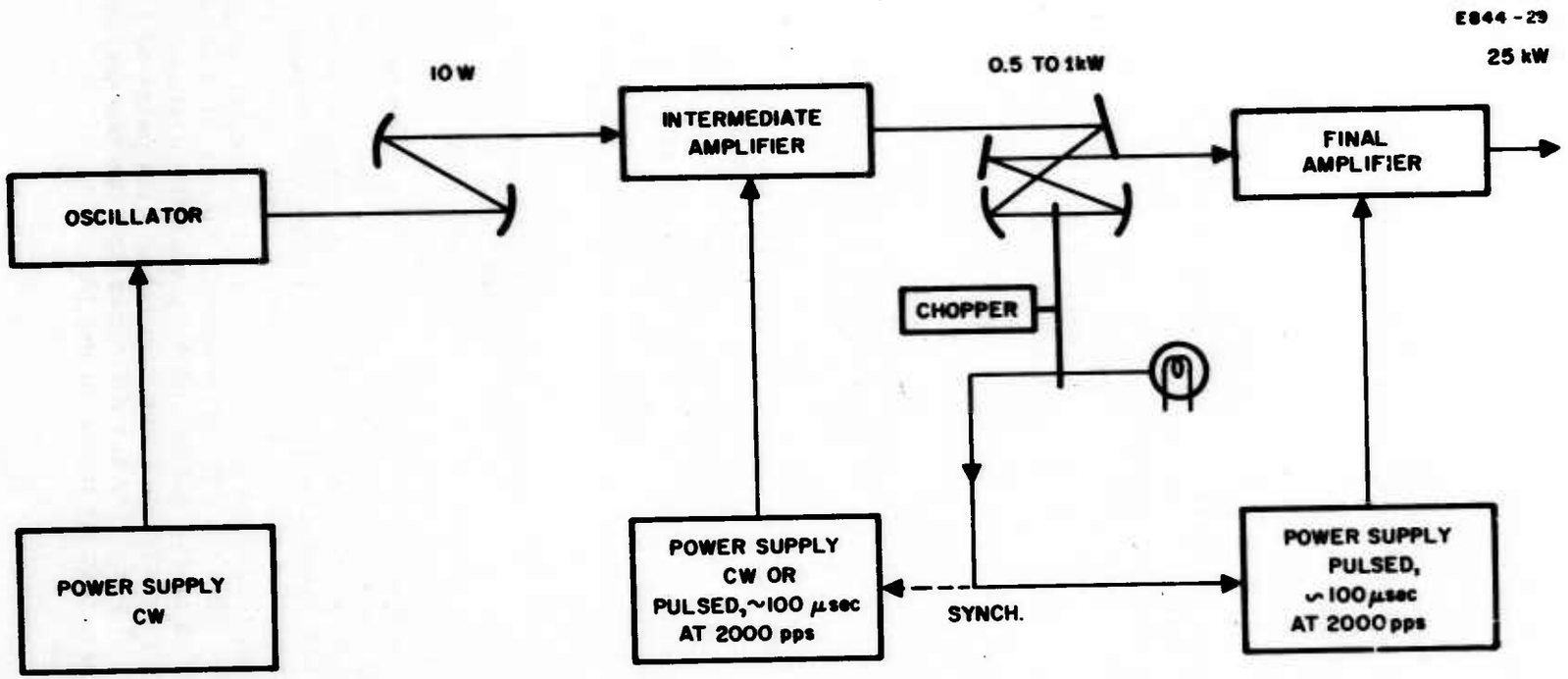

Fig. 30. Functional block diagram of 1 kW transmitter.

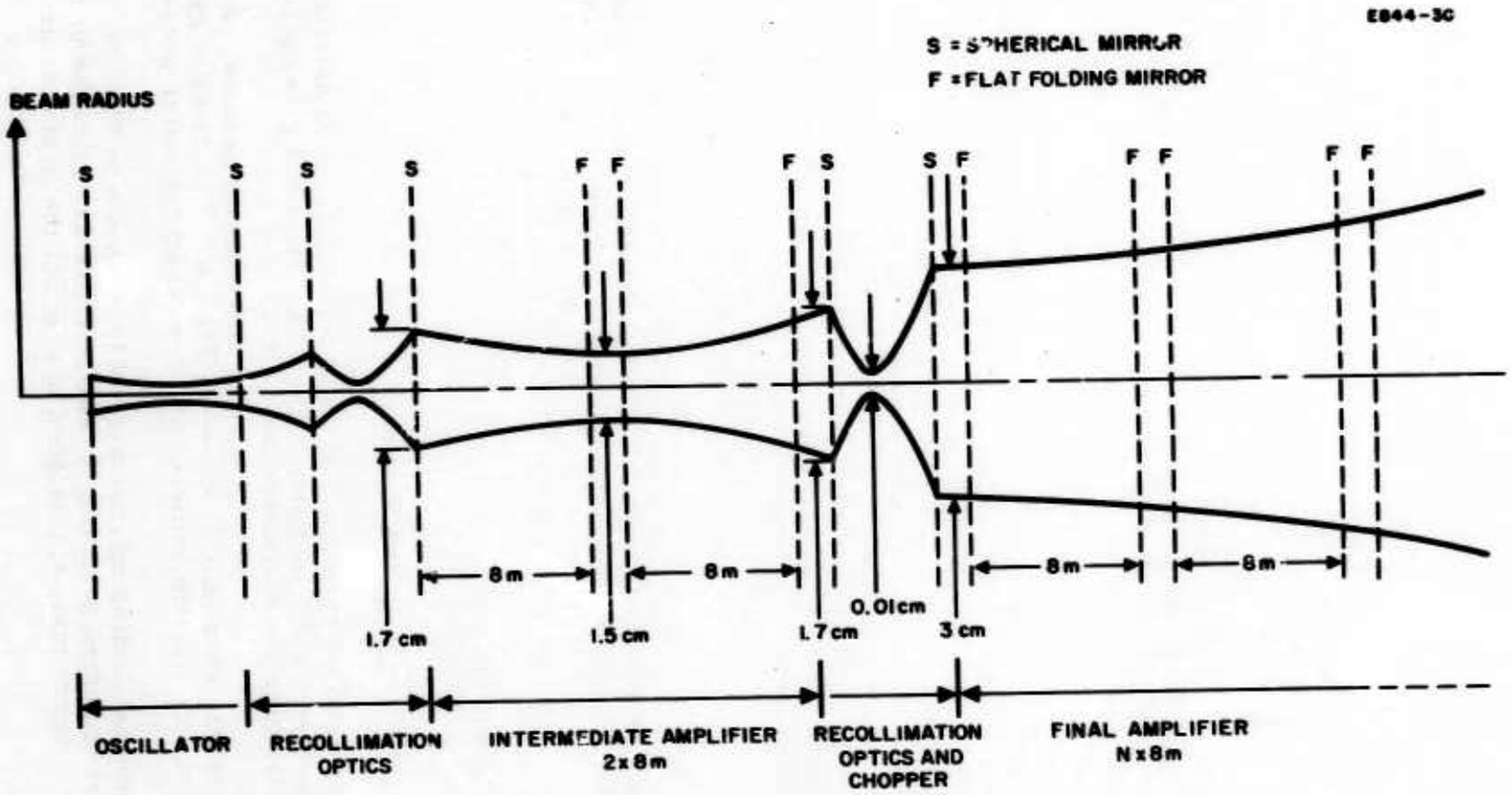

Fig. 31. Schematic representation of the optical path through the transmitter.

The FA will be operated in a pulsed mode, with the input 20 μsec optical pulses being synchronized to the peak gain occurring after the ~100 μsec current pulse, as shown in Fig. 32. The exact choice of current pulse length will be optimized for highest over-all efficiency. The number of 8 m sections required to reach 25 kW peak power must also be determined experimentally. Tables VII through XI give the number of 8 m sections required to make 25 kW peak power under various assumptions of g_o, S_o, and beam collimation. Table VII gives the design based on optimistically extrapolated values of g_o and S_o in a 2 in. diameter pulsed discharge. Only seven amplifier sections are required to make > 25 kW (in fact, six sections would probably suffice). Table VIII shows the effect on the design if S_o is reduced from 200 W/cm^2 to 100 W/cm^2; eleven amplifier sections are required. Table IX shows the further effect of reducing both S_o and g_o from the values of Table VII. With S_o = 100 W/cm^2 (as in Table VIII) and g_o = 2 dB/m, thirteen amplifier sections are required. In contrast, Table X shows that the input power has little effect on the design, as long as it is approximately equal to the saturation flux density of the FA. Table X assumes 500 W input compared with 1600 W input in Table VIII. The number of sections required to exceed 25 kW is the same (eleven). In fact, the difference in output (≈ 1 kW) is approximately the difference in input, as expected in a fully saturated amplifier. Table XI illustrates the importance of positioning the beam waist properly in a fully saturated amplifier. The parameters are identical to those in Table X, except that the beam waist of 3.0 cm has been located 44 m down the tube from the input end. With this arrangement, fourteen sections, instead of eleven, are required to exceed 25 kW.

Although some of the cases look rather discouraging, we must remember that the 25 kW peak power required to make 1 kW average power at 0.04 duty is fairly severe. If the duty were relaxed to 0.1 with 10 kW peak power (as proposed prior to the LREDS study), the number of sections required is considerably smaller, as seen from Tables VII through XI.

B. Fabrication Details and Progress

A more detailed schematic showing the construction details of the intermediate amplifier is given in Fig. 33. Standard glass pipes 6 ft long are used for the discharge tube. Each 6 ft section has an aluminum water jacket sealed on the ends with silastic gaskets. A view of the pieces of this assembly is shown in Fig. 34. The silastic gaskets are held in place by silastic cement and (by design) the water pressure.

The internal folding mirror assembly is shown in Fig. 35. (This picture was taken before polishing.) The mirrors are attached to relatively massive copper pieces, designed to conduct the heat outside of the

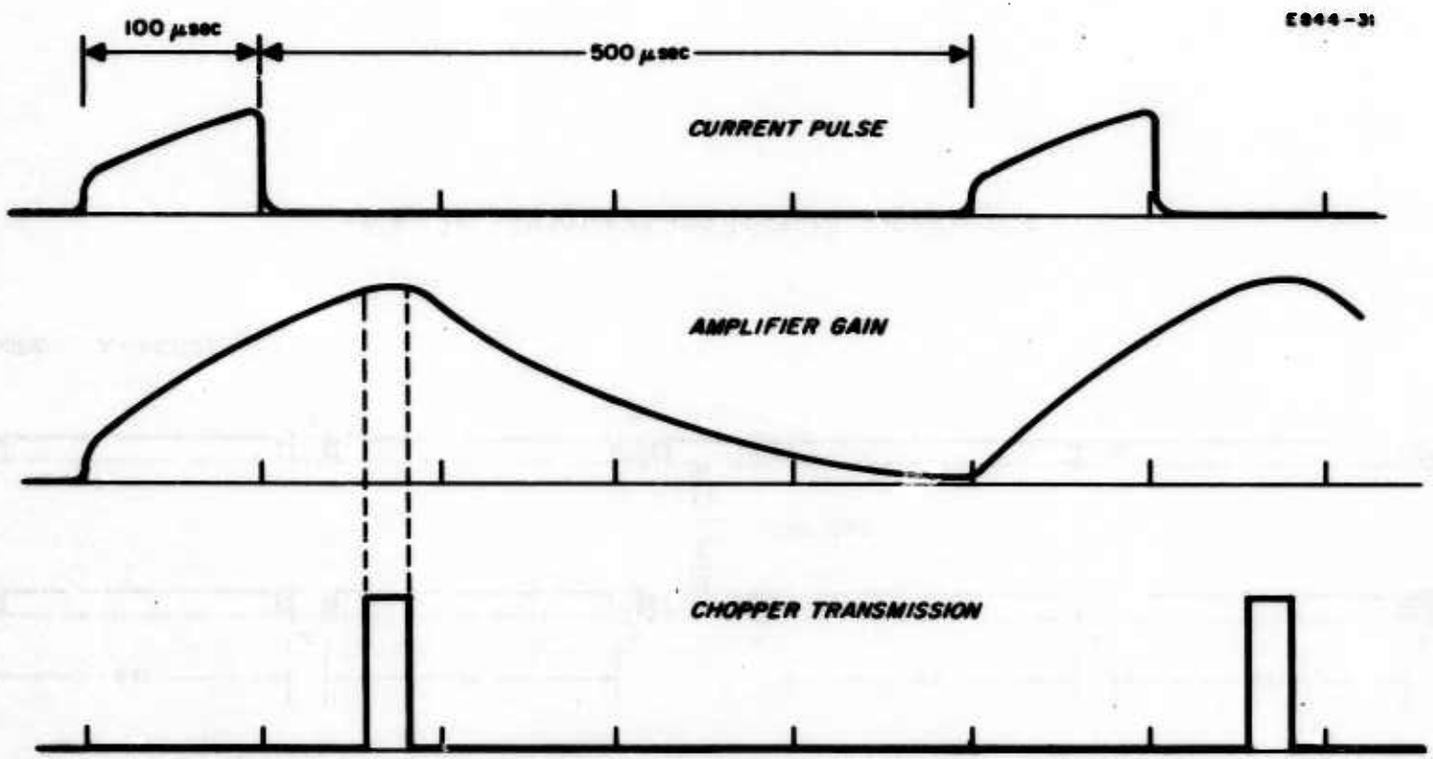

Fig. 32. Schematic representation of current pulse, gain pulse, and chopper timing.

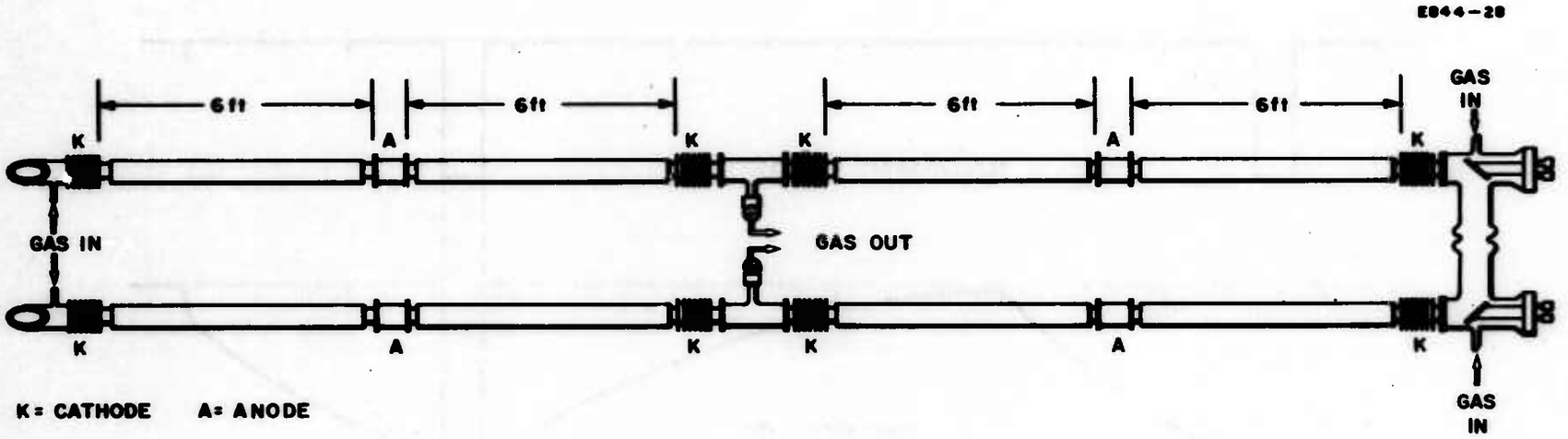

Fig. 33. Details of the 16 m IA construction.

M 5490

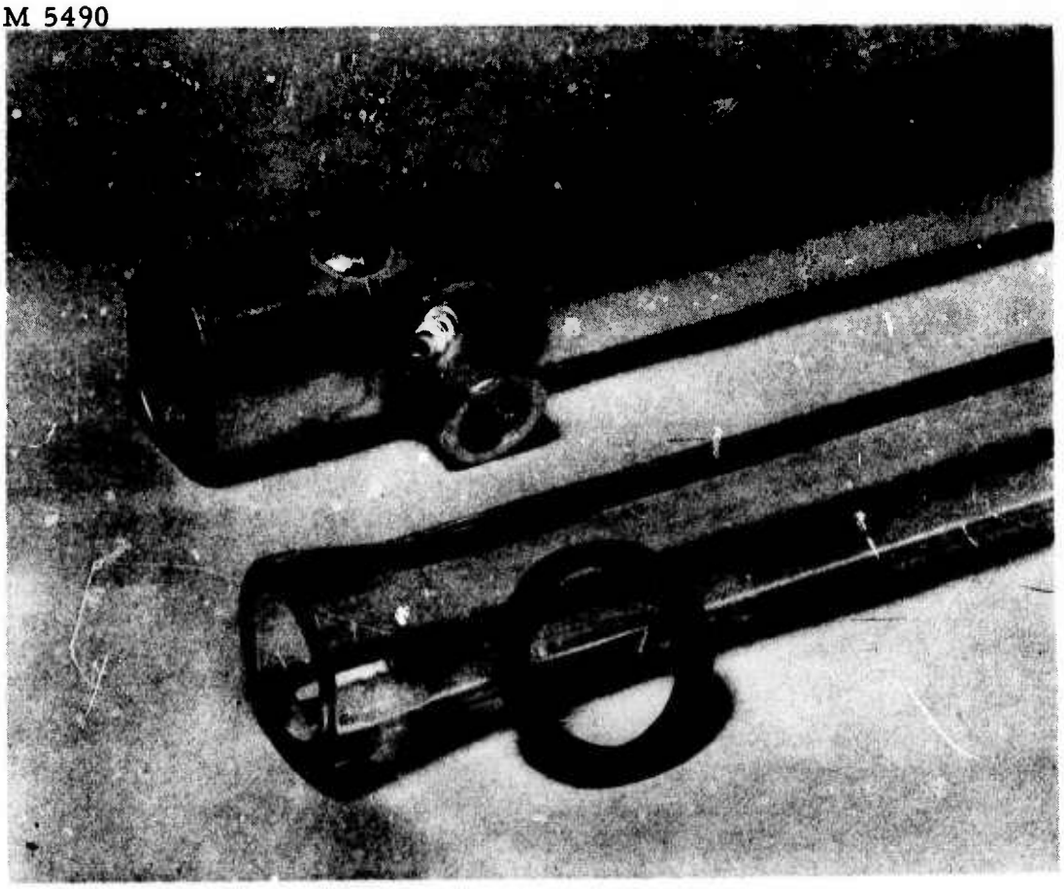

Fig. 34. Exploded view of discharge bore assembly for the IA.

M 5485

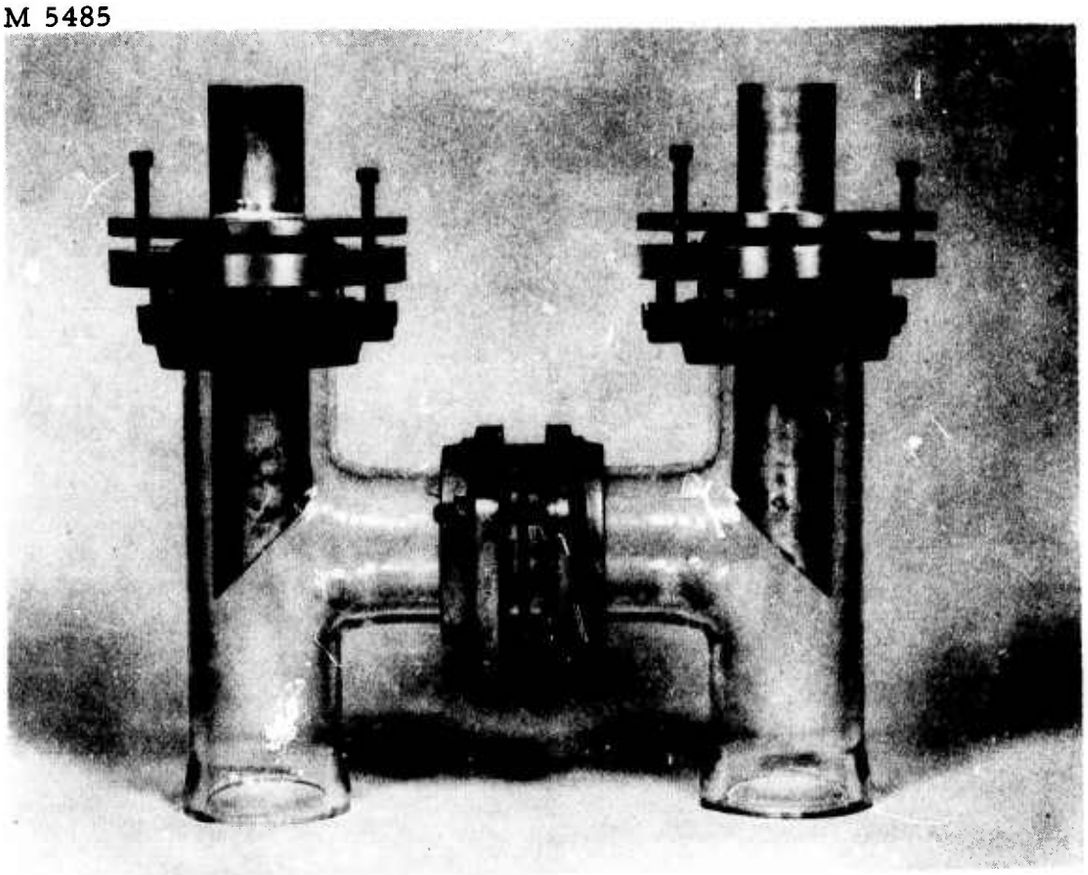

Fig. 35. Folding mirror assembly for 16 m IA.

TABLE VII

Final Amplifier Design

Parameters:

- g_o = 3 dB/m
- S_o = 200 W/cm^2
- P_{input} = 1600 W (typical of a pulsed IA operation)
- Beam Waist = 3.0 cm to $1/e^2$ points
- Beam Waist location: at FA input.

Length from Input, m	Beam Diameter, cm	Power, W	Gain/8 m Section, dB
8	3.022	4748	4.725
16	3.085	8166	2.532
24	3.188	11783	1.770
32	3.328	15637	1.406
40	3.498	19803	1.203
48	3.696	24364	1.078
56	3.918	29408	0.9945

vacuum envelope. Alignment adjustments are provided on the mounting flanges. The techniques for polishing solid copper mirrors so that the scattering and absorption losses are less than those of the usual evaporated gold mirrors were developed under another program. We expect less than 2% total loss at each mirror, with less than 1% absorbed. The massive mirrors are not needed on the IA stage, of course, but the same assembly will be used on the FA sections, so that the technique is being developed with the IA as a test vehicle.

An over-all view of the assembled IA is shown in Fig. 36. The electrodes are made of aluminum and are located in-line between the 6 ft sections. The cathodes are finned to facilitate air cooling. Brewster's angle windows are used for input and output of the IA. Gas inlets are provided at each end of the tube, with a separate pressure monitoring line run in such a way that the pressure gauge measures actual pressure at the tube inlets. Gas is exhausted to a 3 in. diameter foreline through

TABLE VIII

Final Amplifier Design

Parameters	Same as Table VII except $S_o = 100\ W/cm^2$		
Length from input, m	Beam Diameter, cm	Power, W	Gain/8 m Section, dB
8	3.021	3303	3.148
16	3.085	5019	1.995
24	3.188	6814	1.505
32	3.328	8719	1.248
40	3.498	10777	1.097
48	3.696	13031	1.002
56	3.918	15527	0.9382
64	4.158	18307	0.8926
72	4.415	21414	0.8581
80	4.685	24890	0.8304
88	4.967	28773	0.8070

TABLE IX

Final Amplifier Design

Parameters	Same as Table VIII except g_o = 2 dB/m		
Length from Input, m	Beam Diameter, cm	Power, W	Gain/8 m Section, dB
8	3.022	2718	2.302
16	3.085	3815	1.649
24	3.188	4965	1.321
32	3.328	6189	1.135
40	3.498	7515	1.021
48	3.696	8972	0.9469
56	3.918	10589	0.8968
64	4.158	12394	0.8607
72	4.415	14415	0.8332
80	4.685	16678	0.8107
88	4.967	19210	0.7912
96	5.259	22037	0.773
104	5.558	25182	0.7567

TABLE X

Final Amplifier Design

Parameters	Same as Table VIII, except P_{input} = 500 W		
Length from Input, m	Beam Diameter, cm	Power, W	Gain/8 m Section, dB
8	3.022	1973	5.962
16	3.085	3669	2.872
24	3.188	5481	1.920
32	3.328	7416	1.491
40	3.498	9510	1.257
48	3.696	11802	1.115
56	3.918	14335	1.022
64	4.158	17154	0.9568
72	4.415	20299	0.9084
80	4.685	23811	0.8704
88	4.967	27731	0.8391

TABLE XI

Final Amplifier Design

Parameters	Same as Table XI, except the beam waist is located 44 m from the input end of the tube.		
Length from Input, m	Beam Diameter, cm	Power, W	Gain/8 m Section, dB
8	3.409	2394	6.802
16	3.254	4415	2.835
24	3.132	6286	1.712
32	3.048	7995	1.221
40	3.005	9577	0.9614
48	3.005	11081	0.8108
56	3.048	12560	0.7212
64	3.132	14065	0.6690
72	3.254	15650	0.6409
80	3.409	17363	0.6285
88	3.594	19254	0.6263
96	3.804	21370	0.6301
104	4.036	23756	0.6369
112	4.285	26455	0.6447

M 5519

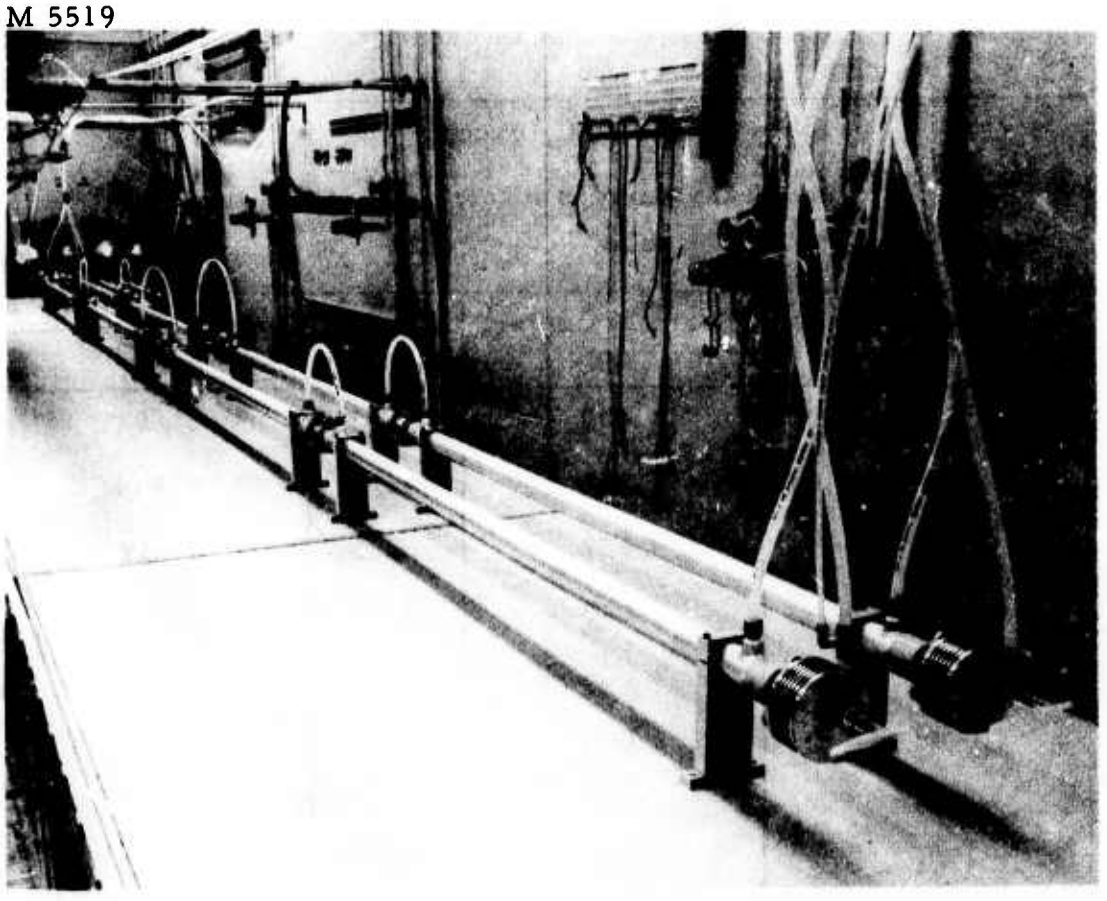

Fig. 36. Over-all view of 16 m IA mounted on the 32 ft table.

two throttle valves located at the center of the tubes. For the initial trials, cooling is accomplished by flowing water from section to section, with four sections in series. If degradation in performance due to wall heating becomes significant, the water cooling path will be rerouted to increase the flow rate.

Construction details of the FA will be essentially identical to those used for the IA, with the exception of the glass pipe i.d. (1 in. for the IA, 2 in. for the FA). A Brewster's angle window will be used on the FA input 8 m section. Future folding mirror assemblies will connect the 8 m sections at both ends, and a Brewster's angle window will be used on the end of the output section.

The 16 m tube is essentially complete. The vacuum and cooling systems have been successfully debugged and the discharge operated. We are now waiting for the folding mirrors to be returned from the optical shop.

V. PROGRAM FOR NEXT QUARTER

The IA will be evaluated with both pulsed and cw discharge excitation and with both pulsed and cw optical excitation. More accurate values for S_o in a 1 in. diameter tube will be obtained. The IA will then be used to drive an 8 m test section of 2 in. tubing to determine pulsed and cw values for g_o and S_o in that diameter. Fabrication of the FA will then proceed, with the objective of realizing 25 kW peak output at 0.04 duty.

REFERENCES

1. C.B. Moore, R.E. Wood, B.B. Hu, and J.T. Yardley, "Vibrational energy transfer in CO_2 laser," University of California, Berkeley (unpublished).

2. G.J. Shulz, "Vibrational excitation of nitrogen by electron impact," Phys. Rev. 125, 229 (1962).

3. L.D. Hocker, M.A. Kovacs, C.K. Rhodes, G.W. Flynn, and A. Javan, "Vibrational relaxation measurements in CO_2 using an induced-fluorescence technique," Phys. Rev. Letters 17, 233 (1966).

4. G.W. Flynn, L.O. Hocker, A. Javan, M.A. Kovacs, and C.K. Rhodes," Progress and application of Q-switching techniques using molecular gas laser," IEEE J. Quantum Electron. 2, 378 (1966).

5. H. Statz, C.L. Tang, and G.F. Koster, "Transition probabilities between laser states in CO_2," J. Appl. Phys. 37, 4278 (1966).

6. A.B. Callear, "Measurement of energy transfer in molecular collisions," Appl. Optics Supp. 2, Chem. Lasers, 145 (1965).

7. K.F. Herzfeld and T.A. Litowitz, Absorption and Dispersion of Ultrasonic Waves (Academic Press, New York, 1959).

8. M.J. Weber and T.F. Deutsch, "Pulsed and steady-state infrared emission studies of CO_2 laser system," J. Quantum Electron. 2, 369 (1966).

9. T.L. Cottrell and J.C. McCoubrey, Molecular Energy Transfer in Gases (Butterworths, London, 1961).

10. P.K. Cheo, "Effects of CO_2, He, and N_2 on the lifetimes of the 00^01 and 10^00 CO_2 laser levels and on pulsed gain at 10.6 μ" (unpublished).

11. M.H. Wallmann, Ann. Physik (Leipzig) 21, 671 (1934).

12. I.M. Metter, Phys. Z. Sovjetunion 12, 233 (1937).

13. T.L. Cottrell and M.A. Day, Molecular Relaxation Processes (Academic Press, New York, 1966).

14. A. Van Itterbeek and P. Mariens, Physica 7, 125 (1940).

15. L. Küchler, Z. Physik Chem. 41B, 199 (1938).

16. A. Euchken and E. Nümann, Z. Physik Chem. 36B, 163 (1937)

17. F. Horrigan, "High Power for Laser Research," Final Technical Report, 15 June 1965 to 14 March 1966, Raytheon Company, Research Division.

18. P.O. Clark and M.R. Smith, Appl. Phys. Letters 9, 367 (1966).

19. E.I. Gordon, A.D. White, and J.D. Rigden, "Gain Saturation at 3.39 microns in the He-Ne Maser," in the Proceedings of the Symposium on Optical Masers, (Polytechnic Institute of Brooklyn, 1963).

20. H. Kogelnik and T.J. Bridges, "A non-resonant multipass CO_2 laser amplifier," IEEE J. Quantum Electron. QE-3, 95 (1967).

21. C.K.N. Patel, "Vibrational rotational laser action in carbon monoxide," Phys. Rev. 141, 71 (1966).

22. P.O. Clark and M.R. Smith, "Pulsed operation of CO_2-N_2-He laser," Appl. Phys. Letters 9, 369 (1966).

23. C. Frapard, M. Roulot, and X. Ziegler, "High peak power 10 μ CO_2 laser," Phys. Letters 20, 384 (1966).

APPENDIX A

MEDIUM DISTORTION EFFECTS

Since optical distortion profiles for CO_2 lasers have been measured by Komai, et al.,* we did not feel it necessary to repeat their work. Interferometric methods were used to measure absolute and relative phase shifts of a helium-neon 6328Å beam passing through the medium as a function of discharge tube radius. Their most significant data are reproduced in Fig. A-1. If the observed distortions simply scale with wavelength as anticipated, the distortion is less than $\pi/20$ rad at 10.6 μ in a 1-in. tube 3 m long. Thus, a total length of about 60 m is anticipated to lead to a reversal in phase from the center to the edge of the tube. Since many of the tubes are larger in diameter and total length is not much longer than this, it is anticipated that simple optical correction can be applied as required.

The saturation distortion effects treated in Section II-C-3 and the possible effects of transient heating in the pulsed discharge case are not included in the measurement by Komai, et al. We expect to look for these effects in the 16 m IA.

*L. G. Komai, et al., Technical Report AFAL-TR-66-257, December 1966, p. 18.

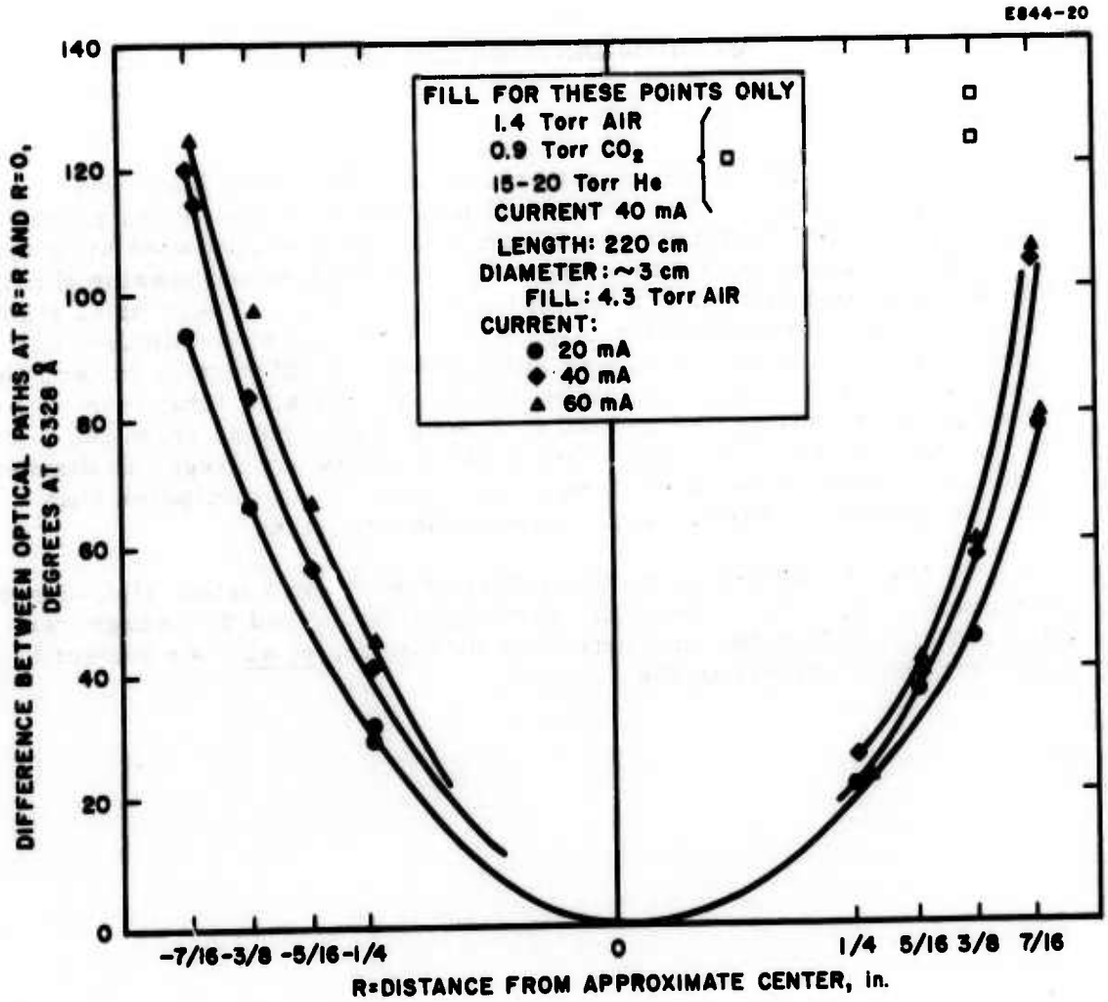

Fig. A-1. Distortion profile for long gas laser tube.

APPENDIX B

EFFECTS OF COUPLED LEVELS ON SATURATION FLUX

We are considering here the effects of single line stimulation on a cw CO_2 amplifier. The result is that the other rotational levels relax very rapidly to the lasering level, act as a pseudo-pump, increase the efficiency, but also increase the saturation power necessary to efficiently extract the energy of inocision.

Consider first a simple four-level system with infinite relaxation rate from the terminal laser level. The excited state population, N_2, then obeys the following equation.

$$\frac{dn_2(x,t)}{dt} = Wn_o - n_2(x,t)\left[\frac{1}{\tau} + \sigma\mu(x,t)\right] \qquad \text{(B-1)}$$

pump — spontaneous decay — stimulated emission

We can write a formal solution to this equation.

$$n_2(x,t) = Wn_o \exp\left[-\int_o^t \left(\frac{1}{\tau} + \sigma\mu(x,t')\,dt'\right]\right. \int_o^t$$

$$\exp\left[+\int_o^{t'} \left(\frac{1}{\tau} + \sigma\mu(x,t'')\,dt''\right.\right. \quad dt''\Big] \qquad \text{(B-2)}$$

Now the flux at x can also be written:

$$\mu(x,t) = \mu(o,t) \exp \int_o^x \sigma n_2(x',t)\,dx' \qquad \text{(B-3)}$$

which differentiates to yield

$$\frac{d\mu(x,t)}{dx} = \mu(x,t)\,\sigma n_2(x,t) \qquad \text{(B-4)}$$

or

$$\frac{d\mu(x,t)}{dx} = \mu(x,t)\,\sigma Wn_o \exp\left[-\int_o^t \left(\frac{1}{\tau} + \sigma\mu(x,t)\right) dt'\right]$$

$$\int_o^t \exp\left[+\int_o^{t'}\left(\frac{1}{\tau} + \sigma\mu(x,t'')\,dt''\right]\right] dt' \qquad \text{(B-5)}$$

This can be readily solved in the equilibrium case, $t \to \infty$ and $\mu(o,t) = \text{const}$. Then,

$$\frac{d\mu(x,\infty)}{dx} = \frac{\mu(x,\infty)\,\sigma Wn_o}{\frac{1}{\tau} + \sigma\mu(x,\infty)} \qquad \text{(B-6)}$$

Integrating this, we get

$$\sigma Wn_o x = \sigma\left(\mu(x,\infty) - \mu(o,\infty)\right) + \frac{1}{\tau}\ln\frac{\mu(x,\infty)}{\mu(o,\infty)} \qquad \text{(B-7)}$$

We would prefer to have $\mu(x,\infty)$ as a function of x, but this is adequate for our purposes.

Equation (B-2) can also be solved for $n_2(x,\infty)$.

$$n_2(x,\infty) \cong \frac{Wn_o}{\frac{1}{\tau} + \sigma\mu(x,\infty)} \qquad \text{(B-8)}$$

It would be convenient here to have an explicit expression for $\mu(x,\infty)$. We note, however, that for large values of $\mu(x,\infty)$, the linear term dominates and we can then write

$$\mu(x,\infty) \cong Wn_o x \qquad \text{(B-9)}$$

Then

$$n_2(x, \infty) \xrightarrow[\text{large } \mu]{} \frac{Wn_o}{\frac{1}{\tau} + \sigma W n_o x} \longrightarrow \frac{1}{\sigma x} \qquad \text{(B-10)}$$

The breaking point between high and low signal is given by $\mu = 1/\sigma\tau$, which is defined as the saturation power (photons/cm^2 sec).

Now consider the case when there are many (M) excited levels, thermally coupled with a fast relaxation time, τ_1. In thermal equilibrium, that fraction of the total band population associated with the j^{th} level ($j = 1, 2, \ldots, M$) is given by the Boltzmann factor, B_j, and it has the approximate* form

$$B_j = \frac{e^{-\gamma j(j-1)/kT}}{\sum_{x=1}^{m} e^{-\gamma j(j-1)/kT}} \qquad \text{(B-11)}$$

where $\gamma \approx 0.39$ cm^{-1} for the CO_2 laser*. Thus, if $2j\gamma \ll kT$ for all j, the distribution of band population over the M levels is roughly uniform, so that we may take $B_j \approx 1/M$.

When there is stimulated emission from a single level, say $j = j_o$, the following rate equations govern the population of the levels:

$$\frac{dn_{2j_o}(x, t)}{dt} = W_{j_o} n_o - n_{2j_o}(x, t)\left(\frac{1}{\tau} + \sigma\mu_{j_o}(x, t)\right)$$

$$+ \sum_{j \neq j_o} \frac{\left(n_{2j}(x, t) - n_{2j_o}(x, t)\frac{B_j}{B_{j_o}}\right)}{\tau_1} \qquad \text{(B-12)}$$

*G. Herzberg, Infrared and Raman Spectra, Chapter 6, p. 371, 395 (D. Van Nostrand Co., Inc., 1964).

$$\frac{dn_{2_j}(x,t)}{dt} = W_j n_o - \frac{n_{2_j}(x,t)}{\tau} - \frac{\left(n_{2_j}(x,t) - n_{2_{j_o}}(x,t)\,\frac{B_j}{B_{j_o}}\right)}{\tau_1} \qquad \text{(B-13)}$$

The last terms on the RHS of these equations simply express the fact that, when perturbed, a system drives toward a distribution of population consistent with the principle of detailed balance: as the j_o state is depleted by stimulated emission, the system drives toward thermal equilibrium within the band of levels by feeding population into the j_o level from all other levels ($j \neq j_o$). Making the approximation that total population is uniformly distributed over the band, as discussed in the preceeding paragraph, Equations (B-12) and (B-13) have the following form in steady state:

$$\frac{dn_{2_{j_o}}(x,\infty)}{dt} = 0 = Wn_o - n_{2_{j_o}}(x,\infty)\left(\frac{1}{\tau} + \sigma\mu_{j_o}(x,\infty)\right) + \frac{(M-1)}{\tau_1}\left(n_{2_j}(x,\infty) - n_{2_{j_o}}(x,\infty)\right) \qquad \text{(B-12a)}$$

$$\frac{dn_{2_j}(x,\infty)}{dt} = 0 = Wn_o - \frac{n_{2_j}(x,\infty)}{\tau} - \frac{\left(n_{2_j}(x,\infty) - n_{2_{j_o}}(x,\infty)\right)}{\tau_1} \qquad \text{(B-13a)}$$

Using (B-13a) to eliminate $n_{2_j}(x,\infty)$ from (B-12a), we get

$$\frac{dn_{2_{j_o}}(x,\infty)}{dt} = 0 = W'n_o - n_{2_{j_o}}(x,\infty)\left(\frac{1}{\tau'} + \sigma\mu_{j_o}(x,\infty)\right) \qquad \text{(B-14)}$$

where

$$W' = MW \qquad \text{(B-15)}$$

and

$$\tau' = \tau/M \qquad \text{(B-16)}$$

Therefore, the saturation power becomes $1/\sigma\tau'$, or $M/\sigma\tau$, which is larger by a factor of M, the number of levels, than that for a single level system. The effective pump rate is also increased by a factor M.

APPENDIX C

COMPUTATIONAL METHOD

The equation

$$\frac{d\,S(z)}{dz} = \frac{g_o\,S(z)}{1 + \frac{S(z)}{S_o}} \qquad \text{(C-1)}$$

is easily solved by numerical integration. The simplest method is to divide the interval (0, L) into equal parts Δz and use the linear approximation over each subinterval:

$$S_j = S_{j-1} + \left(\frac{dS}{dz}\right)_{j-1} \Delta z \qquad \text{(C-2)}$$

$$= S_{j-1} + \frac{g_o\,\Delta z\,S_{j-1}}{1 + \frac{S_{j-1}}{S_o}} \qquad \text{(C-3)}$$

Somewhat improved accuracy is obtained at virtually no increase in computation time (since storage is not an issue in such a simple problem) by using the Milne method*

$$S_j = S_{j-4} + \frac{4}{3}\left\{2\left(\frac{dS}{dz}\right)_{j-3} - \left(\frac{dS}{dz}\right)_{j-2} + 2\left(\frac{dS}{dz}\right)_{j-1}\right\}\Delta z. \qquad \text{(C-4)}$$

*For example, see W. E. Milne, Numerical Solutions of Differential Equations (Wiley and Sons, New York, 1953).

The first three points after S_{in} are computed using the linear approximation (C-3) and the four-point Milne formula (C-4) used thereafter.

When the beam area changes, the power is computed at each point using the local area; thus,

$$P_j = S_j A_j, \qquad \text{(C-5)}$$

where the formula for computing A_j is given in the program.

A program useful in design (ONR-5) is given in List 1. The listing is given for the GE 265 time sharing system using the interpretive routine BASIC. The computation time is 3 to 5 sec. (The variation is a peculiarity of the time-share system.) Lines beginning "REM" are ignored by the computer — they are remarks by the programmer for the information of the program user. A somewhat different notation from that used in the text has been used in the program itself to simplify the subscripting. A typical sequence of runs using this program is shown in List 2. This particular sequence of 5 runs is a reduction of the data from the 5 pass amplifier described by Kogelnik and Bridges* without the approximation of assuming an average area. The value 100 W/cm^2, obtained for S_o in the reference cited below, was used as an input parameter, and a value of 5.5 W output power was obtained, in good agreement with the measured value. The good agreement is not surprising, since the "average area" is a pretty good approximation for a 5-times refocussed beam. The total computation time was 19 seconds and the total time expended on the problem was 5 minutes. (Clock time is recorded on the first line of each run.) The time difference was spent in input/output on the teletypewriter, and by the operater computing (by sliderule) the 6% loss in signal between passes to initiate the next run.

A second example is given in List 3 (ONR-9). This program computes the change in distribution of a gaussian beam as it propagates through a saturable medium. No area expansion is assumed, so that the results are appropriate only for large diameter beams. The input quantity S is the ratio of saturation flux S_o to the flux density on the axis at the input, and the quantity G is the total amplifier small-signal gain, $g_o L$. The program output gives the signal intensity at input and output (each normalized to their values on axis) at 20 radii between 0 and 2 w_o. A typical output is shown in List 4.

---

*H. Kogelnik and T. J. Bridges, IEEE J. Quantum Electron. QE-3, 95 (1967).

LIST 1

```
100 REM THIS PRØGRAM ASSUMES HØMØGENEØUS INTERACTIØN
110 REM    W = BEAM WAIST DIAMETER IN CM TØ 1/E2 PØINTS
120 REM    X = BEAM WAIST PØSITIØN IN METERS
130 REM    P = INPUT PØWER IN WATTS
140 REM    S = SATURATIØN PARAMETER IN WATTS/SQ CM
150 REM    G = SMALL-SIGNAL GAIN IN DB/METER
160 REM    L = TUBE LENGTH IN METERS
170PRINT"VALUES ØF W,X,P,S,G,L";
180INPUT W,X,P,S,G,L
190REM B IS BEAM WAIST AREA IN SQ CM
200 LET B= (3.1416/4)*(W↑2)
210 LET B1 = B/2
220 LET K1 = 1
230 REM K1 IS A FUDGE FACTØR = RATIØ(EXPTL BEAM DIV/GAUSSIAN BEAM DIV)
240 REM K1 MUST BE CHANGED BY MØDIFYING THE PRØGRAM
250 LET C1 = .106*K1/B
260 LET E = L/100
270 LET F = E*.23*G
280 DIM A(200)
290 DIM Q(200)
300 DIM T(200)
310 REM CØMPUTES Q(N), T(N) FØR N = 0 TØ 4
320LET Q(0) = P
330 REM Q(N) IS THE PØWER IN WATTS
340 REM T(N) IS S PRIME X A X DELTAZ
350 FØR N=0 TØ 3
360 LET Z = N*E
370 LET A(N) = B1*(1+(C1*(Z-X))↑2)
380 LET T(N) = Q(N)*(F/(1+Q(N)/(A(N)*S)))
390LET Q(N+1) = Q(N) + T(N)
400 NEXT N
410FØR N = 4 TØ 100
420 LET Z = N*E
430 LET A(N) =B1*(1+(C1*(Z-X))↑2)
440 LETQ(N) = Q(N-4)+1.333333*(2*T(N-3)-T(N-2)+2*T(N-1))
450 LET T(N) =-Q(N)*(F/(1+Q(N)/(A(N)*S)))
460 NEXT N
470PRINT
480 PRINT"L (METERS)", "D(L) (CM)", "P(L) (WATTS)","G(L) (DB)"
490 PRINT
500 LET N = 100
510 PRINT N*E, SQR(8*A(N)/3.1416), Q(N), 4.343*LØG(Q(N)/P)
520END
```

LIST 2

```
KEY
READY.

OLD
OLD PROBLEM NAME--SNR5
READY.
RUN

SNR5      10:13   LAI WED 5/10/87
VALUES OF W,X,P,S,G,L? .842,.5,.968,100,3.8,1
L (METERS)      D(L) (CM)       P(L) (WATTS)    G(L) (DB)
 1.              .389217         1.63548         2.27773

TIME:  4 SECS.


RUN

SNR5      10:14   LAI WED 5/10/87
VALUES OF W,X,P,S,G,L? .248,.5,1.585,100,3.8,1
L (METERS)      D(L) (CM)       P(L) (WATTS)    G(L) (DB)
 1.              .389217         2.41061         1.98575

TIME:  3 SECS.


RUN

SNR5      10:15   LAI WED 5/10/87
VALUES OF W,X,P,S,G,L? .842,.5,3.850,100,3.8,1
L (METERS)      D(L) (CM)       P(L) (WATTS)    G(L) (DB)
 1.              .389217         3.33899         1.71434

TIME:  4 SECS.


RUN

SNR5      10:17   LAI WED 5/10/87
VALUES OF W,X,P,S,G,L? .8[illegible].5,3.15,100,3.8,1
L (METERS)      D(L) (CM)       P(L) (WATTS)    G(L) (DB)
 1.              .389217         4.86784         1.48038

TIME:  4 SECS.


RUN

SNR5      10:18   LAI WED 5/10/87
VALUES OF W,X,P,S,G,L? .842,.5,4.099,100,3.8,1
L (METERS)      D(L) (CM)       P(L) (WATTS)    G(L) (DB)
 1.              .389217         5.9097          1.38878

TIME:  4 SECS.
```

Kayleigh & Dewa's Data Collection

Run #1

Run #2

Run #3

Run #4

Run #5

LIST 3

```
LIST

ØNR9      20:23   LA FRI 05/19/67

100 REM THIS PRØGRAM ASSUMES HØMØGENEØUS INTERACTIØN
110 REM ØNR9 CØMPUTES THE EFFECT ØF SATURATIØN ØN A GAUSSIAN BEAM
120 REM NØ BEAM SPREAD IS ASSUMED
130 REM INPUT PØWER IS ASSUMED AS 1 WATT/ SQ CM AT R=0
140 PRINT "VALUES ØF SATURATIØN FLUX, GAIN";
150 INPUT S,G
160 LET E = 0.01
170 LET F = E*.23*G
180 DIM V(40)
190 DIM P(40)
200 DIM R(40)
210 DIM Q(200)
220 DIM T(200)
230 FØR M=0 TØ 20
240 LET R(M) = 0.1*M
250 LET P(M) = EXP(-2*(R(M)↑2))
260 REM CØMPUTES Q(N), T(N) FØR N = 0 TØ 4
270 LET Q(0) = P(M)
280 REM Q(N) IS THE PØWER IN WATTS
290 REM T(N) IS S PRIME X A X DELTAZ
300 FØR N=0 TØ 3
310 LET Z = N*E
320 LET T(N) = Q(N)*(F/(1+Q(N)/S))
330LET Q(N+1) = Q(N) + T(N)
340 NEXT N
350FØR N = 4 TØ 100
360 LET Z = N*E
370 LETQ(N) = Q(N-4)+1.333333*(2*T(N-3)-T(N-2)+2*T(N-1))
380 LET T(N) = Q(N)*(F/(1+Q(N)/S))
390 NEXT N
400 LET V(M) = Q(100)
410 NEXT M
420PRINT
430 PRINT "RADIUS", "INPUT","ØUTPUT"
440 PRINT
450 FØRM=0 TØ 20
460 PRINT R(M), P(M),V(M)/V(0)
470 NEXT M
480END
```

LIST 4

```
RUN


ØNR9     20:35   LA FRI 05/19/67

VALUES ØF SATURATIØN FLUX, GAIN? 1,48

RADIUS          INPUT           ØUTPUT

 0               1               1
 .1              .980199         .996299
 .2              .923116         .985418
 .3              .83527          .967984
 .4              .726149         .944905
 .5              .606531         .917216
 .6              .486752         .885909
 .7              .375311         .851806
 .8              .278037         .815486
 .9              .197899         .777267
 1.              .135335         .737246
 1.1             8.89216 E-2     .695364
 1.2             5.61348 E-2     .651478
 1.3             3.40475 E-2     .605437
 1.4             1.98411 E-2     .55713
 1.5             .011109         .506535
 1.6             5.97602 E-3     .453743
 1.7             3.08872 E-3     .39899
 1.8             1.53381 E-3     .342689
 1.9             7.31802 E-4     .285495
 2.              3.35463 E-4     .228398

TIME:  20 SECS.
```

APPENDIX D

10.6 μ SIGNAL SOURCES, TEM_{00}

SINGLE FREQUENCY, 100 mW, TEM_{00}

A mechanically stabilized, single frequency 10.6 μ source was constructed for the purpose of making small-signal gain measurements. The characteristics of this laser are summarized below.

Output

The output power was nominally 100 mW in a single P-branch transition. The laser was tunable by means of a piezoelectric transducer mount on the mirrors and could be operated on each of the transitions P(16) to P(22). The output was stable on each transition over a 10 min period under ordinary laboratory conditions.

Cavity

The invar frame shown in Fig. D-1 was used as the structural support. The optical cavity consisted of a 60 cm radius, gold-coated spherical mirror spaced 23.6 cm from a gold-coated flat mirror with a 1 mm output hole coupling. The near-confocal cavity and the small output hole coupling was sufficient to insure TEM_{00} mode operation under proper alignment.

Laser Tube

The laser discharge tube used NaCl Brewster's angle windows, and a 5 mm water cooled pyrex bore with a 12 cm active length. A sealed-off gas mixture of 3 Torr CO_2 + 4 Torr N_2 + 11 Torr He was used. Over 100 hours of operation could be obtained on a single fill.

5 W, TEM_{00}

Output

The output power was nominally 5 W, TEM_{00} mode. With proper cavity spacing, 95% of the power could be obtained in a single P-branch transition. This laser was capable of > 20 W multimode power output when used with a larger coupling hole or dielectric mirrors.

M 4268

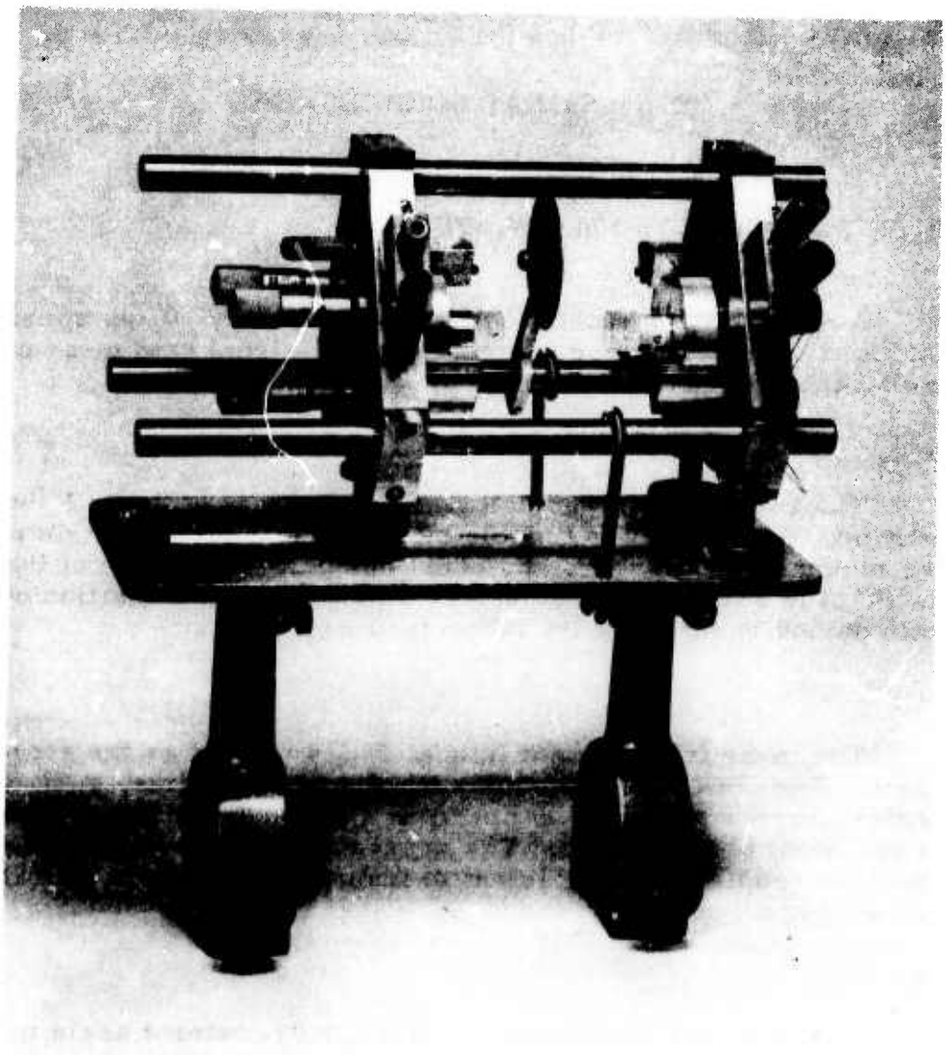

Fig. D-1. Photograph of Fabry-Perot scanning interferometer which was modified for use as a CO_2 laser mirror support structure.

Cavity

The cavity structure used quartz spacer rods for thermal stability, as shown in Fig. D-2. The optical cavity consisted of a 200 cm radius, gold-coated spherical mirror separated 115 cm from a gold-coated flat output mirror with 2 mm coupling hole.

Discharge Tube

The discharge tube was water cooled, with NaCl Brewster's angle windows, and a 10 mm pyrex bore with 100 cm active length. The laser was operated with a flowing gas mixture of 4 Torr CO_2, 5 Torr N_2, and 15 Torr He.

DISCUSSION

Both the above sources are described as operating on the TEM_{00} cavity mode. Undoubtedly this is not true, since no mode selecting irises were used inside the cavities. With the cavity geometries and coupling holes used, the output beam was very closely gaussian in distribution and exhibited the beam divergence associated with a uniphase gaussian beam (see Section III-B-2). Whether or not a high order mode exists inside the cavity, with the output aperture coupling only to a uniphase portion of that mode, is more or less academic for the purposes of the present measurement. In the ultimate application of this equipment, the exact frequency spectrum will be of interest, so that further measurement of oscillator characteristics will then be required.

M 5348

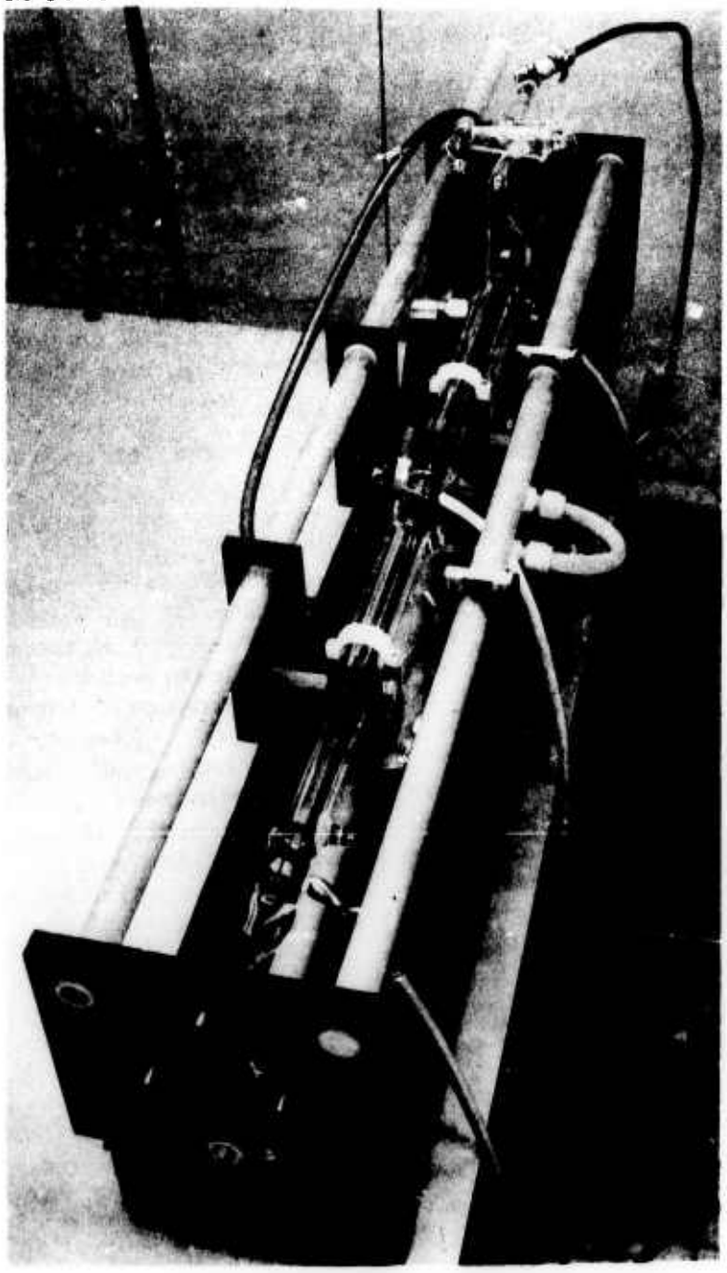

Fig. D-2. CO_2 laser with quartz spacer rods.

UNCLASSIFIED

Security Classification

DOCUMENT CONTROL DATA - R&D

(Security classification of title, body of abstract and indexing annotation must be entered when the overall report is classified)

1. ORIGINATING ACTIVITY (Corporate author) Hughes Research Laboratories 3011 Malibu Canyon Road Malibu, California 90265	2a. REPORT SECURITY CLASSIFICATION Unclassified 2b. GROUP N/A

3. REPORT TITLE

CO_2 OPTICAL RADAR SYSTEM

4. DESCRIPTIVE NOTES (Type of report and inclusive dates)

Semiannual Technical Summary Report, 1 November 1966 through 1 May 1967

5. AUTHOR(S) (Last name, first name, initial)

Bridges, W. B., Smith, M.R.

6. REPORT DATE	7a. TOTAL NO. OF PAGES	7b. NO. OF REFS
May 1967	98	23

8a. CONTRACT OR GRANT NO. NO 0014-67-C-0237, ARPA Order 306 b. PROJECT NO. 259 c. d.	9a. ORIGINATOR'S REPORT NUMBER(S) N/A 9b. OTHER REPORT NO(S) (Any other numbers that may be assigned this report)

10. AVAILABILITY/LIMITATION NOTICES

[redacted]

11. SUPPLEMENTARY NOTES	12. SPONSORING MILITARY ACTIVITY Physics Branch Physical Sciences Division ONR, Washington, D.C.

13. ABSTRACT

Progress is reported on a program to develop and build a 1 kW average power 10.6 μ amplifier for radar applications. Small signal gain and saturation measurements were made on 1-in. diameter amplifier tubes using a CO_2-N_2-He mixture with cw driving signals. Optimum values for cw discharge tubes were 3 dB/m and 60 to 90 W/cm^2; for pulsed discharges (at 500 pps), they were 4 dB/m and more than 200 W/cm^2.

Based on the above values, transmitter designs were made using pulsed operation or a combination of pulsed and cw operation at different stages. The most promising of these designs would use: (1) a 10 W cw oscillator, (2) a folded 16 m, 1 in. diameter tube, (3) a mechanical modulator with recollimating optics, and (4) a final amplifier of 8 m, 2 in. diameter tubes operated with a pulsed discharge. The device would be 32 ft long, including folding and recollimating optics.

The mechanisms of the CO_2-N_2-He laser are summarized and relevant rates and coefficients tabulated. The theory of gain saturation is reviewed and equations derived. Numerical values for small signal gain and saturation flux are calculated and compared with experimental values. Collisional cross relaxation among rotational levels appears to be important, and a method of treating it is presented. We solve the gain saturation equation for simplified cases. Diffraction beam spreading effects on amplifier performance are discussed, and a solution for the effect of gain saturation on the radial beam profile is given.

DD FORM 1 JAN 64 1473

UNCLASSIFIED

Security Classification

UNCLASSIFIED

Security Classification

14. KEY WORDS	LINK A		LINK B		LINK C	
	ROLE	WT	ROLE	WT	ROLE	WT
Gas laser						
10.6 μ optical radar						
CO_2-N_2-He mixture						
Gain measurements						

INSTRUCTIONS

1. **ORIGINATING ACTIVITY:** Enter the name and address of the contractor, subcontractor, grantee, Department of Defense activity or other organization *(corporate author)* issuing the report.

2a. **REPORT SECURITY CLASSIFICATION:** Enter the overall security classification of the report. Indicate whether "Restricted Data" is included. Marking is to be in accordance with appropriate security regulations.

2b. **GROUP:** Automatic downgrading is specified in DoD Directive 5200.10 and Armed Forces Industrial Manual. Enter the group number. Also, when applicable, show that optional markings have been used for Group 3 and Group 4 as authorized.

3. **REPORT TITLE:** Enter the complete report title in all capital letters. Titles in all cases should be unclassified. If a meaningful title cannot be selected without classification, show title classification in all capitals in parenthesis immediately following the title.

4. **DESCRIPTIVE NOTES:** If appropriate, enter the type of report, e.g., interim, progress, summary, annual, or final. Give the inclusive dates when a specific reporting period is covered.

5. **AUTHOR(S):** Enter the name(s) of author(s) as shown on or in the report. Enter last name, first name, middle initial. If military, show rank and branch of service. The name of the principal author is an absolute minimum requirement.

6. **REPORT DATE:** Enter the date of the report as day, month, year; or month, year. If more than one date appears on the report, use date of publication.

7a. **TOTAL NUMBER OF PAGES:** The total page count should follow normal pagination procedures, i.e., enter the number of pages containing information.

7b. **NUMBER OF REFERENCES:** Enter the total number of references cited in the report.

8a. **CONTRACT OR GRANT NUMBER:** If appropriate, enter the applicable number of the contract or grant under which the report was written.

8b, 8c, & 8d. **PROJECT NUMBER:** Enter the appropriate military department identification, such as project number, subproject number, system numbers, task number, etc.

9a. **ORIGINATOR'S REPORT NUMBER(S):** Enter the official report number by which the document will be identified and controlled by the originating activity. This number must be unique to this report.

9b. **OTHER REPORT NUMBER(S):** If the report has been assigned any other report numbers *(either by the originator or by the sponsor)*, also enter this number(s).

10. **AVAILABILITY/LIMITATION NOTICES:** Enter any limitations on further dissemination of the report, other than those imposed by security classification, using standard statements such as:

(1) "Qualified requesters may obtain copies of this report from DDC."

(2) "Foreign announcement and dissemination of this report by DDC is not authorized."

(3) "U. S. Government agencies may obtain copies of this report directly from DDC. Other qualified DDC users shall request through _____."

(4) "U. S. military agencies may obtain copies of this report directly from DDC. Other qualified users shall request through _____."

(5) "All distribution of this report is controlled. Qualified DDC users shall request through _____."

If the report has been furnished to the Office of Technical Services, Department of Commerce, for sale to the public, indicate this fact and enter the price, if known.

11. **SUPPLEMENTARY NOTES:** Use for additional explanatory notes.

12. **SPONSORING MILITARY ACTIVITY:** Enter the name of the departmental project office or laboratory sponsoring *(paying for)* the research and development. Include address.

13. **ABSTRACT:** Enter an abstract giving a brief and factual summary of the document indicative of the report, even though it may also appear elsewhere in the body of the technical report. If additional space is required, a continuation sheet shall be attached.

It is highly desirable that the abstract of classified reports be unclassified. Each paragraph of the abstract shall end with an indication of the military security classification of the information in the paragraph, represented as *(TS), (S), (C), or (U)*.

There is no limitation on the length of the abstract. However, the suggested length is from 150 to 225 words.

14. **KEY WORDS:** Key words are technically meaningful terms or short phrases that characterize a report and may be used as index entries for cataloging the report. Key words must be selected so that no security classification is required. Identifiers, such as equipment model designation, trade name, military project code name, geographic location, may be used as key words but will be followed by an indication of technical context. The assignment of links, rules, and weights is optional.

GPO 888-551

UNCLASSIFIED

Security Classification